AD NUMBER

AD417092

NEW LIMITATION CHANGE

TO

Approved for public release, distribution unlimited

FROM

Distribution authorized to U.S. Gov't. agencies and their contractors; Administrative/Operational Use; Feb 1955. Other requests shall be referred to Defense Atomic Support Agency, Washington, DC.

AUTHORITY

DASA ltr dtd 23 Mar 1964

UNCLASSIFIED

AD 417092 L

DEFENSE DOCUMENTATION CENTER

FOR

SCIENTIFIC AND TECHNICAL INFORMATION

CAMERON STATION, ALEXANDRIA, VIRGINIA

AUTHORITY FOR DOWNGRADING TO READ
DASA LETTER 23 MARCH 1964

UNCLASSIFIED

[redacted]

(5) 782. 500

WT-716

UNCLASSIFIED-FRD Copy No. 176 A

(1)

ion

25

Doc
Cop

SHOT-KNOTHOLE

DA PROVING GROUNDS A/12055

une 1953

1.4

FREE-FIELD MEASUREMENTS OF EARTH STRESS, STRAIN, AND GROUND MOTION

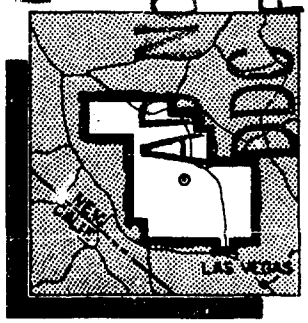

[redacted]

HEADQUARTERS FIELD COMMAND, ARMED FORCES SPECIAL WEAPONS PROJECT
SANDIA BASE, ALBUQUERQUE, NEW MEXICO

Reproduced Direct from Manuscript Copy by
AEC Technical Information Service
Oak Ridge, Tennessee

BEST AVAILABLE COPY

~~WT-716~~

This document consists of 108 pages
No. 176 of 220 copies, Series A

OPERATION UPSHOT-KNOTHOLE

Project 1.4

FREE-FIELD MEASUREMENTS OF EARTH STRESS, STRAIN, AND GROUND MOTION,

REPORT TO THE TEST DIRECTOR

by

W. R. Perret
V. L. Gentry

February ~~1955~~

Sandia Corporation
Albuquerque, New Mexico

BEST AVAILABLE COPY

[redacted]

ABSTRACT

Part I - Project 1.4a

Earth cover provides protection to underground structures against the effects of air shock loading. Part of this protection may result from attenuation of stress with thickness of the cover. Measurements of vertical earth stress at three depths and at five ground ranges were made during Shots 9 and 10 of Operation UPSHOT-KNOTHOLE to detect and evaluate stress attenuation with depth. Data fit equally well the empirical equations

$$P = P_1 \exp - (d - d_1)\, 0.07$$

and

$$P = P_1 \left(\frac{d}{d_1}\right)^{-0.34},$$

in which P and P_1 are the stresses in psi at depths d and d_1 in ft, d_1 being the shallower. Precision in each case is better than ± 25 per cent.

Part II - Project 1.4b

A practical system for measuring free-field earth stresses and strains resulting from transient loads has been tested with sufficient thoroughness to establish its feasibility. Arrays of directionally sensitive earth stress and strain gages and accelerometers were installed 5 ft deep to record these parameters during Shots 1, 9, and 10 of UPSHOT-KNOTHOLE. Duplicate instrumentation showed that stress measurements were reproducible with average deviations of 16 per cent and strain measurements with average deviations of 35 per cent. This test disregards the presently unknown factors related to perturbations of the stress field by the gages. Stress-strain graphs demonstrate hysteresis. Plastic deformation of the soil resulted in rates of energy dissipation as high as 300 μft-lb/ft^3. Data from Shot 10 defined the stress tensor in terms of magnitudes and directions of the three principal stresses as a function of time.

[redacted]

-FRD

FOREWORD

Measurement of free-field phenomena in the earth resulting from airbursts of nuclear weapons was divided under Project 1.4 of UPSHOT-KNOTHOLE into two subprojects: Project 1.4a was concerned with the detection and evaluation of attenuation of vertical earth stress with depth and was intended to give information pertinent to Project 3.8 structural response tests; Project 1.4b involved testing instruments and analytical procedures for determination of stress and strain tensors produced within the earth as a result of a high-yield explosion.

Part I of this report deals entirely with Project 1.4a measurements of vertical stress as a function of depth, time, ground range, and incident air overpressure. Part II is concerned with Project 1.4b systems for measurement and analysis of data for determining stress and strain tensors in the earth as a function of time.

This is one of the reports presenting the results of the 78 projects participating in the Military Effects Tests Program of UPSHOT-KNOTHOLE, which included 11 test detonations. Reference to other pertinent test information is made in WT-782, Summary Report of the Technical Director, Military Effects Program, which includes the following:

a. An over-all description of each detonation including yield, height of burst, ground zero location, time of detonation, ambient atmospheric conditions at detonation, etc., for the 11 shots.
b. Compilation and correlation of all project results on the basic measurements of blast and shock, thermal radiation, and nuclear radiation.
c. Compilation and correlation of the various project results on weapons effects.
d. A summary of each project, including objectives and results.
e. A complete listing of all reports covering the Military Effects Tests Program.

[redacted]

-FRD

CONTENTS

ILLUSTRATIONS

TABLES

PART I

VERTICAL STRESS AS A FUNCTION OF DEPTH AND RANGE

1.1 HISTORICAL BACKGROUND

Experience has shown that buried structures are damaged less by air blast than are similar uncovered structures. Navy structure 3.2.6 1/ survived Easy shot of Operation GREENHOUSE essentially undamaged when covered with loose sand to a minimum depth of 2 feet, but was severely damaged by air shock of approximately the same intensity on Item shot after the earth cover had been removed.

The mechanics of the protective effect of earth cover is not completely understood. Protection afforded by minor thicknesses of earth is almost entirely a result of altered structural response since the earth cover increases the effective mass of the structure, decreasing its response to transient loads. Stability of earth cover over structures which extend above the ground surface requires side slopes of 30-45°. Such slopes have been found to reduce the reflection intensity of air shock waves to about 50-75 per cent of that caused by vertical walls.

Much of the protection afforded by earth cover over deep underground structures is derived from radically different phenomena. It may result in part from attenuation of stresses within the soil column and in part from development of arching above the structure. The latter condition results when, as a consequence of loading, a portion of the structure such as the roof slabs yield sufficiently to cause shear stresses to develop within a zone of soil overlying the structure and extending laterally beyond it. The shear stresses thus developed divert part of the vertical load from the roof to the surrounding soil. This process acts as though arches had developed in the soil above the yielding member of the structure to transmit the load to adjacent soil or parts of the structure. Occurrence of arching depends primarily on a sufficient thickness of soil of the proper type to support relatively high shear stresses. Movement of the structure, particularly of a vibratory nature, or plastic flow of the soil will decrease the stability of arching and reduce its effectiveness.

The thickness of cover which will distinguish between these modes of protection, mass effect or arching, is vague and debatable.

It is safe to anticipate no effective arching for earth cover shallower than the minimum lateral dimension of the covered structures. However, there do not appear to be any data which indicate the relation between the span of the structure and thickness of earth cover for which soil arches will develop under dynamic loading. Moreover, it seems probable that if earth stresses are attenuated with depth, effective attenuation may be anticipated for any thickness of cover sufficient to offer protection through arching over a structure.

Attenuation of stress and arching depend upon mechanical properties of the soil. The nature of soils suggests that if there is relative movement between adjacent soil elements, dissipation of energy and consequently attenuation of stresses may be anticipated. Theoretical studies of earth stress and strain phenomena resulting from steep-fronted transient loads of several hundred milliseconds duration are not yet well advanced. Some doubt has been expressed that any decrease in stress with depths of the order of 5-15 ft should be anticipated.

Measurements of vertical stress at depths as great as 20 ft were made during Operations BUSTER-JANGLE and TUMBLER-SNAPPER to determine experimentally whether attenuation of air-shock-induced stress could be observed. Results from BUSTER-JANGLE[2] were so erratic that no conclusive evidence of attenuation could be deduced. Inadequate control of backfill compaction appeared to be largely responsible for the erratic results.

Gage arrays of two different types were used to measure vertical earth stress at several depths during TUMBLER-SNAPPER.[3] Performance of gages placed in individual holes was unsatisfactory because of unsolved placement problems. Other gages placed in a mound of compacted earth apparently performed satisfactorily, but unanticipated oscillation of the mound obscured conclusive evidence that attenuation of vertical stress occurred.

Free-field measurements of another parameter, vertical component of acceleration,[4] have indicated a decrease in peak acceleration with depth although the data are too limited in number and scope to do more than indicate a trend.

The status of the problem of measuring attenuation of air-shock-induced earth stress with depth was practically unaltered between BUSTER-JANGLE and planning for Operation UPSHOT-KNOTHOLE. However, both previous operations had indicated the critical importance of proper compaction of backfill around and above the gages.

1.2 PLAN AND PURPOSE OF PROJECT 1.4a

Measurement of the vertical component of earth stress at several depths and ground ranges was included in plans for UPSHOT-KNOTHOLE as Project 1.4a. These measurements were designed primarily to determine whether, with adequate control of backfill, attenuation of vertical stress could be observed at depths of 15 ft or less. Identical gage arrays at five ground ranges were planned to improve chances for observing attenuation and indicate possible dependence of such attenuation on the magnitude of the locally incident air shock wave. Location

of the arrays was planned to include anticipated incident peak overpressures ranging from 80 to 10 psi.

Data from these measurements were expected to be comparable with concurrent free-field measurement of vertical stress at several depths in the earth fill adjacent to the buried structures of Project 3.8. 5/ It was anticipated that such comparison might provide a correlation between free-field earth stresses and structural damage.

1.3 INSTRUMENTATION

Carlson-Wiancko earth stress gages of improved design, described in Part II of this report, were used for all but three measurements on Project 1.4a; older-type gages were used in these three instances to determine whether there was any radical difference in performance of the two types. Response of each gage was transmitted over buried cable to a recording shelter, where it was recorded by a Consolidated Engineering Corporation carrier-amplifier photographic recording system backed up by Ampex magnetic tape recorders.6/

Gages were placed at depths of 1, 5, and 15 ft below ground level at distances of 750, 1000, 1250, 1420, and 2000 ft from nominal ground zero for Shots 9 and 10 (Fig. 1.1).

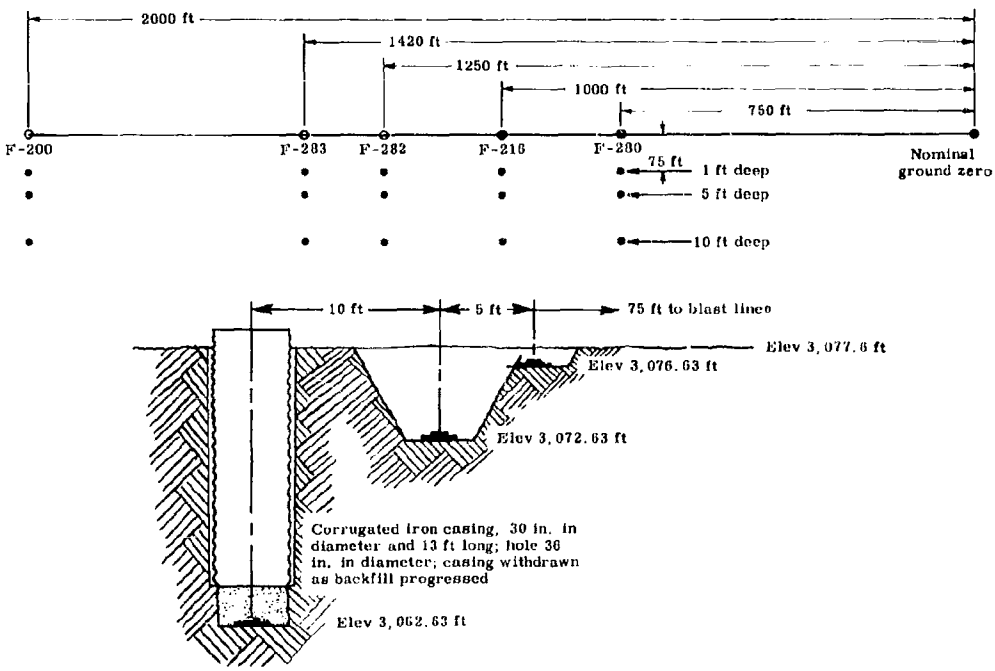

Fig. 1.1 Instrumentation for Earth Stress Attenuation - Shots 9 and 10

These distances included ranges of predicted peak air overpressures between 25 and 12 psi from Shot 9 and between 80 and 10 psi from Shot 10. Incident air overpressures at ground level were obtained from measurements by Project 1.1b and from a pair of ground-baffle gages at Station F-281 for Project 1.4b.

Holes for the earth stress gages were large enough to permit direct hand tamping of the backfill immediately surrounding each instrument. Borings for the 15-ft gages were of sufficient diameter to permit use of 30-in. diameter corrugated iron casing to make the holes safe for occupancy by personnel.

All gages were carefully bedded and leveled in the bottoms of the holes, which had been previously tamped and trimmed to within about 0.1 ft of the prescribed elevation. The final elevation of each gage was determined with a precision of 0.01 ft, and the spread of elevations for all gages at a particular nominal depth was held to 0.24 ft. Screened moist soil was hand tamped around the gages, special precautions being taken to ensure uniformity of the fill and to bond the fill to the relatively undisturbed soil surrounding the hole by wetting the sides of the hole immediately prior to placing the fill.

In the deep holes the initial 13-ft length of casing was withdrawn and replaced by shorter lengths as backfilling progressed. A large pneumatic tamper was used after about 12 to 18 in. of backfill had been hand tamped over the gages to provide reasonable protection. Backfill was placed and tamped in lifts of about 6 in. Uniformity of the compacted backfill to a height of somewhat more than one hole diameter was regarded as extremely important, but as a rule reasonable precautions were taken to maintain uniformity of compaction throughout the entire column. Placement of the gages at the 1- and 5-ft depths differed from that of the deeper ones only in that the sides of the holes were sloped to minimize arching over the gages. Backfill was built up to a height of about 6 in. above nominal ground level and cut back to grade during final preparation of the blast line area.

All backfill was prepared by blade-mixing local surface soil with water to make it somewhat wetter than optimum for compaction because the dry windy climate and blowing dust tended to dry the material very rapidly. As placed and tamped it was probably on the dry side of optimum. Compaction of drier than optimum backfill was desirable to prevent separation of backfill from the undisturbed soil as well as to prevent shrinkage away from the gages.

A few random soil density measurements indicated that the compacted fill was about 10 lb/cu ft more dense than the undisturbed soil. No measurements were made to determine relative compressibilities or moduli of undisturbed and compacted soil. Presence of soluble salts in the playa soil of Frenchman Flat made the low-density undisturbed material relatively hard and rigid as a result of cementation. The same factor probably caused the denser compacted fill to become somewhat more rigid as recementation took place, and it is possible that the compressibilities may have been more closely matched than the measured densities suggest. Tests performed for Project 3.8 5/ show that the shearing strength of compacted soil from Frenchman Flat increased by a factor of 5 to 8 as it dried from optimum water content to about 1/5 of optimum.

1.4 PRESENTATION OF RESULTS

Valid records were obtained for all Project 1.4a gages from Shots 9 and 10. Copies of the stress-time curves from these records are presented in Figs. A.1 through A.5 of Appendix A. Ground and slant ranges for each station shown on the plots are approximate true ranges to the center of each array and differ from true range to a specific gage by a maximum of 11 ft for ground ranges and 2 ft for slant ranges. True ranges diverge widely from the nominal ranges used in planning Project 1.4a because of the large error in ground zero for Shot 9 and the direction of the error for Shot 10 (Fig. 1.2).

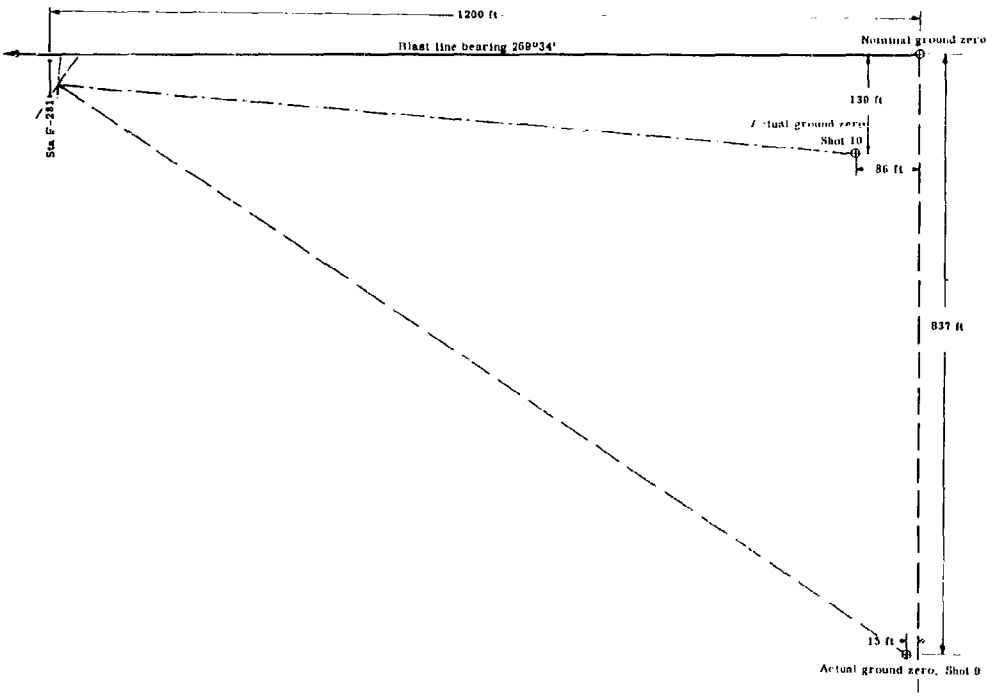

Fig. 1.2 Relative Positions, Nominal and True Ground Zeros - Shots 9 and 10

Pertinent data from these gages are presented in Tables 1.1 (Shot 9) and 1.2 (Shot 10). Incident air overpressures measured by Stanford Research Institute for Project 1.1b[7] are included, as are those measured at Station F-281 as a part of Project 1.4b.

Peak earth stresses and incident air overpressures are plotted as functions of ground range in Fig. 1.3 for Shot 9 and Fig. 1.4 for Shot 10. These curves emphasize coherence of the air overpressures

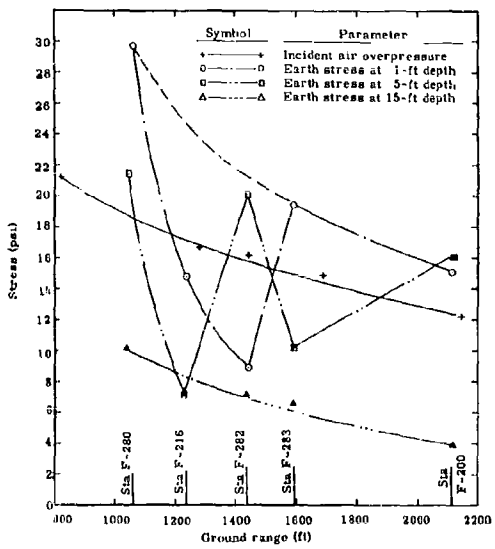

Fig. 1.3 Vertical Earth Stress - Shot 9

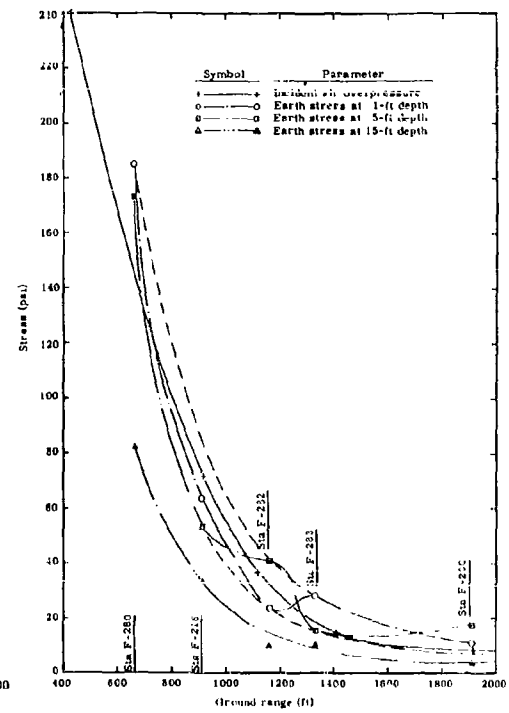

Fig. 1.4 Vertical Earth Stress - Shot 10

and of the earth stresses observed at the 15-ft gages. This coherence contrasts notably with the erratic character of some of the data from the 1- and 5-ft gages. Curves were drawn through all data points except where deviation from a smooth curve is small. Light dashed curves have been drawn for the 1-ft data from Shot 9 and the 1- and 5-ft data from Shot 10 to indicate a possible smooth curve which conforms in general to the shapes of the incident air overpressure and the 15-ft gage curves.

1.5 ANALYSIS AND DISCUSSION OF RESULTS

Data from the earth stress gages at different depths will be useful for determining variations of air-shock-induced stresses with increasing depth if it can be established that the major source of these stresses is the air overpressure incident at the adjacent ground surface. The criteria of adequacy of data are comparisons of arrival times, durations, and stress magnitudes as well as similarities of air overpressure-time and earth stress-time wave forms.

Direct comparison of air overpressure and earth stress data is valid only for comparable ground ranges. Consequently comparison of air and ground data for Shot 9 (Table 1.1) is limited to those from Stations F-281 (air only), F-282, and F-200; comparison of data from Station F-216 is of doubtful value because of the large difference in ground ranges to the air pressure and earth stress gages. Similarly air and ground data for Shot 10 (Table 1.2) are comparable at Stations F-216 and F-200 but are of doubtful comparability at Stations F-281 and F-282.

Comparison of data from three depths at a single station to establish that the indicated stresses are derived from a common source is not subject to these limitations because ground ranges to all gages at any station are nearly identical, differing appreciably only at Station F-280 for Shot 9.

The general pattern of arrival times in Tables 1.1 and 1.2 is roughly consistent with differences in ground range and gage depth. However, arrival times are not suitably precise for analysis of Shot 9 data in terms of comparative propagation velocities because the obliquity of the array to the air shock front resulted in a very complex system of propagation paths to the gages. Arrival times for earth stresses from Shot 10 at several stations show the apparent vertical component of propagation velocity between the 5- and 15-ft depths to be about 900 ft/sec. This velocity component is reasonable for the soil conditions at Frenchman Flat and the relative positions of the gages.

Rise times of the earth stresses from Shots 9 and 10 increase directly with depth and inversely with incident overpressure. Exceptions to these trends are usually in the direction of greater rise times and may be a consequence of errors in record interpretation. Rise times for the 1-ft gages are short and are probably characteristic of the incident air shock, having been affected to a negligible degree by traversing 1 ft of soil. The increase in rise time with depth is consistent with transmission of stress through a medium in which plastic deformation occurs. The increased rise time as a function of magnitude of incident air overpressure is consistent with, although somewhat greater than, the rise time of the air shock.

Postive-phase duration in the air shock wave for Shot 9 is greater than in the measured earth stress. There is also a general decrease of positive phase duration with depth. However, these data have the same lack of congruity as do arrival times. Positive-phase durations for Shot 10 follow a clearer pattern of increase with ground range and decrease with depth except for anomalies in data from the 5-ft gages at Stations F-280, F-216, and F-283, and in the air overpressure data from Station F-281. Durations of the precursor shock wave from Shot 10 follow a pattern roughly similar to that for positive-phase duration out to a ground range of about 1400 ft; beyond, it becomes difficult to distinguish the precursor from the main shock wave.

Peak stress-ground range curves for the 15-ft gages at all stations (Figs. 1.3 and 1.4) parallel the trend established by the data from the incident air shock wave. Data from the 1- and 5-ft gages were too erratic to define clearly any similar trends. Observation of earth stresses greater than the incident air overpressures has not been

TABLE 1.1 - Vertical Stress Data Shot 9 - Project 1.4a

Station number	Gage depth (ft)	Ground range (ft)	Slant range (ft)	Arrival time (sec)	Rise time (sec)	Peak stress (psi)	Pos phase duration (sec)	Max impulse intensity (psi-sec)
F-214	Surface	820	2558	1.097	-	21.2	0.703	-
F-280	1	1063	2643	1.1676	0.004	29.7	0.632	6.41
	5	1052	2641	1.1678	0.014	21.4	0.573	4.27
	15	1044	2640	1.1863	0.012	10.1	*	0.73
F-216	Surface	1281	2741	1.237	-	16.7	0.663	-
	1	1240	2722	1.2557	0.005	14.8	0.514	1.99
	5	1237	2721	1.2294	0.010	7.1	0.240	0.27
	15	1231	2718	1.2398	0.018	7.2	0.329	0.62
F-281	Surface	1444	2820	1.2988	0.006	16.2	0.660	-
F-282	1	1446	2822	1.3000	0.004	8.9	0.723	0.99
	5	1443	2820	1.3014	0.014	20.1	0.749	3.55
	15	1438	2818	1.3109	0.021	7.1	0.385	0.42
F-283	1	1592	2900	1.3613	0.004	19.5	0.639	3.18
	5	1590	2898	1.3615	0.015	10.2	0.539	1.40
	15	1587	2896	1.3626	0.021	6.6	0.432	0.65
F-217	Surface	1696	2958	1.400	-	13.9	0.740	-
F-200	Surface	2147	3238	1.613	-	11.2	0.767	-
	1	2120	3220	1.5967	0.14	15.1	0.723	4.07
	5	2119	3219	1.5833	0.034	16.1	0.560	3.20
	15	2115	3216	1.5840	0.048	3.8	0.581	0.50

*Indeterminate

TABLE 1.2 - Vertical Stress Data Shot 10 - Project 1.4a

Station number	Gage depth (ft)	Ground range (ft)	Slant range (ft)	Precursor shock: Arrival time (sec)	Precursor shock: Rise time (sec)	Precursor shock: Peak stress (psi)	Precursor shock: Duration (sec)	Main shock: Rise time (sec)	Main shock: Peak stress (psi)	Main shock: Pos phase duration (sec)	Main shock: Max impulse intensity (psi-sec)
F-215	Surface	430	678	0.0915	-	53	0.005	-	240	0.188	-
F-280	1	666	847	0.1371	0.006	40	0.019	0.009	165	0.188	8.86
	5	666	847	0.1377	0.015	31	0.021	0.024	173	0.241	10.11
	15	665	846	0.1485	0.022	17.2	0.026	0.018	82.8	0.133	2.51
F-216	Surface	920	1060	0.1915	-	16.9	0.06	-	71.5	0.269	-
	1	915	1055	0.1938	0.007	16.9	0.053	0.011	63.4	0.250	3.95
	5	915	1054	0.1946	0.012	7.9	0.053	0.023	53.3	0.254	2.93
	15	914	1054	0.2089	0.019	10.7	0.047	0.030	33.5	0.208	1.51
F-281	Surface	1121	1238	0.2482	0.021	16.4	0.091	0.025	36.7	0.313	-
F-282	1	1165	1277	0.2658	0.014	8.0	0.104	0.015	23.5	0.346	2.02
	5	1164	1277	0.2677	0.014	21.7	0.094	0.034	40.5	0.345	4.29
	15	1164	1277	0.2785	0.024	7.6	0.089	0.042	9.7	0.333	0.87
F-283	1	1334	1434	0.3231	0.007	16.2	0.149	0.021	28.1	0.408	4.07
	5	1334	1434	0.3272	0.015	10.4	0.155	0.016	15.5	0.422	2.55
	15	1334	1433	0.3370	0.021	7.8	0.163	0.025	10.4	0.295	1.21
F-217	Surface	1415	1509	0.3510	-	11.6	*	-	14.3	0.457	-
F-200	Surface	1918	1990	0.5960	-	7.7	*	-	8.1	0.671	-
	1	1914	1985	0.6000	0.013	8.5	0.034	0.012	10.9	0.593	3.52
	5	1914	1984	0.5845	0.031	10.8	0.043	0.017	17.6	0.531	5.017
	15	1914	1984	0.5809	-	*	*	-	3.4	0.387	0.44

*Indeterminate

uncommon in measurements of vertical earth stress at shallow depths. However, the erratic data from the shallower gages, which contrast strongly with the coherent results from those at 15 ft, render the high measured stresses less dependable than the data from the deep gages. If the indicated peak stresses for the 1-ft gages at Stations F-216 and F-282 are assumed to be low by 10-20 psi for both Shots 9 and 10, a smooth curve through the remaining data conforms roughly to that for the air pressure data, as illustrated by the light dashed curves of Figs. 1.3 and 1.4. A similar curve has been drawn for the 5-ft data from Shot 10 by assuming that the indicated peak stresses for that depth at Stations F-282 and F-200 are too great. Such excessively high stresses may be the result of overcompaction or excessive rigidity of the backfill. Conversely the low stresses indicated by the 1-ft data at these stations and by the 5-ft gage at Station F-216 may have been caused by high compressibility of the soil or shrinkage of the backfill. The minor scatter in the data from 15-ft gages suggests either that the compacted backfill was more uniformly placed over them or that its relatively small volume compared with that of the undisturbed earth above the gages obscured any irregularities introduced by the backfill.

Data on arrival times and peak stresses suggest that the air shock incident at the station is the source of the observed earth stresses. A stronger indication that air overpressure is the major source of the earth stress is given by superposition, with coincident arrival times, of the air overpressure curve from Station F-281 and the earth stress curves for the 1- and 5-ft gages at Station F-282 for Shot 10 (Fig. 1.5). The pattern registered by the earth stress gages is very similar to that registered by the air pressure gage except for discrepancies in magnitude. Stress-time curves of Figs. A.1 through A.5 also reveal similarity between curves for the gages of each group, and characteristic features of the earth stress curves are also found in air overpressure curves from stations too remote for direct comparison.

The 1-ft gages at Stations F-282 and F-200 indicated lower peak stresses than the 5-ft gages. This condition is a reversal of the trend at the other three stations and is contradicted by data from the 15-ft gages at all five stations. Rise times, arrival times, and positive-phase durations support the data as tabulated. Consequently this reversal in stress magnitudes must be considered real and probably the result of discrepancies in gage and backfill placement.

No essential difference in performance between older and newer gages is evident from the stress-time curves (Figs. A.2, A.4, and A.5). The 5-ft gage (old) did register considerably higher stresses than the 1-ft gage (new) at Station F-282, but a similar situation was observed at Station F-200 where both gages were new ones (Figs. 1.3 and 1.4). Data from the 15-ft gage (old) at Station F-283 deviated less from the curves of peak stress vs ground range than did data for new gages at two other stations.

There seems to be no clear-cut general evidence of ground-transmitted stress from remote ground incidence of the air shock. It is possible that the minor signal at about 1.5 sec in the record from the

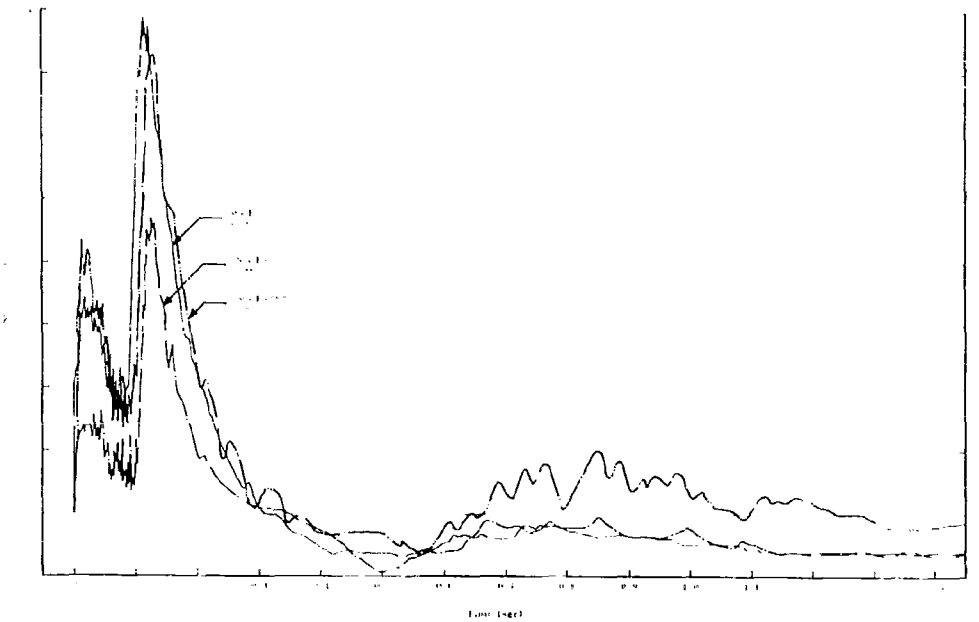

Fig. 1.5 Comparison of Air Overpressure and Vertical Earth Stress - Shot 10

15-ft gage at Station F-280 for Shot 9 (Fig. A.1) may represent refracted or reflected earth stress originating from incidence of the air shock in the vicinity of ground zero. This signal is repeated at the shallower gages with a finite time lag and decreased amplitude, suggesting transmission upward. A similar phenomenon appears in the records from Station F-283 for Shot 9 (Fig. A.2), but no correspondingly distinct evidence appears at other stations for this shot. Data from Shot 10 give no evidence of similar ground-transmitted signals, perhaps because they are obscured by perturbations introduced by the precursor shock. The secondary positive signals which appear about 0.5 sec after main shock arrivals from Shot 10 at Station F-280 (Fig. A.3) and at progressively greater intervals after main shock arrival at more remote stations are the result of a secondary shock in the air overpressure. The increasing time interval between the main and secondary events at increasing ground ranges is not consistent with arrival of a secondary event through the earth from the vicinity of ground zero.

The effect of gage depth on observed stresses has been investigated by plotting stress magnitude against depth. Data for this study were read at points judged to represent common events on the stress-time curves for a single station. Several comparable sets of data, including peak stresses, were derived from each group of gages. Such

events did not occur simultaneously at all depths but lagged at the deeper gages by intervals consistent with the corresponding lags in arrival time. Stress varied as an inverse function of depth, but the variation was not linear. Tests were made to determine whether attenuation could be better expressed by an equation of the form

$$P = P_1 \exp - \beta (d - d_1) \qquad (1.1)$$

or

$$P = P_1 (d / d_1)^{-a}, \qquad (1.2)$$

where P and P_1 are stresses which exist at depths d and d_1 and β and a are constants.

Semilogarithmic plots of all sets of comparable data for each station were made, and a linear relation for each set was sought. Data for all three depths fell very nearly on a straight line in some instances, and in general they could be roughly approximated by a straight line. Peak stress data usually approximated linearity about as well as did data representing other events in the stress-time curves. Therefore they were used as a basis for final analysis of data from each station. However, the results may be considered to represent the stress-depth relation of the whole stress transient rather than of peak stresses only.

Semilog and log-log plots of peak stress versus depth for Shot 9 are presented in Figs. 1.6 and 1.7. Corresponding plots for Shot 10 are presented as Figs. 1.8 and 1.9. The coherence and negligible scatter of data from the 15-ft gages for both shots indicated that they were the most trustworthy and should be given maximum weight. Conversely data from some of the 5-ft gages, particularly at Station F-282 and F-200, were ignored because of their anomalous nature. Data from Shot 9 for the 5-ft gages at Station F-216 and from Shot 10 for the 5-ft gages at Station F-280 were similarly ignored, the former being excessively low, the latter anomalously high. Data from the 1-ft gages were given full weight although this procedure was sometimes arbitrary and resulted in inconsistently flat slopes. The scarcity of data and the large proportion of intermediate data points that were ignored because of anomalies left little choice in the lines drawn to represent the stress-depth relation since only two points remained.

All data from several stations fell on, or nearly on, a straight line on one or the other of the graphs. Data from Station F-283 fit a straight line on the log-log plots for both Shots 9 and 10. Data from Station F-280 for Shot 9 and from Station F-216 for Shot 10 fell on a straight line on the semilog plot. Several other sets of data are reasonably well represented by straight lines. Analytic plots of data from Station F-282 for Shot 9 substantiate evidence from Fig. 1.2 that they were too irregular to yield a logical relation between stress and depth. Data from this station for Shot 10 are more reasonable, but again they are the most irregular of the five sets of information available.

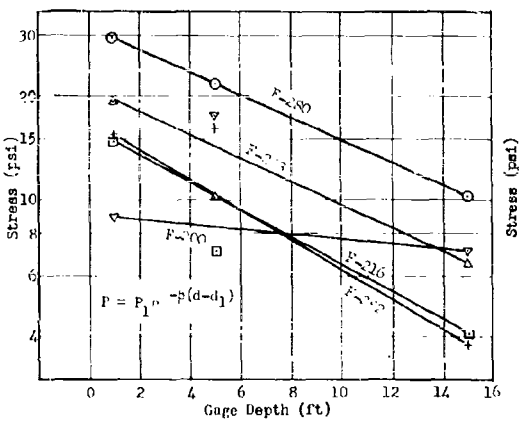

Fig. 1.6 Vertical Earth Stress Attenuation - Shot 9

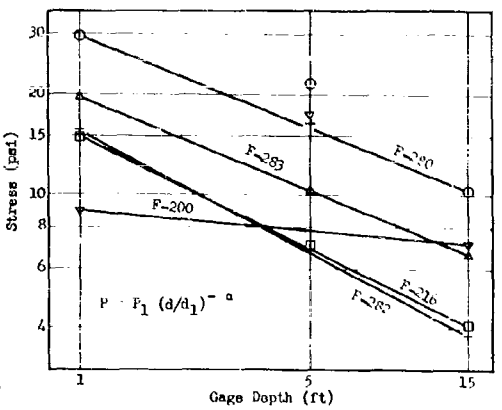

Fig. 1.7 Vertical Earth Stress Attenuation - Shot 9

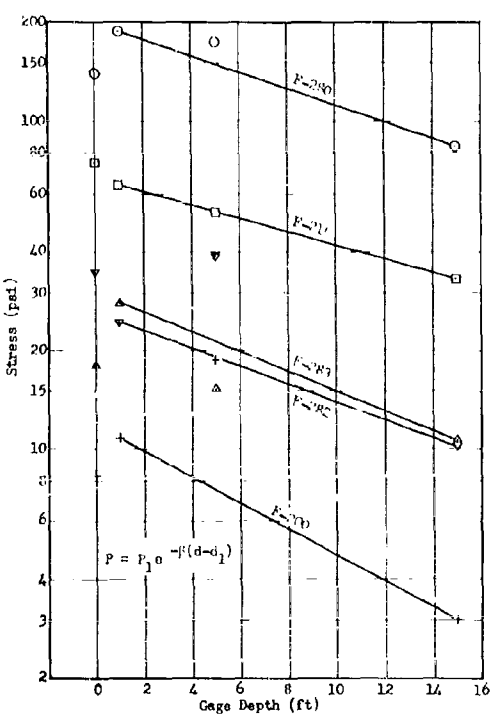

Fig. 1.8 Vertical Earth Stress Attenuation - Shot 10

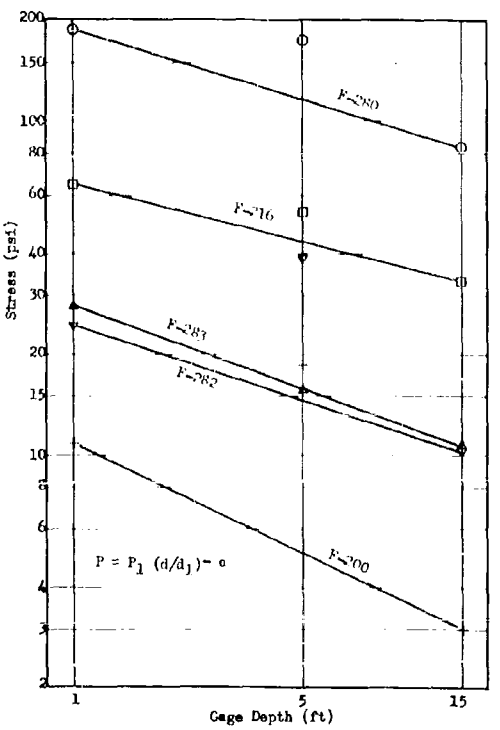

Fig. 1.9 Vertical Earth Stress Attenuation - Shot 10

TABLE 1.3 - Attenuation Factors

Station number	Peak Overpressure (psi)		$\beta(ft^{-1})$		a	
	Shot 9	Shot 10	Shot 9	Shot 10	Shot 9	Shot 10
F-280	19	140	0.077	0.058	0.39	0.30
F-216	17	72	0.052	0.046	0.26	0.14
F-282	16	33	0.016	0.063	0.09	0.30
F-283	15	19	0.077	0.071	0.40	0.36
F-200	12	8	0.098	0.083	0.49	0.45
		Mean	0.076	0.064	0.39	0.35

Attenuation factors for Shot 9 at Station F-282 and for Shot 10 at Station F-216 were unusually low and have been neglected in computing the mean values in Table 1.3. There is a definite suggestion of increasing values of β and a with decreasing peak incident overpressure (increasing ground range) for Shot 10; no trend of this sort is evident for Shot 9. This apparent inconsistency is, however, a consequence of the relative spread of peak overpressure represented. The peak overpressures incident at the last two stations for Shot 10 are commensurate with the full range of overpressures for Shot 9, and the attenuation factors for Shot 10 at these two stations are roughly comparable with those for Shot 9 at all stations. Scatter of the basic data and the somewhat arbritary procedures adopted in their analysis preclude use of the resulting factors for more than rough estimates based on average values or indication of trends. The analysis shows that attenuation of vertical earth stress as a function of depth may be expressed equally well by the equation

$$P = P_1 \exp \left[- 0.07 \, (d - d_1) \right] ,$$

or by the equation

$$P = P_1 \, (d / d_1)^{-0.37}$$

where depths are measured in feet. The factor β is probably accurate within $\pm$ 20 per cent and the exponent a within $\pm$ 25 per cent.

It is comforting to note the close agreement between the values of β and a as calculated from data for Shots 9 and 10. It is somewhat disturbing, however, that the fit of the data is no better for one form of analysis than for the other. Results of the two forms of analysis as shown in Figs. 1.6 through 1.9 certainly do not provide a basis for regarding one type of attenuation more favorably than the other. There are intuitive grounds for preferring the logarithmic type of

attenuation, but in the absence of stronger experimental evidence for differentiation between the logarithmic and inverse power types of attenuation, intuition hardly seems sufficient grounds for tipping the balance.

Integration of the stress-time curves gives curves of impulse intensity or impulse per square inch as a function of time for each gage at the five stations. Families of curves for each station are presented in Appendix A as Figs. A.6 through A.9. Integration was performed by summation of trapezoidal areas derived from original record data and entered on punched cards. IBM machines were used for the mathematical operations. No correction was made for zero drift or residual stresses which were evident in some of the recorded data. Errors from these sources do not become excessive during the first portion of the integrated curve and probably do not affect the maxima by more than 10 per cent. Beyond the maxima the integrated curves are strongly affected by the cumulative effect of residual stresses, but these latter portions of the curves are of little interest.

The curves of impulse intensity versus time and the peak impulse intensities listed in Tables 1.1 and 1.2 are presented for information only. No special significance is attached to them. Variation of impulse with depth is analogous to that of earth stress but more pronounced because both stress magnitude and positive-phase duration decrease with depth. Curves for Shot 10 show the effect of the precursor shock on impulse intensity. The precursor makes an appreciable contribution because of its duration even though it involves relatively low stresses. The rise in the precursor portion of the curve is not steep, but its contribution to the maximum impulse is equivalent to a high peak stress of a nonprecursor shock wave since such a peak would have a short duration compared with that of a well developed precursor shock.

1.6 CONCLUSIONS AND RECOMMENDATIONS

1. Observed earth stresses were induced by incidence of air shock at the ground surface in the vicinity of the gages.
2. The vertical component of earth stress so induced decreases with depth. The attenuation may be expressed equally well by the equations

$$P = P_1 \exp\left[-0.07\ (d - d_1)\right]$$

or

$$P = P_1\ (d / d_1)^{-0.37}\ ,$$

where P and P_1 are the peak stresses in psi at depths d and d_1 in ft. The constants in both equations are probably good within $\pm$ 25 per cent.
3. Stress magnitudes of the entire stress-time sequence are attenuated in essentially the same manner as peak stresses.

4. Data from Shot 10 suggest that rate of attenuation increases with decreasing incident overpressure. This increase appears to be roughly logarithmic, but the data are not adequate to be conclusive.
5. Rise time of earth stress increases and positive-phase duration decreases with depth. Arrival times lag with increasing depth.
6. Peak impulse intensities vary with depth analogously to, but more rapidly than, the stresses.

Unsolved instrumentation problems and incomplete knowledge of the phenomena of transmission of air-shock-induced earth stress cause the results of these measurements to be subject to controversy. The situation will not be clarified by more tests of the same sort because these uncertainties are fundamentally the result of instrumentation problems. The following recommendations are presented as a basis for removing these uncertainties:

1. Effects on measured stresses of instrument characteristics and of materials and methods of gage placement should be studied. Such studies should be made initially in soils typical of test sites but ultimately should include soils typical of target areas. The goal of these tests would be firm knowledge of the reliability of indicated stresses in terms of stresses in the undisturbed medium. Static loads and dynamic loads induced by high-explosives charges of moderate size would be used for these tests. Cognizance would have to be taken of possible adverse effects of the short time factor inherent in small charges since the goal of the instrumentation is use under conditions produced by very large charges.
2. Full-scale free-field measurements similar to those of Project 1.4a should be performed at Nevada Proving Ground after instrumentation problems have reached a reasonable solution. The full-scale experiment should include earth stress and earth strain measurements at several depths, including the maximum feasible for gage placement. Incident overpressure levels should range from 300 to 30 psi. Such tests should include means for observing the effects of degree of compaction of the soil on possible attenuation of stresses.

The ultimate purpose of free-field measurements of earth stress attenuation is correlation between free-field phenomena and structural response or damage to underground facilities. Such tests must consequently be closely related to experiments of the type performed by Project 3.8 of UPSHOT-KNOTHOLE, and the recommendations contained in the final report on Project 3.8 tests of buried structures are considered desirable.

Theoretical studies aimed specifically at better understanding of the transmission and dissipation of steep-fronted transient stresses in soils would aid materially in interpreting free-field data from stress measurements.

PART II

DERIVATION OF EARTH STRESS-STRAIN SYSTEMS AND GROUND-MOTION STUDIES

2.1 THEORETICAL BACKGROUND

Damage to an underground structure as a result of an explosion will be directly related to the transient force field or one of its definitive parameters, and will result from the response of the structure or its elements to one or more of these phenomena. Consequently the problem of predicting damage to underground structures is more complex than simply defining the force field produced in the earth by an explosion. In fact, it is resolved into problems of (1) defining the force field by free-field parameters, (2) interaction of the structure with the force field, and (3) determining consequent loading and structural response. Structural tests of the type undertaken by Project 3.8 of UPSHOT-KNOTHOLE[5] will give answers to the third problem and may help clarify the second. Specific cases involving a particular structure at a known distance from an explosion of known magnitude can be treated by direct measurement of structural response. However, this approach must necessarily be of limited scope, and the general approach would be far more useful if free-field phenomena were understood and could be correlated with structural response and damage.

Definition of the transient force field in the absence of a structure requires knowledge of the stress and strain tensors and the acceleration, velocity, or displacement of soil particles at various distances from the explosion and at various instants of time following detonation. Knowledge of all three parameters -- stress, strain, and motion -- is required because structures of different types will be affected more strongly by one or the other. Initially the feasibility of measuring these parameters in the free field must be established. Ultimately such measurements as are feasible must be made in the free earth and in the earth adjacent to structures and the results correlated with measured loading and response of structural elements.

2.1.1 Earth Stress Systems

Derivation of principal stresses and strains and of stress and strain tensors is treated in considerable detail in textbooks on theory

of elasticity and stress analysis.[8] These sources are usually concerned with static conditions, but the methods of analysis can be applied to instantaneous values of transient phenomena.

The stress tensor at a point in a medium is defined by the magnitude and directions of the normal and shear stresses* on any group of three orthogonal planes at the point. This definition requires measurement of at least six parameters, three normal stresses and three shear stresses. An equally valid and often more useful definition of the stress tensor is in terms of magnitudes and directions of the principal stresses; these are the normal stresses on the three principal planes, which are mutually orthogonal and so oriented that all shear stresses on them vanish. The normal and shear stresses on any plane through the common point of the principal planes can be derived from the principal stresses.

Techniques and procedures for measurements from which the stress tensor may be derived have been developed by the Corps of Engineers, US Army,[9] in the course of studies of stress distribution in earth-fill structures and externally loaded runway subgrades. In these studies loading was static, and either plane or radially symmetric stress could be assumed.

Measuring transient earth stresses introduces several problems not encountered in static measurements. Time dependence of loading and its consequences, such as altered plastic behavior of the soil and inertial effects, are the most evident differences. Instrumentation problems differ appreciably, although the relative difficulty of static and dynamic measurements may be debatable. Instruments suitable for measuring shear stresses in soils under static load do not appear to be practical for use under transient loads, and shear stresses must consequently be derived from measured normal stresses. Assumption of either a plane or radially symmetrical stress system is less likely to be permissible under dynamic than under static loading. Consequently measurements under dynamic conditions should be designed to furnish sufficient component data to permit analysis as a three-dimensional stress system.

Stress tensors derived from earth stress measurements during dynamic loading are customarily for dynamic stresses only and do not define the total stress condition because the tensor for static earth stress is ignored in both observation and analysis. This situation results principally from differences in instrumentation for the two classes of measurements. The static stress tensor may be determined from independent static measurements either before or after dynamic loading. The complete stress condition is then defined by the sum of the static and dynamic tensors.

Numerous measurements of earth pressure resulting from underground explosions have been made by means of oil-bag pressure gages.[10] The value of these measurements is uncertain because of their doubtful

* Normal stress on a plane is the force intensity or force per unit area acting perpendicular to the plane. The corresponding shear stress is the force intensity acting parallel to the plane.

relation to stresses and their critical dependence on such factors as the column of fluid in the gage hole. They proved useful, however, in providing a basis for correlation between phenomena produced by explosions of various magnitudes in several types of soil.[11]

The first tests of instrumentation to measure transient earth stress were made in conjunction with the underground high-explosive tests of Project 1 (9) of JANGLE.[12] At the invitation of Stanford Research Institute, Sandia Corporation installed instrumentation to measure four components of earth stress on Shots HE-1 and HE-3.[13] Carlson-Wiancko earth stress gages were placed 5 ft deep, oriented to respond to normal stresses on the vertical, radial, and two 45° vertical radial planes* at a specific ground range. The preliminary nature of these tests and the limited time and number of recording channels available prompted assumption of a radially symmetrical stress system. Results indicated that measuring techniques for static earth stress components could be adapted to dynamic stress measurements. Certain alterations of instrument design[3] were found necessary, however, to eliminate undesirable mechanical resonance (ringing) of the gages.

More recently Stanford Research Institute has measured earth stress components as a part of Project Mole.[10] Unidirectional stress gages were oriented within the earth to respond to normal stresses on the vertical, radial, and tangential planes as well as on several of the 45° bisecting planes of the orthogonal group. Check tests included duplication of gages at several orientations as well as variation of depth and placement conditions. Stress component data were insufficient for complete three-dimensional analysis, but considerable information pertinent to transient earth stress problems was obtained.

2.1.2 Earth Strain Systems

Knowledge of the strain tensor at a point in the earth is important to understanding underground damage phenomena. Correlation of stresses and strains as a function of time gives needed information concerning the elastoplastic behavior of soil under transient loading. Moreover, certain categories of structures are more sensitive to strain phenomena in the earth than to stress loading.

Static earth strain components have been measured as a part of stress-distribution studies of loaded runway subgrades.[2] Strain gages developed at the Ohio River Division Laboratory (ORDL) of the Corps of Engineers, US Army, have proved satisfactory for measurement of static earth strains. However, results obtained by Stanford Research Institute with ORDL strain gages subjected to transient loading during Phase I of Project Mole were not wholly satisfactory although more recent information has tempered initial adverse evaluation.[10]

---

* The direction of a plane is defined as the direction of the normal to it throughout this report, and consequently corresponds to the direction of the normal stress which acts on it.

Sandia Laboratory developed an earth strain gage, similar in principle to the ORDL gage, for Project 19.1h of TUMBLER-SNAPPER.[3] It was designed to have greater sensitivity, smaller maximum range, and density more closely approximating that of the soil; characteristics considered essential for proper response to transient earth strains. Tests of these Sandia gages during TUMBLER-SNAPPER showed them to be suitable in principle but indicated that transducers of greater electrical sturdiness were needed to survive the zero-time electrical transients associated with nuclear detonations.

2.1.3 Earth Accelerations

Measurement of one or more mutually orthogonal components of earth acceleration furnishes information from which motion of the earth and of the underground portions of some structures may be derived for correlation with damage. Integration of the acceleration-time data provides velocity-time data which may, in turn, be integrated to give displacement-time information. Accelerometers are the most suitable instruments for measurement of earth motion produced by nuclear explosions. Magnitudes and durations of velocities and displacements are so great that development of velocity or displacement gages has not been practicable.

Earth acceleration components resulting from air and underground nuclear and high-explosives bursts have been measured by numerous agencies.[14] Instrumentation techniques are well established, and data-handling procedures are comparatively simple. Patterns of recorded accelerations have not been generally simple or consistent. In fact, about the only consistently dependable feature of these measurements has been the strong initial downward acceleration that characterizes arrival of the air-shock-induced signal at the vertical-component accelerometer. Reasonable displacement information, derived from double integration of the acceleration-time records, has been reported in some instances. Displacement data so derived are, of course, subject to the errors inherent to integration and correction for variation of record zero, but data which permit such manipulation without obviously gross errors produce reasonable information.

2.2 PLAN OF THE EXPERIMENT

Loading of the earth by air shock from nuclear air bursts provides excellent conditions for testing and verifying both instrumentation and analytical procedures for determining earth stress tensors. Such loading induces a stress tensor characterized by a major principal stress directed very nearly vertically and considerably greater than the other two principal stresses. Magnitudes and durations of load-induced phenomena would be sufficient to minimize the effect of the finite size of an instrument array on the assumption that all measured stresses represent data at a single point within the earth. Neither of these conditions was realized in tests prior to UPSHOT-KNOTHOLE.

Project 1.4b was conceived, therefore, as a test of instrumentation and analysis for derivation of induced earth stress tensors.

Stress component measurements were to be adequate for complete determination of the tensor and were to be supplemented by tests of improved Sandia earth strain gages and routine measurements of acceleration components. Measurements were planned for three shots of UPSHOT-KNOTHOLE, and all instrumentation was to be placed at a depth of 5 ft except that for ground-baffle measurements of air overpressure at the surface.

Instrumentation for Shot 1 provided for observation at the anticipated 20-psi air overpressure ground range of six stress components, the corresponding six strain components, three acceleration components, and incident air overpressures (Fig. 2.1). Duplicate instrumentation was included to provide a reliability check on the measurements of two stress and one strain component. Tests planned for Shots 9 and 10 at Frenchman Flat were more comprehensive than for Shot 1 and included instrumentation for measuring nine stress, six strain, and three acceleration components in the earth as well as incident air overpressure (Fig. 2.2). Multiple instrumentation was planned for two stress and one strain component for reliability checks. Identity of nominal ground zeros for Shots 9 and 10 permitted use of a single instrument array for both tests, but differences in burst height and yield required the use of set ranges for anticipated peak incident overpressure of 20 psi for Shot 9 and 30 psi for Shot 10. Limited recording facilities necessitated measurement of only nine stress components, including one duplication, for Shot 9. However, all instrumentation for this project was operated during Shot 10.

2.3 INSTRUMENTATION

Instrumentation used for Project 1.4b measurements was generally similar to that used during previous tests at Nevada Proving Ground. The Carlson-Wiancko earth stress gages and Sandia earth strain gages were modified as described below. Wiancko accelerometers and Wiancko air pressure gages were of standard design. Each end instrument was connected through a buried 4-conductor shielded cable to an amplifier and recorder in a remote subterranean shelter.[9] All end instruments were calibrated on assigned recording channels, and recorder set ranges and calibration steps were adjusted prior to placement of the earth gages in the ground. Circuits of the gages at Station F-281 were checked between Shots 9 and 10, but recalibration for Shot 10 was not feasible except for the ground-baffle gages.

2.3.1 End Instruments

Modification of the Carlson-Wiancko earth stress gage[3] was a purely geometric one to improve its response aspect for earth stress. Prior to modification it had been proven an electrically and mechanically reliable instrument for dynamic measurements. However, the apparent compressibility of the unmodified gage was appreciably lower than that of its load-responsive flat cylindrical portion because of the transducer housing (Fig. 2.3 left). Studies of the effect of gage compressibility on the distribution of static stress in soil have shown that if this compressibility is low compared with that of the soil,

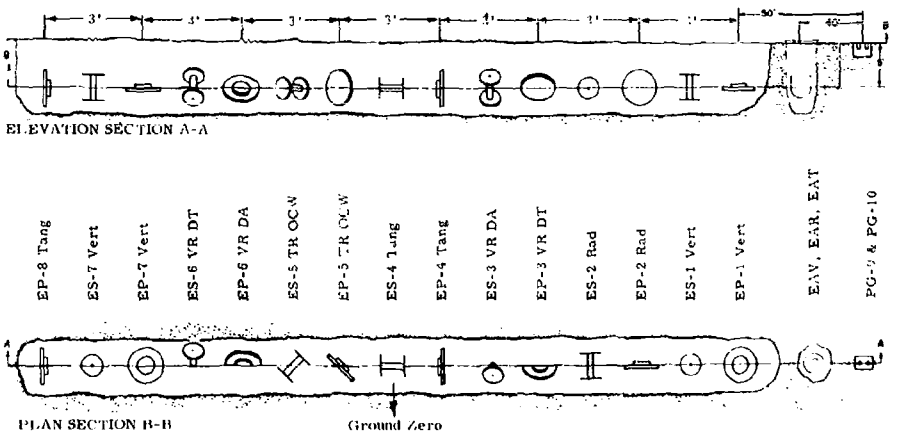

Fig. 2.1 Instrumentation, Area T-3

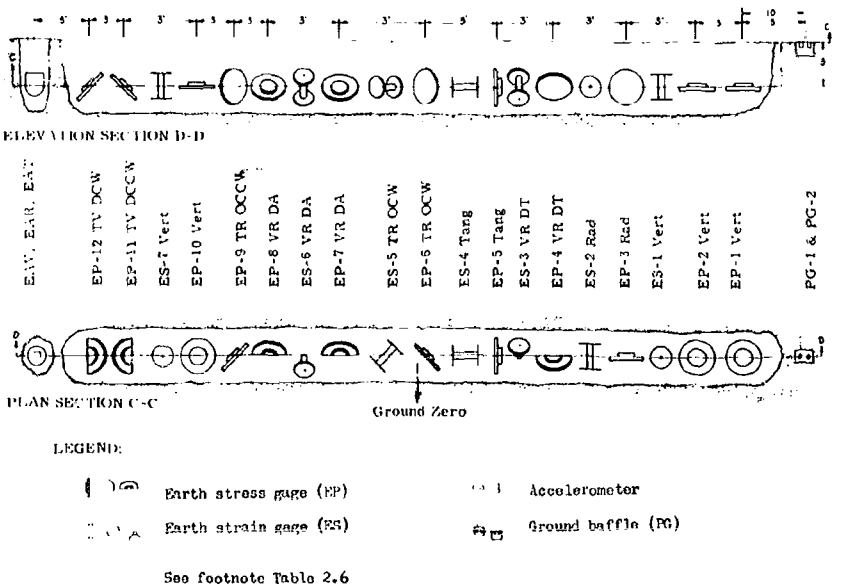

Fig. 2.2 Instrumentation, Frenchman Flat

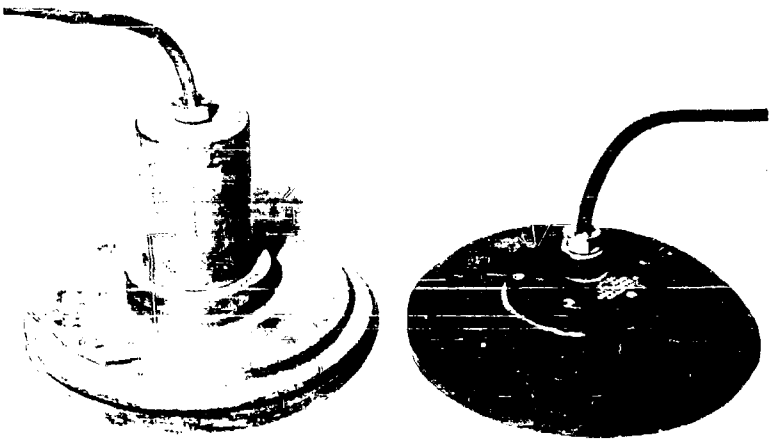

Fig. 2.3 Carlson-Wiancko Earth Stress Gages; Unmodified (left), Modified (right)

concentration of stress occurs at the gage. The relative significance of the ratio of instrument and soil compressibilities for transient dynamic versus static soil loads is not fully understood. It is probable that higher stress-strain ratios of the soil under dynamic loads brings the ratio of gage and soil compressibilities closer to the ideal. Nevertheless it was considered advisable to improve gage geometry as a means of improving stress response. Reorientation of the transducer element at the expense of a slight loss in sensitivity permitted reduction of the height of the transducer housing from 4.5 to 0.75 in. (Fig. 2.3, right). These gages were redesigned with the cooperation of Dr. Roy W. Carlson and the Wiancko Engineering Co.

Earth strain gages for Project 1.4b were similar to those initially tested in the earth mound during TUMBLER-SNAPPER.[3] Electrical weakness of the prototype gage was overcome by use of better transducer elements. Improved mechanical characteristics resulted from more rigid end plates and a longer sliding surface of reduced area. The gage length was increased to 5 in. to alleviate the crowded conditions in the transducer connector portion of the prototype gages. A better density match with the adjacent soil was obtained by use of different construction materials. The over-all density of the improved gages was about 100 lb/ft^3, approximately the density of the compacted Nevada Proving Ground soil in the backfill.

Accelerometers[14,15] were mounted in a case fabricated from a standard 10-in. bull plug.* The cover plate of the case provided means

* A bull plug is a standard pipe fitting for terminating a large-diameter pipeline.

for mounting three accelerometers with response axes mutually orthogonal (Fig. 2.4). The assembly was designed to have a density approximately equal to that of the surrounding soil.

Duplicate air pressure gages[15,16] were placed in a concrete block ground baffle adjacent to the earth gages to indicate the incident overpressure at the ground surface.

2.3.2 Placement of End Instruments

Instrumentation for Project 1.4b was installed at Station S-285 (Area T-3, 1450 ft from ground zero) for Shot 1 and at Station F-281 (Frenchman Flat, 1200 ft from nominal ground zero) for Shots 9 and 10. All instrumentation except the air overpressure gages in ground baffles was offset normally from the blast line at the specified stations. Earth stress and strain gages were placed in trenches 5 ft deep having a bottom width of about 2 ft and a width of about 7 feet at the surface. Stress gages were placed at 3-ft intervals, and strain gages were approximately midway between. Orientation was controlled within ±3 degrees, and gage elevations were held within ±0.1 ft of the prescribed direction and depth. Backfill materials and controls were similar to those described in Part I, Section 1.3. Details of gage layout and placement procedures are discussed in Appendix B.

The accelerometer assemblies were placed in holes 5 ft deep and 12 in. in diameter. Accelerometers were oriented with respect to nominal ground zero by means of the sight-tube jig described in Appendix B. The assembly was bonded to the soil, after orientation, by a Calseal grout and the hole backfilled with tamped soil.

2.4 RESULTS

Raw data from Project 1.4b comprised oscillograph and magnetic tape records of the various gage output signals as a function of time. These records were read and translated into stresses, strains, and accelerations by automatic computers and were furnished for analysis as tabulations of these parameters.

Reduced data were plotted as curves of the parameters versus time, and are appropriately grouped in Appendix C to assist in comparison of duplicate data or of corresponding parameters. Overlapping of curves plotted on a single axis system for comparison has been minimized by use of offset ordinate scales.

Specific information from the parameter-time curves has been tabulated. Data in the tables, as well as in the curves, are identified by the symbols used in Figs. 2.1 and 2.2 and defined in a footnote to Table 2.6. However, the tabular information is arranged to emphasize comparable information rather than in the order position in the gage arrays.

2.4.1 Shot 1

Data from all 19 information channels at Sta 3-285 for Shot 1 are presented in Tables 2.1 and 2.2 and in Figs. C.1 through C.7.

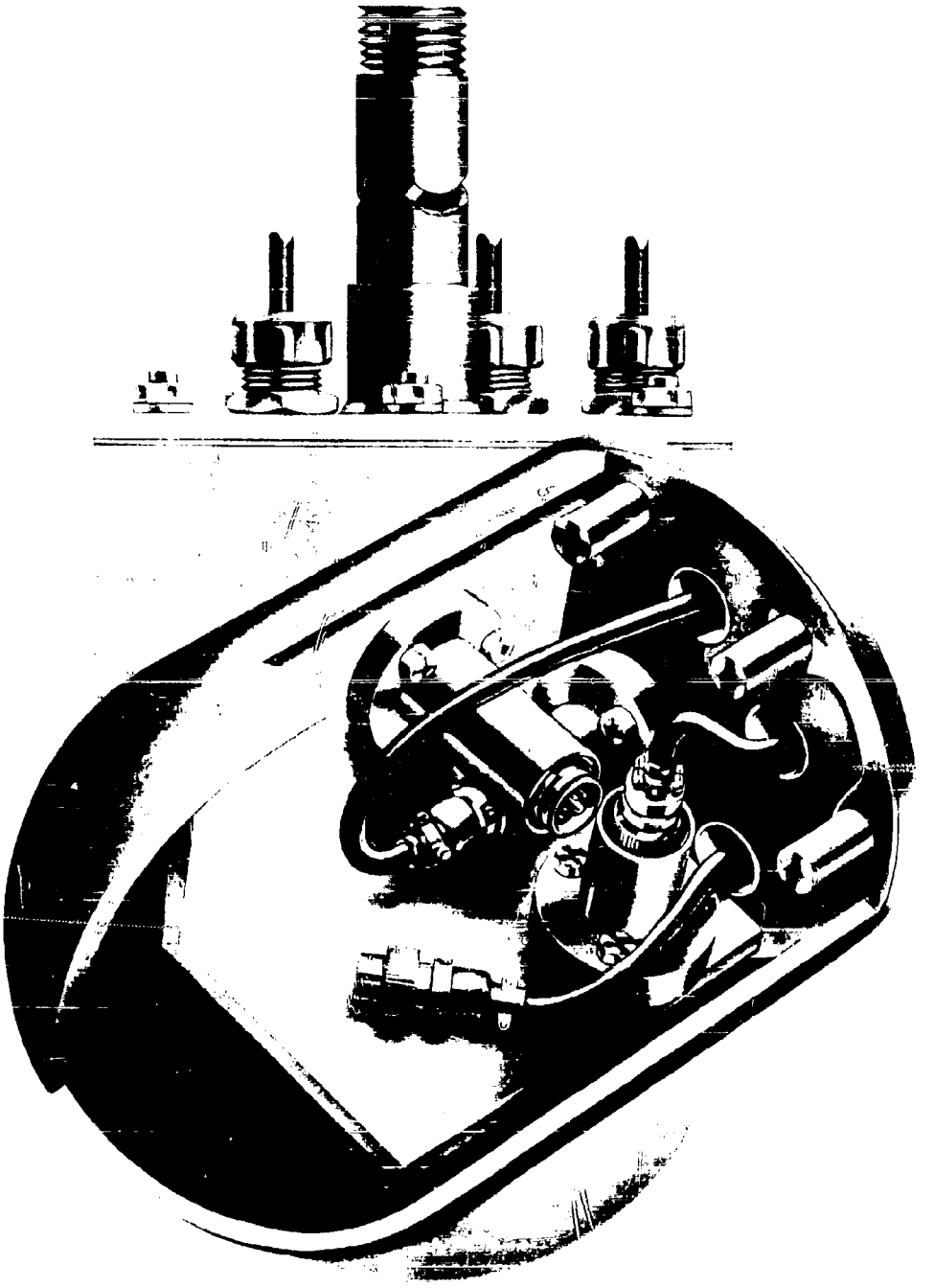

Fig. 2.4 Three-Component Accelerometer Mount

TABLE 2.1 - Free-Field Earth Stress and Strain Data - Shot 1
(Ground range: 1450 ft)

Gage*	Component†	Arrival time (sec)	Rise time (sec)	Peak stress (psi)	Peak strain (10^{-4} in./in.)	Positive phase duration (sec)
PG-9	Air pressure	0.2810	0.016	14.45	-	0.58
EP-1	Vert	0.2910	0.019	31.56	-	0.64
ES-1	Vert	0.2915	0.026	-	6.0	0.71
EP-7	Vert	0.2962	0.014	27.43	-	0.62
ES-7	Vert	0.2984	0.020	-	17.0	0.76
EP-2	Rad	0.2931	0.019	9.23	-	0.69
ES-2	Rad	0.2944	0.034	-	2.7	0.71
EP-3	VR DT	0.2943	0.020	17.29	-	0.63
ES-6	VR DT	0.2990	0.012	-	10.0	0.66
EP-4	Tang	0.2946	0.020	6.96	-	0.62
ES-4	Tang	0.2977	0.004	-	1.3	0.61
EP-8	Tang	0.2955	0.014	9.54	-	0.63
EP-5	TR	0.2953	0.007	8.98	-	0.64
ES-5	TR	0.2979	0.005	-	2.2	0.90
EP-6	VR DA	0.2966	0.012	18.30	-	0.66
ES-3	VR DA	0.2946	0.011	-	6.6	0.91

TABLE 2.2 - Free-Field Earth Acceleration Data - Shot 1
(Ground range: 1450 ft)

Gage*	Direction†	Arrival time (sec)	Peak acceleration (g)	Peak velocity (ft/sec)	Displacement Peak (in.)	Displacement Residual (in.)
EAV	up	0.2872	1.51	0.52	0.82	-
	down		2.31	0.50	0.56	0.24
EAR	in	0.2872	0.70	0.42	0.33	-
	out		1.37	0.26	0.30	0.05
EAT	CCW	0.2877	0.63	0.18	0.10	-
	CW		0.31	0.22	0.10	0.04

* See Fig. 2.1

† See footnote Table 2.6

2.4.2 Shot 9

Only 21 of the 24 end instruments at Sta F-281 were operational during Shot 9 because their recorder channels were assigned to other instrumentation. Consequently no data were obtained from earth stress gages EP-1, EP-8, and EP-11. Circuit failures external to the gages rendered two of the remaining channels inoperative, and no data were obtained from stress gage EP-5 and strain gage ES-5. Parameter-time curves for the 19 channels which yielded information are included in Figs. C.8 through C.14, and corresponding numerical data appear in Tables 2.3 and 2.4.

TABLE 2.3 - Free-Field Earth Stress and Strain Data - Shot 9
(Ground Range: 1430 ft)

Gage*	Component†	Arrival time (sec)	Rise time (sec)	Peak stress (psi)	Peak strain (10^{-4} in./in.)	Positive phase duration (sec)
PG-1	Air pressure	1.2987	0.006	15.89	-	0.64
PG-2	Air pressure	1.2989	0.006	16.41	-	0.68
EP-1	Vert	Not connected to recorder				
EP-2	Vert	1.2967	0.012	19.46	-	0.70
ES-1	Vert	1.3011	0.018	-	7.2	0.80
EP-10	Vert	1.2949	0.013	19.49	-	0.68
ES-7	Vert	1.2952	0.012	-	11.0	-
EP-3	Rad	1.3000	0.005	3.60	-	0.56
ES-2	Rad	1.3022	0.003	-	2.4	-
EP-4	VR DT	1.2911	0.014	8.64	-	0.92
ES-3	VR DT	1.2911	0.013	-	2.7	1.41
EP-5	Tang	Circuit failure				
ES-4	Tang	1.3000	0.002	-	0.6	-
EP-6	TR OCW	1.2983	0.005	3.42	-	0.49
ES-5	TR OCW	Circuit failure				
EP-7	VR DA	1.2964	0.006	11.86	-	0.54
ES-6	VR DA	1.2975	0.005	-	8.9	0.90
EP-8	VR DA	Not connected to recorder				
EP-9	TR OCCW	1.2959	0.005	4.64	-	0.75
EP-11	TV DCCW	Not connected to recorder				
EP-12	TV DCW	1.2955	0.007	4.49	-	0.59

* See Fig. 2.2

† See footnote Table 2.6

TABLE 2.4 - Free-Field Earth Acceleration Data - Shot 9
(Ground Range: 1430 ft)

Gage*	Direction†	Arrival time (sec)	Peak acceleration (g)	Peak velocity (ft/sec)	Displacement Peak (in.)	Displacement Residual (in.)
EAV	up	1.2935	0.70	0.11	0.00	-
	down		4.34	0.55	0.57	0.25
EAR	in	1.2933	0.80	0.14	0.22	0.02
	out		1.65	0.12	0.03	-
EAT	CCW	1.2935	0.57	0.08	0.08	-
	CW		0.46	0.06	0.05	0.05

* See Fig. 2.2

† See footnote Table 2.6

2.4.3 Shot 10

All 24 information channels at Sta F-281 were operating during Shot 10 and produced valid data, given in Figs. C.15 through C.22 and Tables 2.5 and 2.6.

Partition of the air overpressure from Shot 10 into a precursor shock and main shock as indicated in Fig. C.15 required subdivision of arrival times and peak values of the parameters (Tables 2.5 and 2.6). The positive phase durations in Table 2.5 represent the time interval from arrival of the precursor to crossover into the negative phase of the phenomenon.

2.5 DISCUSSION OF RESULTS

Analytical operations to which measured parameters must be subjected to evaluate their usefulness are defined in general terms in Section 2.2. Comparison of incident overpressure and vertical stress measurements will verify the source of observed earth parameters. A measure of reliability of the instrumentation as placed can be obtained from comparison of data from duplicate component gages. Comparisons of corresponding earth stress and strain components can indicate the elastoplastic behavior of the soil.

Derivation of principal stresses was feasible for only one of the three sets of data because insufficient component measurements were obtained from Shots 1 and 9. The principal stress can be approximated for Shot 1 if radial symmetry is assumed, but the angle of 34° between the blast line, which controlled orientation of the earth gages for Shot 9, and the line from true ground zero through the center of the array precludes computation of the principal stresses (Fig. 1.2).

TABLE 2.5 - Free-Field Earth Stress and Strain Data - Shot 10 (Ground Range: 1120 ft)

Gage*	Component†	Precursor Shock				Main Shock				Positive phase duration
		Arrival time	Rise time	Peak stress	Peak strain	Arrival time	Rise time	Peak stress	Peak strain	
		(sec)	(sec)	(psi)	(10^{-4} in./in.)	(sec)	(sec)	(psi)	(10^{-4} in./in.)	(sec)
PG-1	Air pressure	0.2485	0.014	17.16	-	0.3342	0.027	39.57	-	0.31
PG-2	Air pressure	0.2477	0.015	15.65	-	0.3392	0.022	33.60	-	0.31
EP-1	Vert	0.2517	0.011	10.51	-	0.3375	0.032	33.51	-	0.29
EP-2	Vert	0.2509	0.010	22.98	-	0.3364	0.034	56.12	-	0.36
ES-1	Vert	0.2514	0.025	-	5.8	0.3408	0.032	-	13.3	0.43
EP-10	Vert	0.2538	0.009	24.63	-	0.3417	0.025	59.92	-	0.33
ES-7	Vert	0.2548	0.007	-	9.0	0.3421	0.028	-	21.2	0.43
EP-3	Rad	0.2522	0.009	3.59	-	0.3362	0.033	4.31	-	0.35
ES-2	Rad	0.2642	0.019	-	0.4	0.3418	0.035	-	6.5	0.64
EP-4	VR DT	0.2535	0.006	5.76	-	0.3400	0.031	10.73	-	0.36
ES-3	VR DT	0.2556	0.020	-	2.1	0.3570	0.016	-	5.2	0.47
EP-5	Tang	0.2526	0.009	3.07	-	0.3469	0.022	6.00	-	0.51
ES-4	Tang	0.2681	0.019	-	1.0	0.3591	0.067	-	3.7	0.75
EP-6	TR OCW	0.2556	0.005	3.81	-	0.3450	0.020	4.60	-	0.44
ES-5	TR OCW	0.2557	0.011	-	3.2	0.3483	0.075	-	12.6	-
EP-7	VR DA	0.2514	0.010	13.16	-	0.3391	0.025	20.08	-	0.25
ES-6	VR DA	0.2414	0.020	-	3.5	0.3405	0.027	-	6.1	0.37
EP-8	VR DA	0.2535	0.007	12.14	-	0.3393	0.026	22.33	-	0.26
EP-9	TR OCCW	0.2532	0.008	5.61	-	0.3411	0.027	7.68	-	0.36
EP-11	TV DCCW	0.2537	0.009	7.85	-	0.3448	0.022	19.80	-	0.30
EP-12	TV DCW	0.2532	0.007	5.49	-	0.3369	0.030	13.25	-	0.35

* See Fig. 2.2.

† See footnote Table 2.6.

TABLE 2.6 - Free-Field Earth Acceleration Data - Shot 10 (Ground range: 1120 ft)

		Precursor Shock				Main Shock				
Gage*	Direction†	Arrival time (sec)	Peak accel (g)	Peak velocity (ft/sec)	Peak displacement (in.)	Arrival time (sec)	Peak accel (g)	Peak velocity (ft/sec)	Peak displacement (in.)	Residual displacement (in.)
EAV	up	0.2518	-	-	-	0.3397	1.56	0.44	0.17	-
	down		2.52	0.62	0.22		2.95	1.20	0.82	0.20
EAR	in	0.2514	0.64	0.12	0.07	0.3541	1.39	0.49	0.55	-
	out		-	-	-		0.45	0.36	0.33	0.03
EAT	CCW	0.2514	0.60	0.06	0.006	0.3472	0.74	0.23	0.22	-
	CW		-	-	-		0.78	0.23	0.41	0.04

* See Fig. 2.2

† Components:
Vert or V = vertical
Rad or R = radial
Tang or T = tangential
VR = 45° planes between V and R
TR = 45° planes between T and R
TV = 45° planes between T and V

Directions of oblique components:
DA = downward away from ground zero
DT = downward toward ground zero
OCW = outward clockwise
OCCW = outward counterclockwise
DCW = downward clockwise
DCCW = downward counterclockwise

Comparison of air overpressure and vertical earth stress for each shot shows that these parameters vary in essentially similar patterns, although the incident overpressures are lower. There is also close similarity in the time variations of most of the other stress and strain components, as evidenced by the curves in Appendix C. These facts establish conclusively that all but minor portions of the earth stresses and strains resulted directly from incidence of the air shock wave at the ground surface adjacent to the gage array.

2.5.1 Reliability of Duplicate Observations

Comparison of duplicate observations of the same parameters as a function of time is one measure of the ability of similar gages, placed under similar conditions and subject to similar loading histories, to register similar parameter-time patterns. Variations of individual gage characteristics are ignored since reliability of the gages under repeated static calibration and transient unloading tests is probably better than 97 per cent.

The effect of the presence of gages and of disturbance of a volume of soil inherent to installing them is also ignored. It is realized that under certain conditions these factors may so distort the stress distribution in the soil as to cause the gages to indicate stresses differing by factors as high as 2 or 3 from those in the undisturbed medium. However, magnitudes of these effects have been measured and computed for static loads only, and projection of the assumptions on which such estimates are based to distortion of transient stress distribution may be questionable in the present state of knowledge of dynamic behavior of soils.

The instrumentation plan for Shot 1 (Fig. 2.1) included three sets of duplicate observations: EP-1 and EP-7, spaced 18 ft apart, measured vertical earth stress; EP-4 and EP-8, 12 ft apart, measured tangential stress; and ES-1 and ES-7 measured vertical earth strain. Duplicate observations were limited for Shot 9 (Fig. 2.2) to vertical stress, EP-2 and EP-10, and vertical strain, ES-1 and ES-7. Data from Shot 10 (Fig. 2.2) provided more comparable observations: three vertical stresses, EP-1, EP-2, and EP-10; two 45° vertical-radial stresses, EP-7 and EP-8; and two vertical strains, ES-1 and ES-7.

The study of reliability is based on comparison of data samples from duplicate gages. Sample data were taken throughout the positive phase of measured stresses and strains and were chosen by identity of shape of minor features of the record trace pairs as well as by approximate simultaneity. Mean values of sample pairs and deviations of the data from these means were computed. Reproducibility of the data is expressed as the average of the deviations and as the range of deviations. Results of this study are presented in Table 2.7. The only features of the data in Table 2.7 which require clarification are the effects of residual strains, and the possibly anomalous stresses indicated by EP-1 for Shot 10.

TABLE 2.7 - Comparison of Duplicate Data

Shot	Parameter component	Number of observations	Deviation from mean (%)	
			Range	Average
1	Vert stress	72	4-42	16
	Tang stress	67	0-31	13
	Vert strain	66	10-54	35
9	Vert stress	20	10-22	6
	Vert strain	15	16-32	26
10	Vert stress*	13	25-91	55
	Vert stress†	13	0-18	8
	Vert-rad stress	14	1-36	14
	Vert strain	14	3-21	14

* Data from EP-1 and EP-2
† Data from EP-2 and EP-10 (see text)

Extension of the strain-time curves beyond the negative phase shows, in all cases, a residual strain, probably indicative of plastic deformation of the soil in the vicinity of the gages. It is also noted in Appendix B that placement of earth strain gages to respond to the vertical component involves considerable difficulty in attaining uniformity of compaction of the soil between the end plates while retaining the proper mechanical setting of the transducer. Consequently performance of two such gages in response to approximately equal transient loads may indicate a much wider spread of strains than would be anticipated from corresponding stress measurements. Adjustment of the vertical strain data from duplicate gages to equal residual strains makes the deviation of the data from the mean much less than it is for the raw data. ES-1 and ES-7 showed residual strains for Shot 1 of 0.4×10^{-4} and 5×10^{-4} in./in., and the peak strain after correction was twice as great for ES-7 as for ES-1. These data, as well as the consistent one-sidedness (ES-7 always greater) of the entire strain-time comparison, suggest a generally lower compacted density of the soil in the vicinity of ES-7 and particularly beneath the upper end plate of that gage. Residual strains from the vertical gages for Shots 9 and 10 were more comparable: they were about 5×10^{-4} in./in. for Shot 9 with a difference of only 10^{-4} in./in. between ES-1 and ES-7 and 8×10^{-4} in./in. for Shot 10 with approximately the same difference between readings.

Two of the vertical stress gages, EP-1 and EP-2, at Sta F-281 (Fig. 2.2) were separated by only 3 ft while the third, EP-10, was 24 ft from EP-2. However, EP-2 and EP-10 each showed stresses for Shot 10 which were about 1.7 times those indicated by EP-1 and 1.5 times

the incident air overpressure. The apparent anomaly of the EP-1 stress data makes evaluation of information from the three gages difficult since labeling the EP-1 data anomalous may be questioned in the light of close agreement with incident air overpressure. However, vertical earth stresses at 5 ft exceeded incident air overpressures by 20 to 100 per cent for Shots 1, 9, and 10 of this series and Shot 7 of TUMBLER-SNAPPER. There is some reason to expect that vertical earth stress might exceed incident overpressures by as much as 100 per cent because of differences in acoustic impedance across the air-earth boundary. Principal stresses computed from Shot 10 data have also given strong support to the higher values of vertical earth stress. Consequently data from EP-2 and EP-10 are considered the most reliable.

2.5.2 Stress-Strain Relations

Curves of corresponding components of earth stress as a function of strain give information concerning the elastic and plastic response of soils to loading. Plastic deformation of the soil under load implies time lags between application of a stress and stabilization of the corresponding strain. This lag is taken into account in measuring static stress-strain characteristics by retaining a series of incremental loads for periods that vary from minutes to days and result in approximately complete equilibrium for each increment. Transient loads produced in soil by shock obviously do not permit stabilization of plastic strain because they change too rapidly. Consequently, measured transient earth strains may be expected to lag corresponding measured stresses. These lags are random and small and usually not much greater than differences in arrival times. Average measured deviations of the strain lags from arrival time differences were about 1.3 msec. It is practicable to correlate major and minor features of corresponding stress- and strain-time curves such as peaks and some features of the precursor shocks, disregarding exact time correlations. This type of correlation is not dependable within the sharply rising front of the shock wave or in the smoother portion of a clean wave beyond the peak.

Uncertainty of correlation makes doubtful the true shape of the loading branch (initial loading to peak) of a stress-strain curve as well as some portions of the unloading branch (peak to negative phase). Consequently such regions of the curves are represented by straight lines. The curvature and minor loops of the precursor shock region (Shot 10) and the unloading branch represent spikes and troughs and are reasonably dependable. Fortunately most of the stress- and strain-time curves were sufficiently ragged beyond the peaks and throughout the precursor shock to facilitate correlation. The stress-strain curves form open hysteresis loops in which the enclosed areas between loading and unloading branches represent energy dissipated through deformation of the soil. The loops are not closed because plastic deformation resulted in residual strains. Arbitrary closure of the loops permits estimation of the energy dissipated through hysteresis.

Stress-strain curves were plotted for a single set of vertical component measurements for Shot 1 (Fig. 2.5) and for duplicate vertical

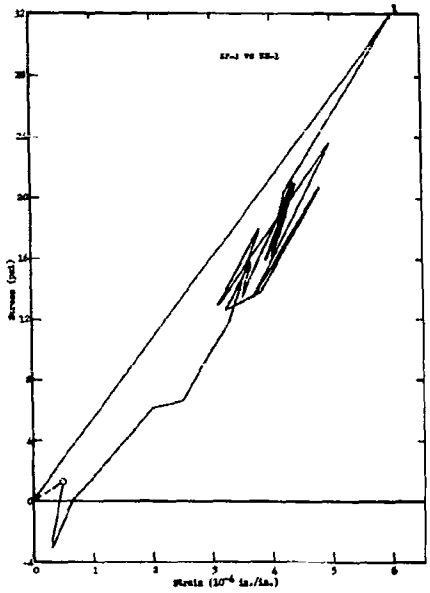

Fig. 2.5 Vertical Earth Stress vs Strain - Shot 1

and orthogonal vertical-radial oblique data for both Shots 9 and 10. All of these curves show hysteresis and residual strain (circled end points of solid curves). Equal areas within the several hysteresis loops as drawn do not represent similar stress-strain energies because of scaled differences. The product of the units in which the stresses and strains are presented (psi and 10^{-4} in./in.) result in energy density rather than energy, and areas within the hysteresis loops represent micro-foot-pounds per cubic foot.

The forms of the stress-strain curves from vertical components for Shot 9 (Fig. 2.6) are similar as are those from the two sets of vertical-radial oblique data (Figs. 2.7 and 2.8). These curves are considerably smoother than that from Shot 1 (Fig. 2.5) or those from Shot 10 because the incident shock and induced earth stresses were relatively clean waves.

Evidence of the precursor shock appears in the stress-strain curves from Shot 10 as a lobe and some ragged oscillations in the loading branches. The duplicate vertical component curves (Fig. 2.9) and the orthogonal oblique pair (Figs. 2.10 and 2.11) all exhibit generally similar shapes as they did for Shot 9.

Energy dissipation densities derived from the stress-strain curves are presented in Table 2.8 with corresponding values of peak stress, strain, and positive-phase durations. Duplicate vertical component data are identified by the pertinent stress gage symbol. The energy densities computed from the hysteresis curve areas are probably subject to errors of the order of 50 per cent. The principal sources of these errors are the uncertainties attached to gage placement and the assumption of linear stress-strain relationships between observed points on the curves. The latter assumption is especially questionable within the loading branch of the curve where consolidation or shearing of the soil during loading would require nonlinearity between stress and strain. Consideration of the stress-strain ratios at maximum stress and the computed energy densities suggests that for the duplicate vertical component data the error in curve areas may be more serious than in the measured parameters. Comparison of the stress-strain ratios for Shot 9 shows that that from EP-2 data is about 1.5 times that from EP-10, and the same comparison for Shot 10 gives the same factor. On the other hand, comparison of the corresponding energy densities for Shot 9 indicates a ratio of 0.58 and a ratio of 0.61 for similar comparison of Shot 10 energy densities, roughly the inverse of the stress-strain ratios.

However, the energy data give some reasonable indication of the expected dissipation caused by plastic deformation of the soil.

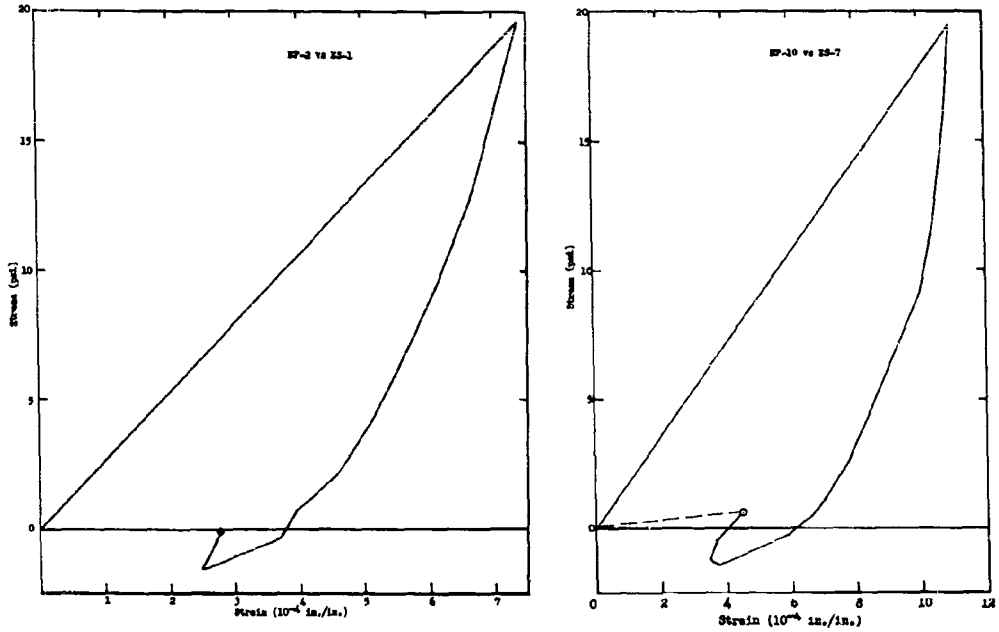

Fig. 2.6 Duplicate Vertical Earth Stress vs Strain - Shot 9

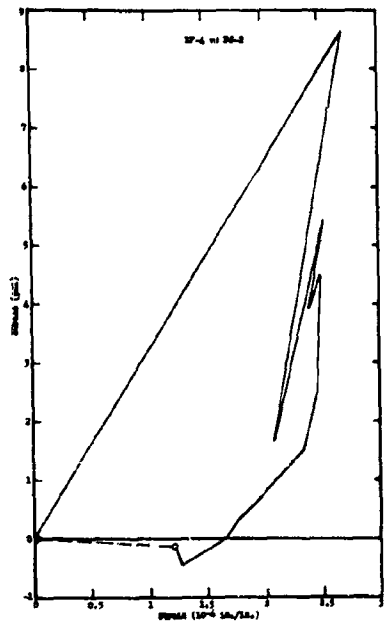

Fig. 2.7 Oblique Earth Stress vs Strain - Shot 9

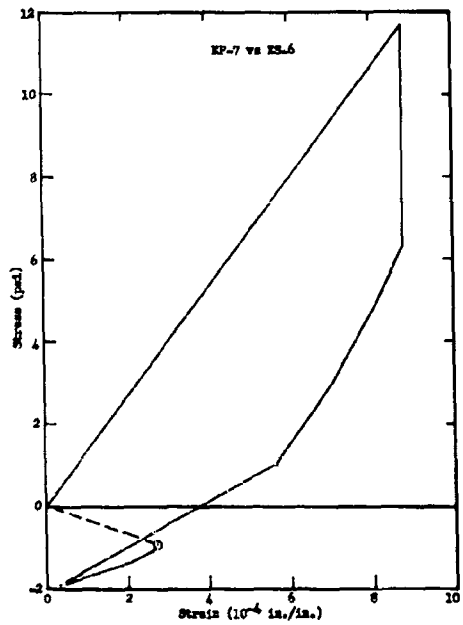

Fig. 2.8 Oblique Earth Stress vs Strain - Shot 9

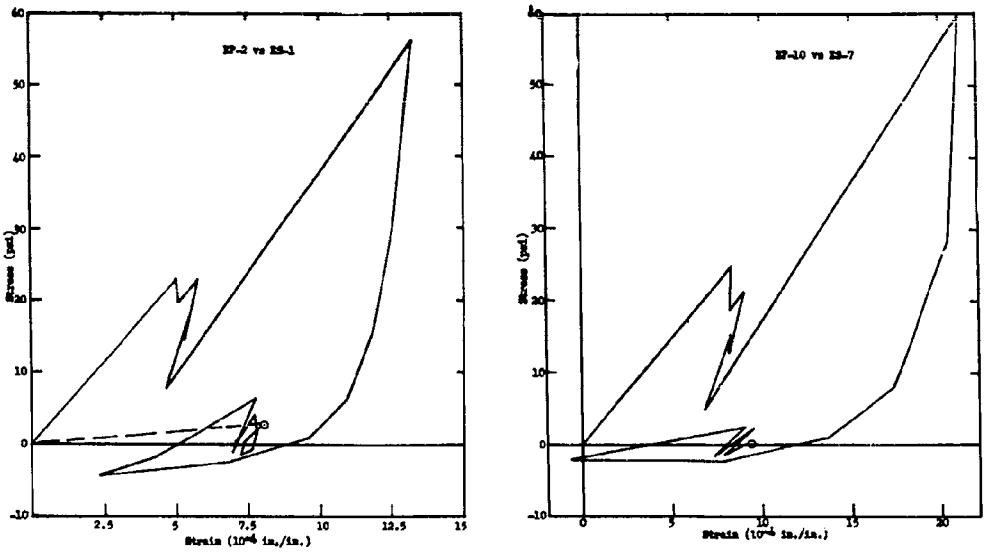

Fig. 2.9 Duplicate Vertical Earth Stress vs Strain - Shot 10

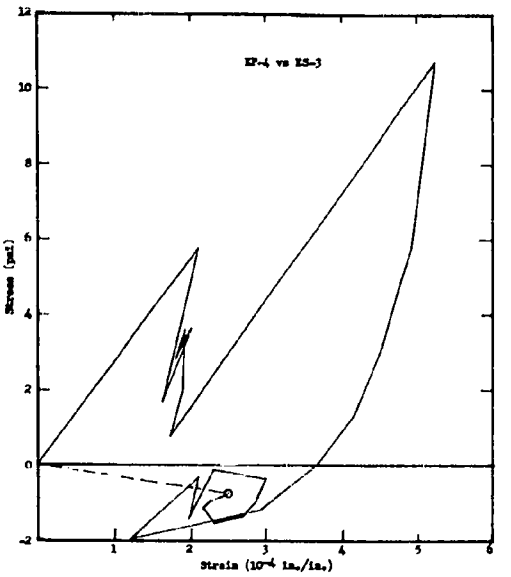

Fig. 2.10 Oblique Earth Stress vs Strain - Shot 10

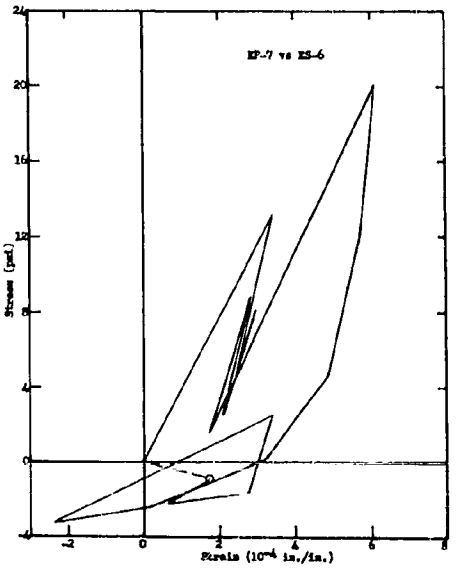

Fig. 2.11 Oblique Earth Stress vs Strain - Shot 10

TABLE 2.8 - Stress-Strain Energy Dissipation

Shot	Component	Peak stress (psi)	Peak strain (10^{-4} in./in.)	Pos phase duration (sec)	Density of energy dissipation (μft-lb/cu ft)
1	Vert	31.6	6.0	0.67	12
9	Vert (EP-2)	19.5	7.2	0.70	32
	Vert (EP-10)	19.5	11.0	0.68	55
	Vert-Rad (DT)	8.6	2.7	0.92	6.4
	Vert-Rad (DA)	11.9	8.9	0.50	28
10	Vert (EP-2)	56.1	13.3	0.43	200
	Vert (EP-10)	59.9	21.2	0.43	330
	Vert-Rad (DT)	10.7	5.2	0.42	16
	Vert-Rad (DA)	20.1	6.1	0.31	38

Stress- and strain-time curves for the components used in comparing stress-strain relations (Figs. C.2, C.9, C.10, C.16, and C.18) show that in all cases the transient loads resulted in permanent compressive strains (circled points on the curves) which are interpreted as plastic deformations. These appear to be a relatively large part of the peak strains. However, both peak and residual strains are small when the magnitudes of the corresponding applied loads are considered. Evidently the peak strains are relatively small because of lag in response of the soil to sudden loading. They probably represent mostly elastic strain, which is recovered before the end of the positive phase of the transient stress but to which is added throughout the positive phase plastic strain which is not recovered except as the low-intensity forces of the negative phase may affect it. Lag in deformation of the soil under the transient load accounts for the appreciably longer positive-phase durations for strain gage data.

2.5.3 Stress Tensors

Stress measurements from Shot 1 included components for determining the principal stresses if radial symmetry is assumed. The measured tangential earth stress is considered to be the minor principal stress, and data from the vertical, radial, and vertical-radial oblique stress gages are used as though a plane stress system existed. Computations are similar to those described in an earlier report.[13] Results of this analysis showed that the major principal stress was only slightly greater than the mean measured vertical stress, and that it was directed between 10° and 20° from the vertical. These results are based on data read from the stress-time curves at identical times and

include errors introduced by the finite spread of the gage array and asymmetry of the shock front.

Identity of the stress-time pattern, as indicated by similarity of peak or trough shape and approximate position in the stress-time sequence, defined comparable stresses for different components of the Shot 10 data. Data representing a single nominal instant actually involved a range of times as great as 10 msec over the group of stress-time curves. However, in view of the spread of the gage array and the evident correspondence of stress-time patterns for different gages, the assumption of simultaneity was considered reasonable, and mean values were used to define the nominal time for each set of stress data. Only events which could be readily identified on all or nearly all stress-time curves (Figs. C.15 through C.20) were considered suitable for analysis. Data representing 14 such events during the positive phase of stress-time curves for Shot 10 were compiled for use in computing principal stresses.

The theoretical background and procedure for deriving principal stresses for three-dimensional conditions are described in Appendix D; definitions of the stress system are included there to refresh the reader's memory of basic stress relations. The basis for these relations is the existence of stress equilibrium. Equilibrium is not necessarily a general condition during transient loading of a soil mass, but it probably does exist instantaneously throughout the load cycle and is probably more fully realized at maxima and minima than during intermediate portions of the cycle. Therefore the assumption that the derived data represent conditions when all stresses are in equilibrium is reasonable and permits analysis as described in Appendix D.

Data for stress analysis should satisfy tests for the static equilibrium of stresses. The simplest test for such equilibrium is equality of the sums of the normal stresses on all triads of mutually orthogonal planes through a point. This is only one index and is a necessary but not a sufficient condition for equilibrium. Its simplicity and the fact that it may be expected to yield indicative, if not conclusive, evidence of equilibrium recommended its use.

Observed stresses must accordingly satisfy the equality

$$\begin{aligned} \sigma_V + \sigma_R + \sigma_T &= \sigma_{VR\ DA} + \sigma_{VR\ DT} + \sigma_T \\ &= \sigma_{VT\ DCW} + \sigma_{VT\ DCCW} + \sigma_R \\ &= \sigma_{RT\ OCW} + \sigma_{RT\ OCCW} + \sigma_V, \end{aligned}$$

or the more practical forms in which common terms in each pair of sums are eliminated:

$$\left(\sigma_V + \sigma_R\right) - \left(\sigma_{VR\ DA} + \sigma_{VR\ DT}\right) = \Delta\sigma_{VR} \cong 0$$

$$\left(\sigma_V + \sigma_T\right) - \left(\sigma_{VT\ DCW} + \sigma_{VT\ DCCW}\right) = \Delta\sigma_{VT} \cong 0$$

$$\left(\sigma_R + \sigma_T\right) - \left(\sigma_{RT\ OCW} + \sigma_{RT\ OCCW}\right) = \Delta\sigma_{RT} \cong 0.$$

It is recognized that anticipated instrumentation errors might be dominant and yield inequalities. Random inequalities of magnitudes similar to those of anticipated errors could be regarded as indicative of approximate stress equilibrium. However, absence of randomness must be regarded as principally indicative of nonuniform stress distribution and can not distinguish between effects of gage placement and nonequilibrium of stresses.

Inequalities $\Delta\sigma_{VR}$, $\Delta\sigma_{VT}$, and $\Delta\sigma_{RT}$ are derived for each of the 14 sets of observations. These differences are normalized to give comparable values of $\Delta\sigma / \overline{\Sigma\sigma}$ where $\overline{\Sigma\sigma}$ represents the arithmetic mean of the summed stress pairs, i.e.,

$$\overline{\Sigma\sigma}_{VR} = \left[\frac{\sigma_V + \sigma_R + \sigma_{VR\ DA} + \sigma_{VR\ DT}}{2}\right],$$

which may be thought of as the sum of each stress pair if stress equilibrium were realized. The mean of these normalized differences and the probable deviation, e, of any observation from the mean are the criteria of equilibrium. Three sets of vertical stress data - EP-1 alone, the mean of EP-1, EP-2, and EP-10, and the mean of EP-2 and EP-10 data (of Fig. 2.2 and discussion of Shot 10 data in Section 2.5.1) - are used for the equilibrium tests.

Results of this analysis are tabulated (Table 2.9) to compare mean values of normalized inequalities with probable deviations of any of these observations from the mean. Differences in stress sums for EP-1 and σ_{RT} data are fairly random, those for the latter being nearly evenly balanced between positive and negative differences. Differences derived from averaged vertical stress observations are, on the contrary, very one-sided, sums including σ_V being greater in all instances.

TABLE 2.9 - Stress Equilibrium Check - Shot 10

Source of σ_V data	$\frac{\Delta\sigma_{VR}}{\overline{\Sigma\sigma}_{VR}}$ (%)	e_{VR} (%)	$\frac{\Delta\sigma_{VT}}{\overline{\Sigma\sigma}_{VT}}$ (%)	e_{VT} (%)	$\frac{\Delta\sigma_{RT}}{\overline{\Sigma\sigma}_{RT}}$ (%)	e_{RT} (%)
EP-1	34	21	30	32	6	18
(EP-1 + EP-2 + EP-10)/2	46	19	47	11	6	18
(EP-2 + EP-10)/2	68	19	70	7	6	18

Table 2.9 shows no conclusive evidence either for or against the stress equilibrium. On the basis of the mean of the normalized difference, which is sensitive to randomness of sign, data from EP-1 show departures from equilibrium of the order of the anticipated instrumentation error. Probable deviations from the mean normalized differences are insensitive to sign, and the third set of data is considerably better than those for EP-1 and somewhat better than mean data from all three gages. But although these values indicate deviations well within the range of anticipated instrumentation error, they can not distinguish the equilibrium criterion from either instrumentation error or distorted stress distribution in the vicinity of instrumentation. Perturbation of stress distribution caused by recompaction of the soil mass during gage installation or the presence of gages within the soil may result in relatively large one-sided deviations of stress sums without interfering with instantaneous stress equilibrium.

Principal stresses representative of the stress tensor in the earth at 14 instants after arrival of the air shock above the gage array were computed despite the indeterminate results of the stress equilibrium check. These computations, outlined in Appendix D, include derivation of (1) shear stresses in the V-, R-, and T-planes, (2) major, intermediate, and minor principal stresses, (3) angles between each principal stress and the three coordinate axes, and (4) maximum shear stress. The first two were performed for three sets of vertical stress data: EP-1 data only; the mean of EP-1, EP-2, and EP-10 data; and the mean of EP-2 and EP-10 data. The remaining computations were made using only the mean data from EP-2 and EP-10.

Shear stresses on the vertical, radial, and tangential planes, derived from measured normal stresses as described in Appendix D, are shown as functions of time in Fig. 2.12. Stress equilibrium (assumed if not rigorously proven) requires the equalities $\tau_{VR} = \tau_{RV}$, $\tau_{VT} = \tau_{TV}$, and $\tau_{RT} = \tau_{TR}$. These shear stresses and the normal stresses, σ_V, σ_R, and σ_T appear in the cubic equation (Eq D.5) from which the principal stresses are derived (Appendix D).

Analysis based on σ_V data from EP-1 resulted in imaginary roots of the cubic equation at one or more points near the end of the positive phase and in negative stresses (tensions) during the precursor portion of the minor principal stress as great as 85 per cent of the maximum compressive stress in that part of the shock wave. Shear stresses in the vertical plane were large, having an average value nearly equal to σ_V. Derived angles between the major principal stress and the axes were erratic, and except in the immediate vicinity of the main shock peak, showed the stress to be inclined almost 60° to the vertical axis. The major principal stress differed radically from σ_V in magnitude as well as direction. Consequently if the reasoning which recommended performance of this experiment in connection with an air burst weapon is sound, either EP-1 data lead to false results - a likely conclusion in view of the tensions, imaginary roots, high shear stresses in the V-plane, and departure of the major principal stress from vertical - or induced stresses are propagated through the earth near the surface at a relatively steep angle despite generation at the surface.

Choice between data representing means for the three vertical gages and those derived from EP-2 and EP-10 alone is not so obvious as was elimination of EP-1 data. Average shear stresses in the vertical plane were somewhat smaller for the 2-gage mean data, and probable deviation of the normalized differences of stress sums in Table 2.6 was also more favorable for them. Directions of the major principal stresses derived from the two sets of data differed by only about 5° although the 3-gage data gave the larger inclination to the vertical axis. Therefore a conclusive choice is not possible, but the 2-gage mean data seem the better.

Curves for principal stresses derived from mean data from EP-2 and EP-10 as a function of time (Figs. 2.13, 2.14, and 2.15) are self-explanatory. Similar curves for the angle between stresses and coordinate axes in the same figures need discussion only from the standpoint that orientation of the two lesser principal stresses is less precise. Deriving the angles in the latter cases involves operations with large differences of small numbers, and results are much more sensitive to inaccuracies in derived stresses. However, these stresses and their directions are relatively insignificant because the major principal stress is greater than either by a factor of at least 8. The intermediate and minor principal stresses are thus essentially of only academic interest under the conditions produced by air shock loading on the earth.

It is of interest to note the differences in general direction of the two lesser principal stresses during the precursor and main shock phases of loading. During the precursor shock the intermediate stress is directed nearly midway between the radial and tangential axes; during the main shock it is very nearly parallel to the tangential axis. The minor principal stress shows a similar trend: nearly parallel to the radial axis during the main shock, between the radial and tangential axes during the precursor shock. Inaccuracies of computations for precursor data are sufficient to account for the erratic oscillation of the angles for σ_2 and σ_3, but it seems probable that trends described are real if not strongly defined.

Shear stresses derived from principal stresses in accordance with the equation

$$\tau_{max} = \frac{(\sigma_1 - \sigma_3)}{2}$$

are maxima and act on the plane which bisects the angle between major and minor principal planes. The maximum shear stress, τ_{max}, is shown as a function of time in Fig. 2.16.

Magnitudes of the maximum shear stress are several times greater than those of the shears derived from measured normal stresses (Fig 2.12). This situation is contrary to that between the major principal stress and the measured normal stress on the V-plane. However, consideration of the directions of the planes in which the derived shears act show them to be more nearly coincident with the principal planes - in which shears vanish - than is the plane of maximum shear.

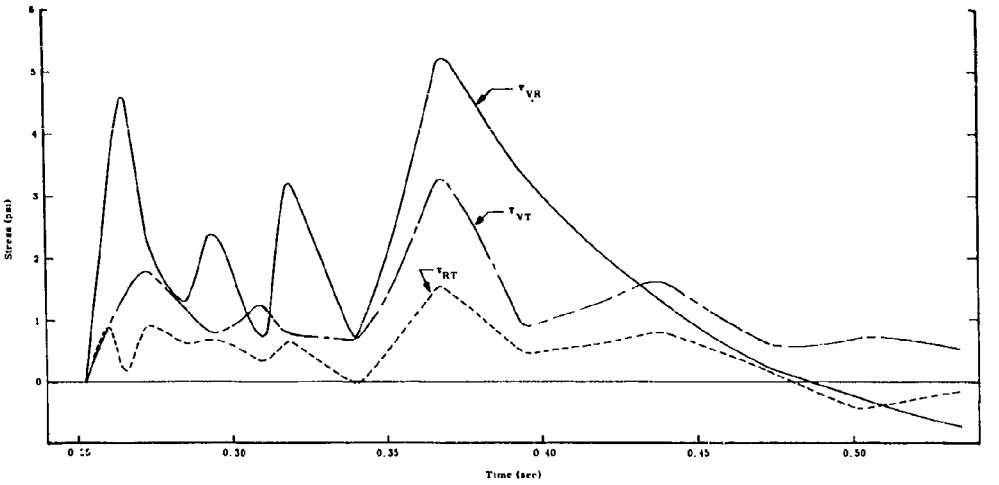

Fig. 2.12 Shear Stress vs Time - Shot 10

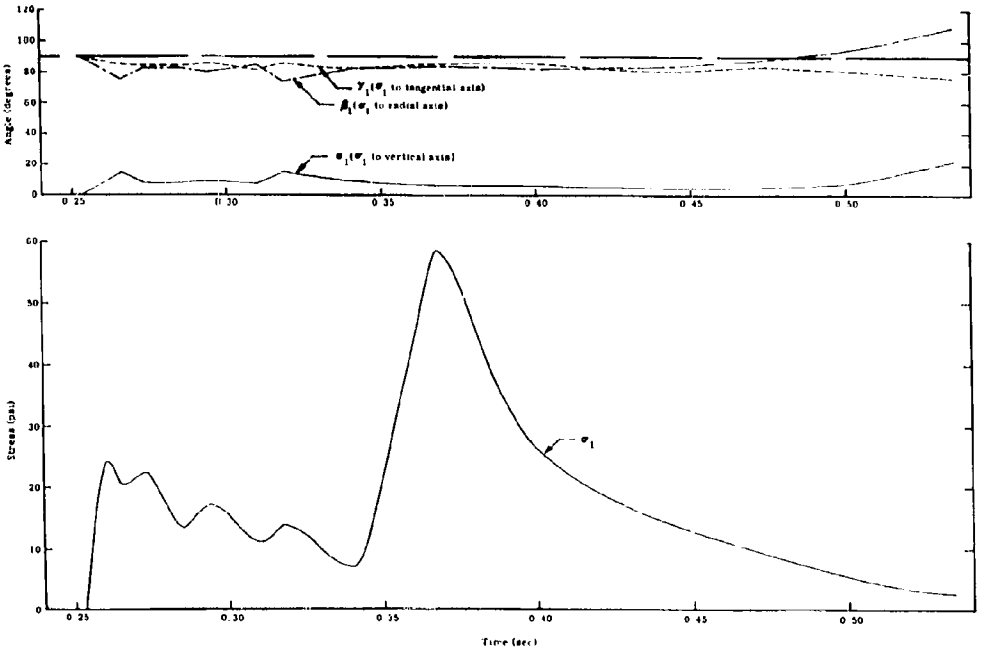

Fig. 2.13 Major Principal Stress and Orientation vs Time - Shot 10

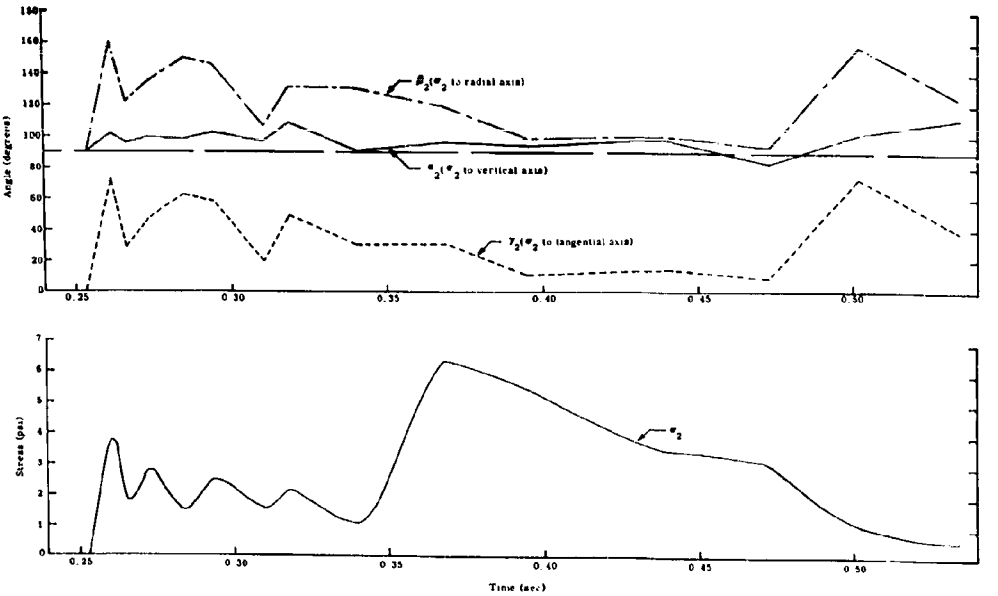

Fig. 2.14 Intermediate Principal Stress and Orientation vs Time - Shot 10

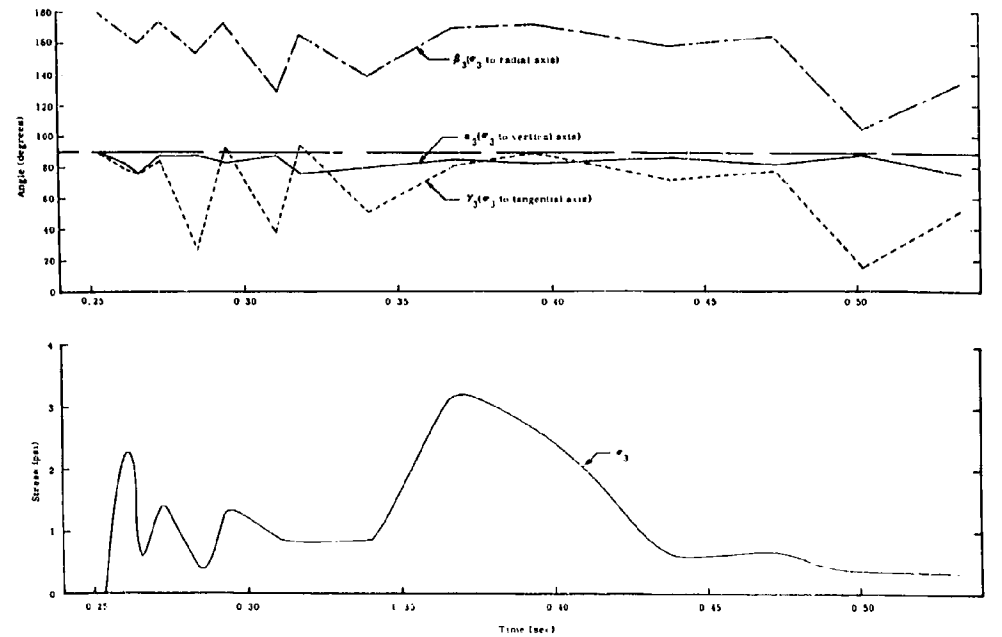

Fig. 2.15 Minor Principal Stress and Orientation vs Time - Shot 10

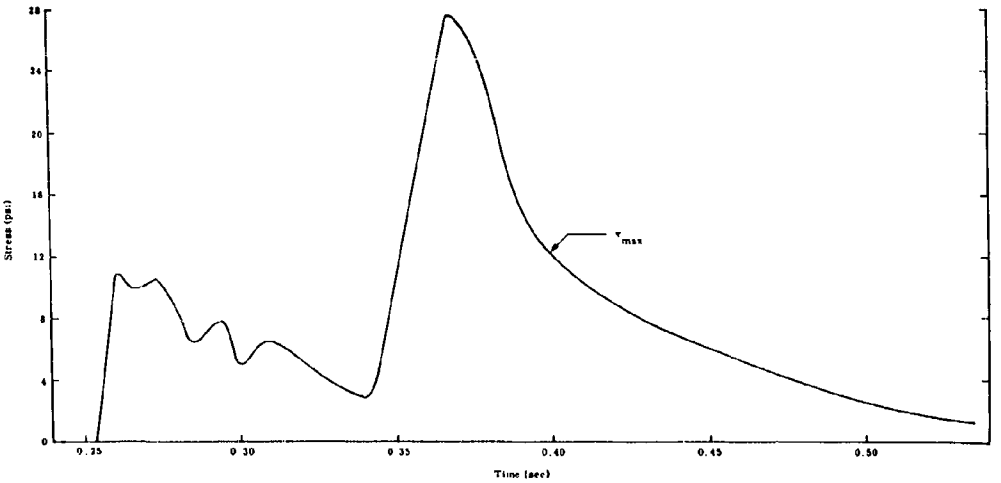

Fig. 2.16 Maximum Shear Stress vs Time - Shot 10

2.5.4 Ground Motion

Particle velocity and displacement may be derived from measured particle acceleration by integration with respect to time. A velocity-time curve resulting from integration of acceleration-time data is subject to the restriction that the velocity must ultimately become zero. Normal field data frequently require some adjustment to satisfy the final zero velocity requirement.

Displacement-time curves are derived from the corrected velocity-time data by a similar integration process. Adjustment of displacements is less clear-cut than for velocities. Frequently no adjustment is necessary to provide a displacement-time curve which appears reasonable. However, it is not always feasible to make the proper velocity correction from inspection of that curve only, and consideration of first approximation curves of both velocity and displacement may be necessary for logical correction. The simplest correction is an assumed zero shift of the acceleration curve which will have the effect of linear increase or decrease in velocity, and results in a parabolic correction of the displacement curve. Correction may also be made by assuming a linear zero drift in the acceleration data which results in a parabolic correction in the velocity curve and a third-power correction in the displacement curve. Combinations of these corrections may be helpful, but usually the less complex corrections yield reasonable results provided the original data are reliable and the time interval is short.

Integration and adjustment of the data may be used with reasonable success for data from phenomena of a few seconds duration. However, durations of the order of tens of seconds are difficult to handle because errors are cumulative and real basic information may become hopelessly lost in the effects of minor correction errors.

Free-field measurements of vertical, radial, and tangential components of earth acceleration were made during Shots 1, 9, and 10. Parameter-time curves of acceleration, velocity, and displacement for Shot 1 are presented in Figs. C.5 - C.7; for Shot 9 in Figs. C.12 - C.14; and for Shot 10 in Figs. C.21 - C.23. Arrows on parameter axes of these curves indicate direction of motion.

Maximum accelerations, velocities, and displacements and residual displacements for each component are compiled in Tables 2.2, 2.4, and 2.6. Residual displacements are those at which each displacement is assumed to remain constant since they occur at times after accelerations and velocities are assumed to become vanishingly small.

Acceleration-time curves for Shots 1 and 9 show no appreciable departures from zero following crossover after the positive phase of the stress data. However, sufficient deviation from zero appears in several of the velocity-time curves beyond the positive stress phase to suggest integration to a later time.

The period during which the velocities are assumed to be significant are represented by the solid curves for both velocity and displacement; the dashed portions indicate continuing trends resulting from long-period minor departures of the acceleration curves from zero. These departures emphasize one of the difficulties of properly adjusting the acceleration zero to give reasonable velocity data.

Integration of acceleration data from Shot 10 measurements has been carried well beyond the start of the negative phase because a relatively strong secondary signal was recorded at about 0.9 sec. This signal corresponds to the strong secondary events noted at about the same time on all stress and strain measurements, probably a secondary shock in the air wave as suggested weakly by the air overpressure records (Fig. C.15). Extension of integration to times corresponding to the negative-phase portion of the stress data has probably had little effect on the vertical and radial velocity and displacement curves, all of which could have been terminated at about 0.8 sec and approximately zero velocity without altering the early portions of the curves. Similar correction to zero velocity either at the positive phase or later in the negative phase was not feasible for tangential accelerometer data, partly because signal strengths were 20 per cent or less of set range after about 0.6 sec.

Arrival of the main shock following the precursor shock at about 0.35 sec is evident in all three acceleration components for Shot 10 and to a lesser degree in the derived velocity and displacement data. There is a suggestion of a similar occurrence in the Shot 1 data shortly before 0.6 sec, but this effect is not so well corroborated by the stress and strain curves for Shot 1 as by those for Shot 10.

Peak and residual displacements seem reasonable with the possible exception of that shown for the upward peak of EAV displacement (0.82 in.) for Shot 1. This displacement, greater than the peak downward displacement, may have resulted from incorrect adjustment of the acceleration curve. The adjustments, which were of the order of 0.03 to 0.005 g, were very small but often affected radically later parts of the displacement curves.

The most optimistic attempts at correlation between displacement-time curves and the earth strain curves yielded only one case of apparently similar parameter-time behavior. The vertical displacement curve (Fig. C.21) and the vertical strain curves (ES-1 and ES-7) for Shot 10 (Figs. C.16 and C.18) are of generally comparable shape. Perhaps to expect correlation of these two parameters, one measured by gages which are very sensitive to placement conditions, the other derived by a double integration process which involved arbitrary zero adjustments, is asking too much of the data.

Other considerations must enter into speculation on the relation between strains and displacements, however. Strains are purely local parameters and can actually represent local displacement only if the variation of strains over a volume of the medium is known. Thus the instantaneous vertical displacement at a point within the soil represents the integral of the instantaneous strains induced within a column of soil extending from the point of measurement to some depth below which loads and strains become vanishingly small. This displacement will be independent of the strains above the measurement point at the instant under consideration and will, in fact, depend on conditions of load and strain in the overlying material only as these conditions affect and have affected transmittal of load. Correlation of displacement with strain would therefore appear to require knowledge not only of the strain at the measuring point but at a sufficient number of points to establish strain as a function of distance and the locus of vanishingly small strains.

2.6 CONCLUSION

Conclusions are divided into those dealing with stress-strain characteristics of transiently loaded soil, derivation of the stress tensor, and derivation of velocity and displacement information from measured accelerations.

1. It is feasible to install existing stress and strain instruments in the earth at depths as great as 15 ft, except in unusual soil conditions.

2. Reproducibility of measurements of earth stress and strain components, using the methods outlined (as expressed by the average deviation from the mean of duplicate measurements), is better than 16 per cent for stress gages and about 25 per cent for earth strain gages.

3. Stress-strain data from component measurements in the earth provide a basis for estimating energy dissipation caused by plastic deformation of the soil under transient loading. This rate of energy loss was computed to be of the order of 30 μft-lb/cu ft at the 5 ft depth when the vertical stress is of the order of 20 to 30 psi and 300 μft-lb/cu ft when the vertical stress is about 60 psi.

4. Earth stress tensors and, by inference, earth strain tensors in the form of principal stresses and principal strains, may be derived from measurements of properly oriented components of the transient earth stresses and earth strains produced by air or underground explosions. The assumption of instantaneous equilibrium of stress for the purpose of using analytical procedures based on static stress equilibrium is

feasible although analysis of the data does not necessarily indicate fulfillment of the equilibrium condition.

5. Use of earth acceleration-time data for derivation of velocity and displacement-time information is feasible within certain limits of precision of the data and duration of the transient phenomena, as established by several previous tests.[14] Correlation between earth displacement data so derived and measured earth strains is not clearly established although fair agreement was indicated in one case.

It is interesting to consider the results of this study of earth stress and strain measurements in terms of the applications which the techniques might find in solving problems of underground effects of explosions and establishing bases for theoretical treatment of such problems. Correlation of free-field phenomena with damage and structural response, is, of course, necessary to usefulness of free-field measurements and is not yet an accomplished fact, possibly because of inadequate knowledge of structural response and of the coupling of soil and structural loads. This discussion will, however, deal with free-field measurements and assume their usefulness to the basic problems of damage. The assumption will also be made that methods and techniques of installing gages in the earth will have been developed, at least to such a point that realistic corrections can be made in the data for the influence of perturbations in the stress system caused by the gages and by the disturbance of the soil.

Air bursts of nuclear weapons, particularly those at heights of the order of one or two fireball radii, induce large transient stresses in the earth within a sizable area around ground zero. Such stresses are evidently predominantly vertical for peak incident overpressures of 35 to 40 psi, lateral stresses being 10 per cent or less of the vertical stresses. There is no reason to believe that this situation would change at higher incident overpressure levels except possibly toward an even lower ratio of lateral to vertical stresses. Consequently free-field measurements concerned with damage to underground structures from air burst weapons can be limited to the vertical component of various phenomena and to the region within the limits of loading which may produce serious structural response. The principal problems involve the rate of dissipation of the energy within the soil and its meaning to structural response. Correlation of vertical stress- and strain-time data as a function of depth and analysis of stress-strain relations as a function of depth can be expected to give useful information. An additional effect suggested by Part I is that variation of the rate of stress attenuation or energy dissipation with depth as a function of peak incident overpressure probably merits inclusion in a study of the type suggested above. The apparent increased rate of stress attenuation at higher incident overpressures might well be a highly significant factor in the effectiveness of earth cover protection for underground structures.

All these effects, to be useful either empirically or theoretically, must be correlated with structural response studies of the type initiated by Program 3.8 of UPSHOT-KNOTHOLE.[5]

Application of free-field measurements of earth stress and strain to underground explosions is considerably broader than for air bursts.

There is no obvious predominance of a single component as for air bursts. Radial components of parameters are usually greater for underground bursts, but vertical components are frequently nearly as large as the radial because of reflection and refraction effects. The tangential component may be negligible in some situations so that radial symmetry and plane stress may be assumed. However, gross inhomogeneities of the soil, dissymmetry and development of shears may be expected to make tangential components significant in many cases. No sufficiently comprehensive earth stress-strain measurements have been made in connection with underground explosions to determine satisfactorily the full significance of the various component measurements to an understanding of the free-field phenomena. The finite size of gages and the number required for experimental studies of stress and strain tensor measurement techniques using underground bursts of moderately small underground high-explosives charges -- of the order of several hundred pounds of TNT -- require gage placement at such relatively remote ground ranges (in terms of damage criteria) that effects of soil inhomogeneities, shears, and dissymmetry may be obscured.

Knowledge of the stress and strain tensors as a function of position with respect to ground zero could provide a more realistic basis for estimates of underground structural damage than the current rule of thumb. Similarly knowledge of the stress-strain pattern would be helpful in estimating loading on structures. These are free-field measurements, which, to have usefulness, must be correlated with structural response. An intermediate step in this correlation, which has so far been neglected and which is probably very important, is measurement of tensors in the soil immediately adjacent to structures. It is probably in this zone that significant differences between free-field phenomena and structural loading will be resolved. The plastic nature of soil and yielding of structural elements under load cause a serious difference between loading and response of soil in the free-field region and the corresponding effects at a structure. Free-field information would also serve to establish boundary values for theoretical studies of diffraction in the vicinity of underground structures.

It does not seem probable that a sound basis for design or damage estimates for underground structures will be available until the stress-strain reactions of the soil around the structure are understood in sufficient detail to give a realistic picture of the loading pattern on the structure.

APPENDIX A

STRESS-TIME AND IMPULSE INTENSITY-TIME WAVE FORMS FOR PROJECT 1.4a

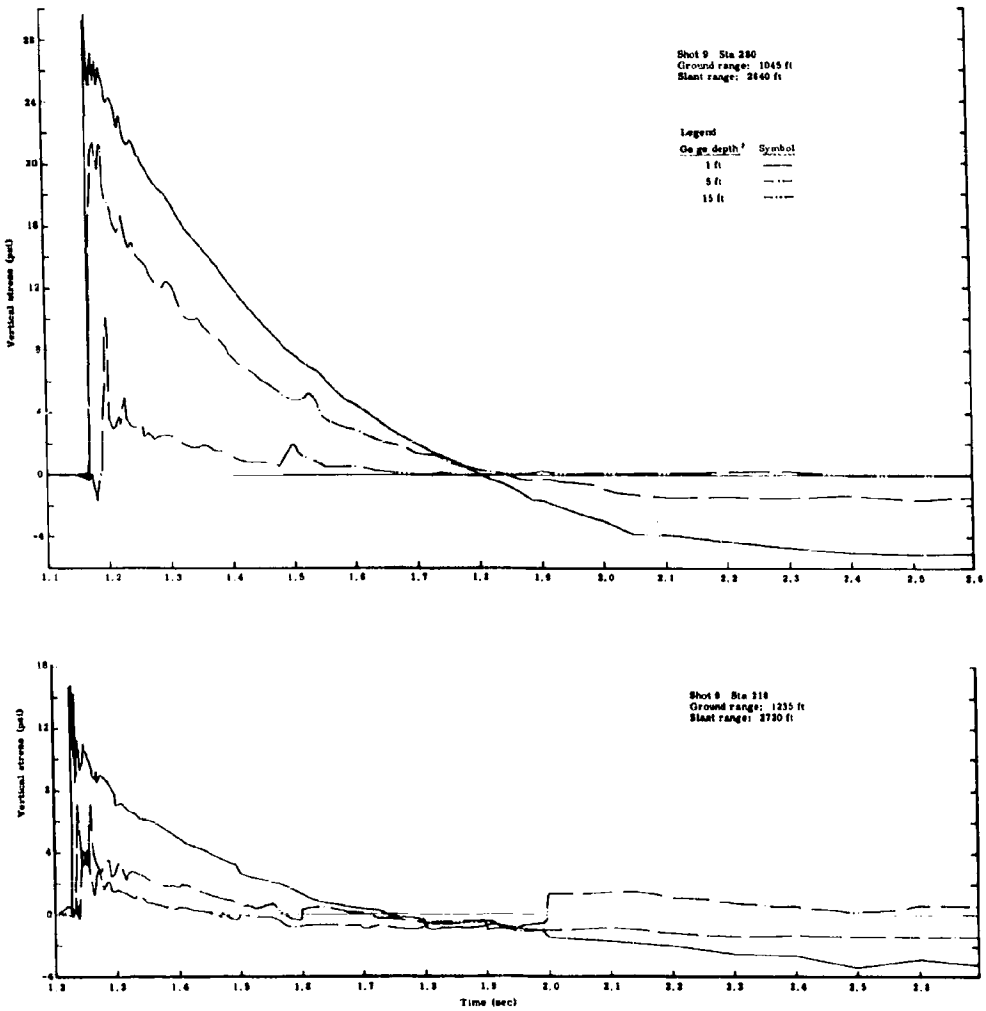

Fig. A.1 Earth Stress vs Time vs Depth

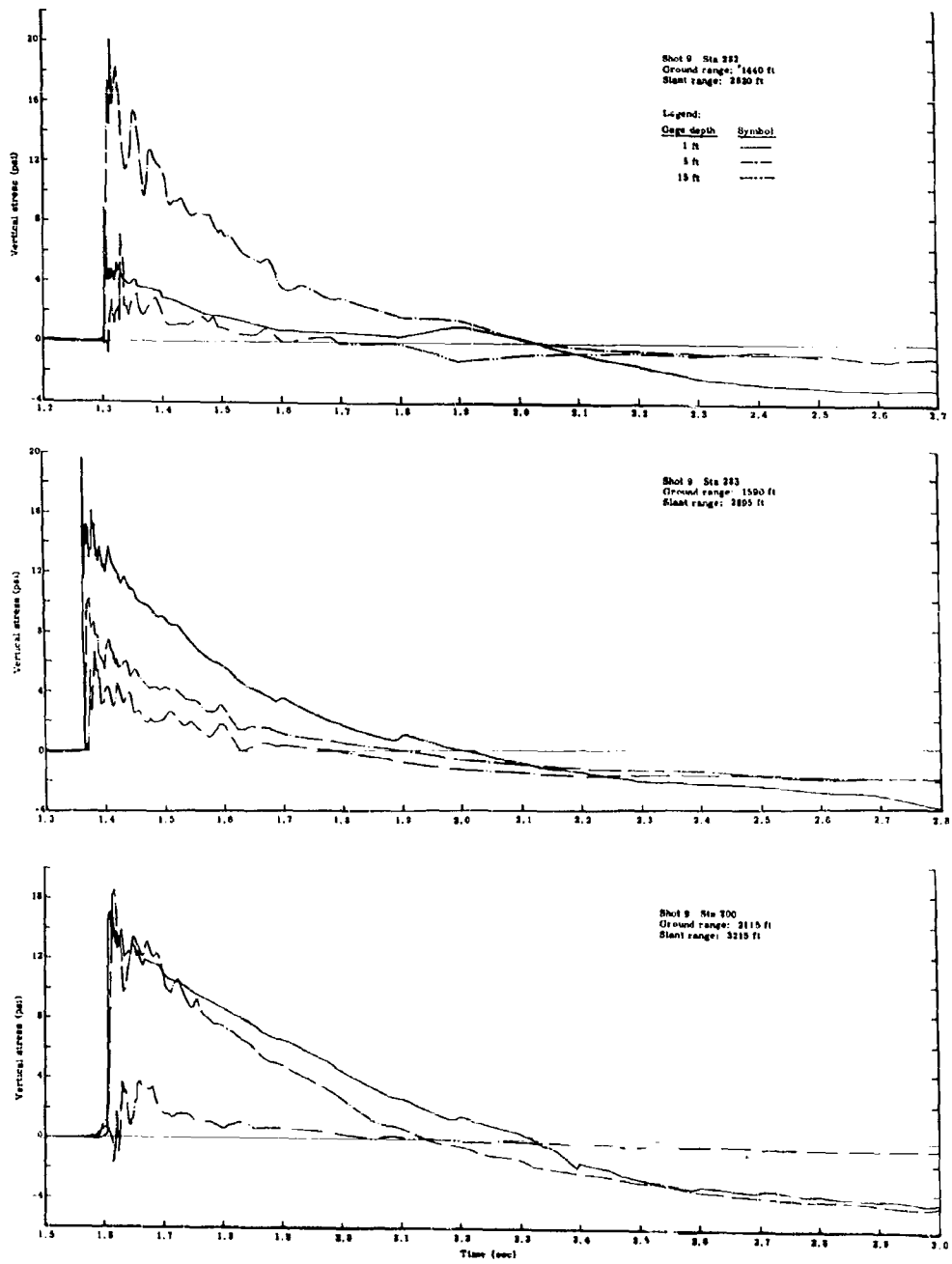

Fig. A.2 Earth Stress vs Time vs Depth

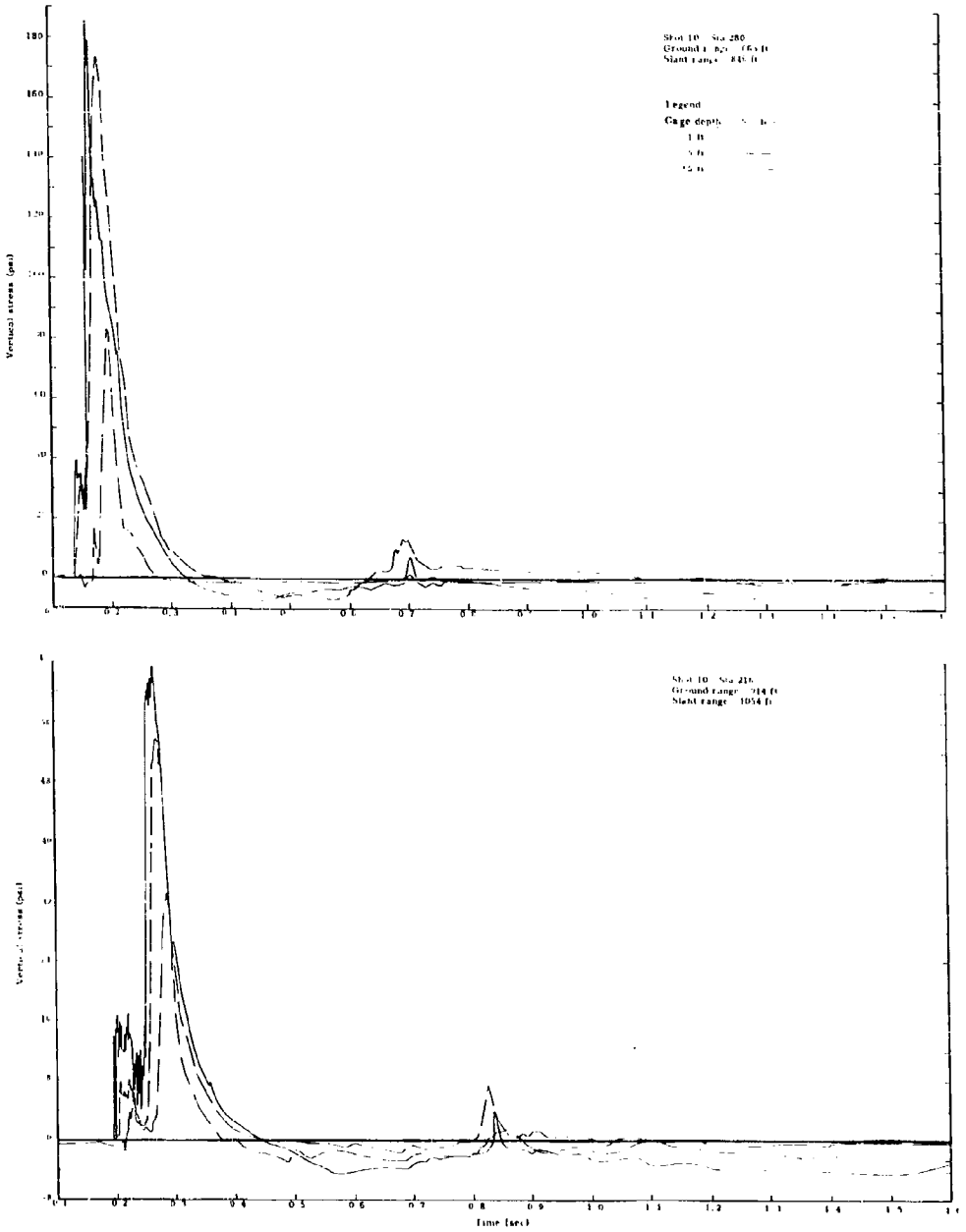

Fig. A.3 Earth Stress vs Time vs Depth

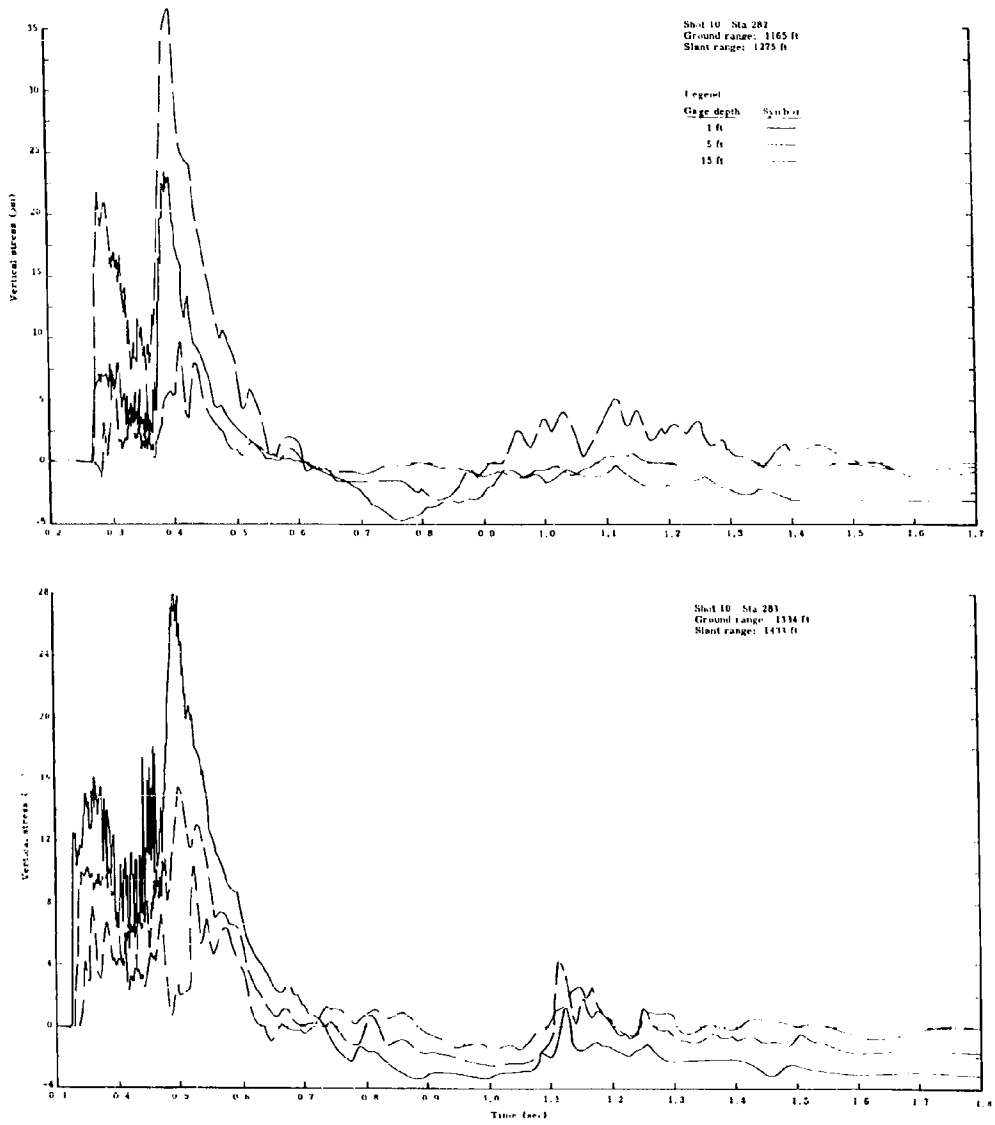

Fig. A.4 Earth Stress vs Time vs Depth

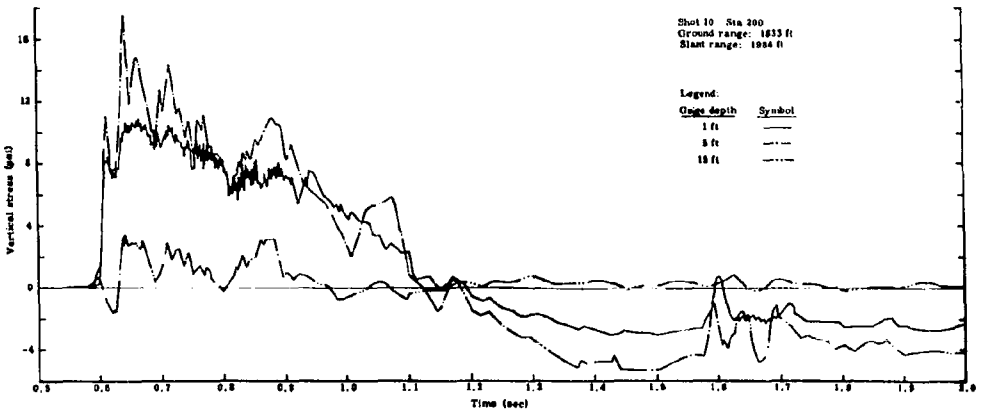

Fig. A.5 Earth Stress vs Time vs Depth

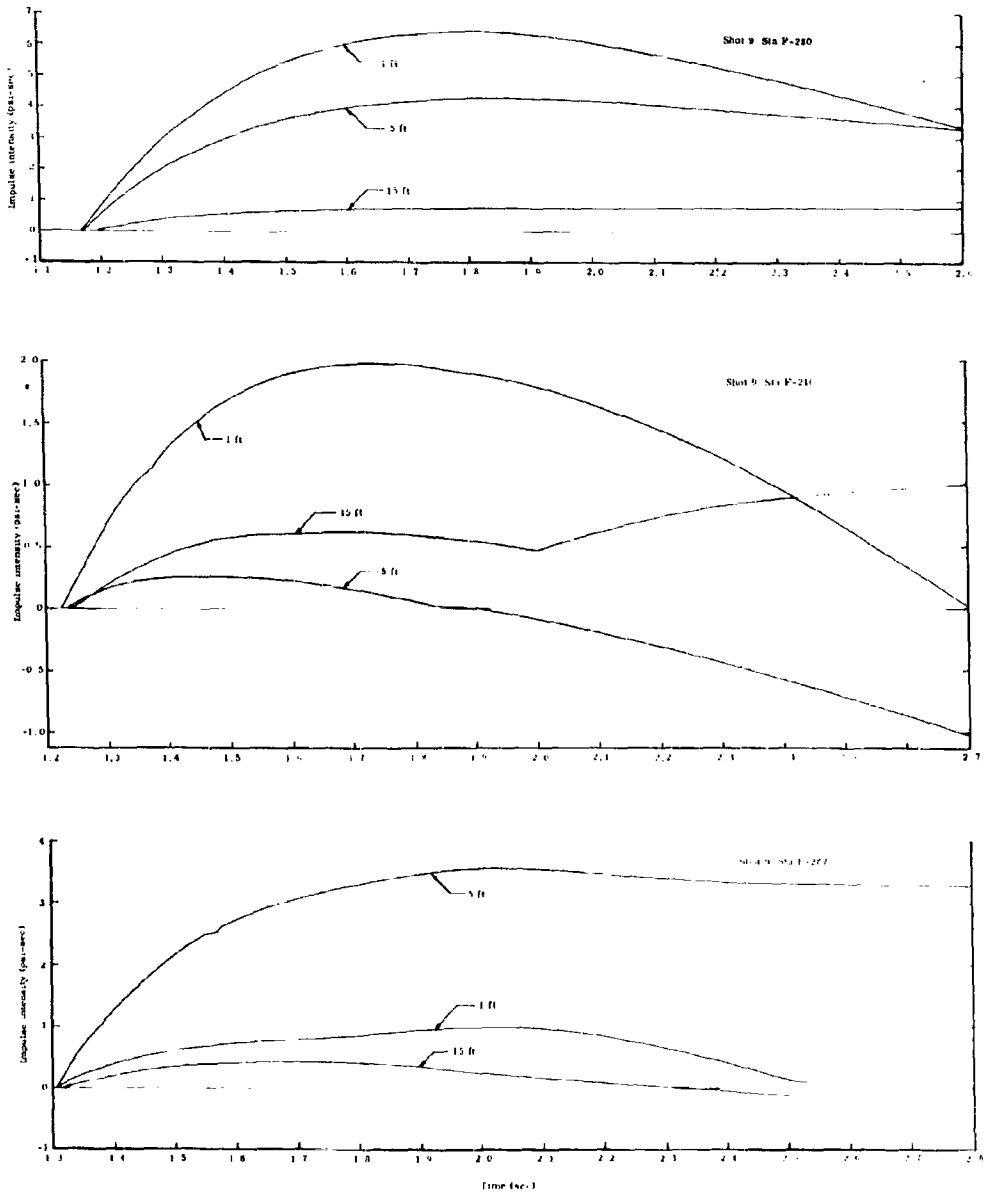

Fig. A.6 Impulse Intensity vs Time vs Depth

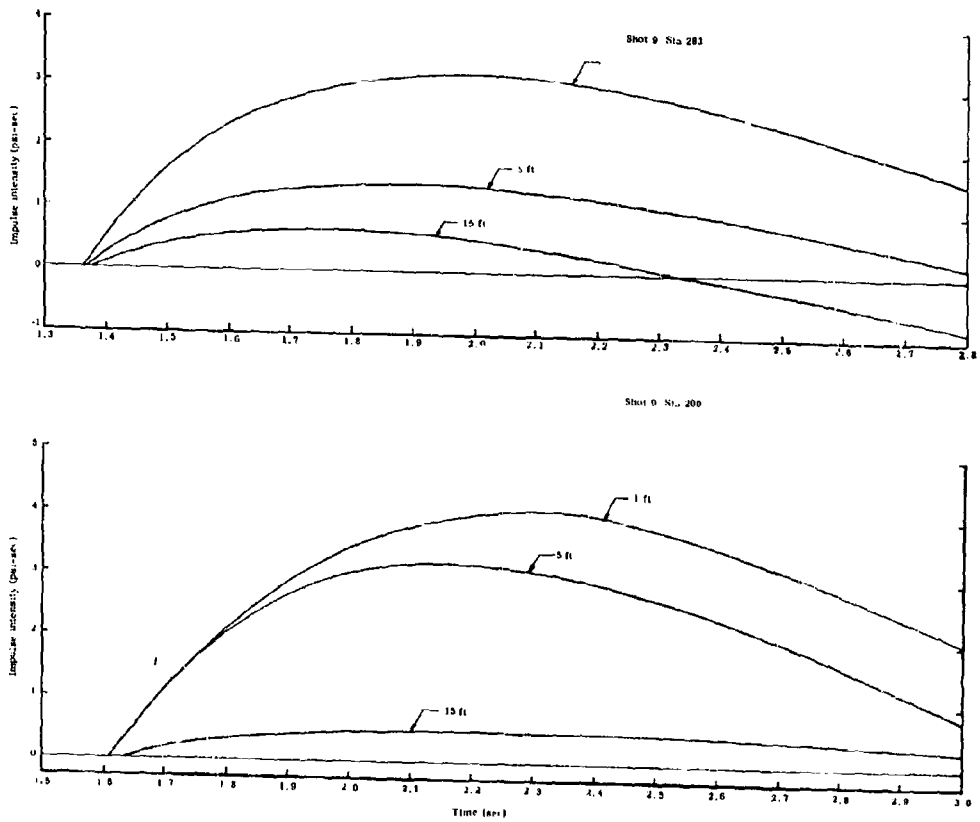

Fig. A.7 Impulse Intensity vs Time vs Depth

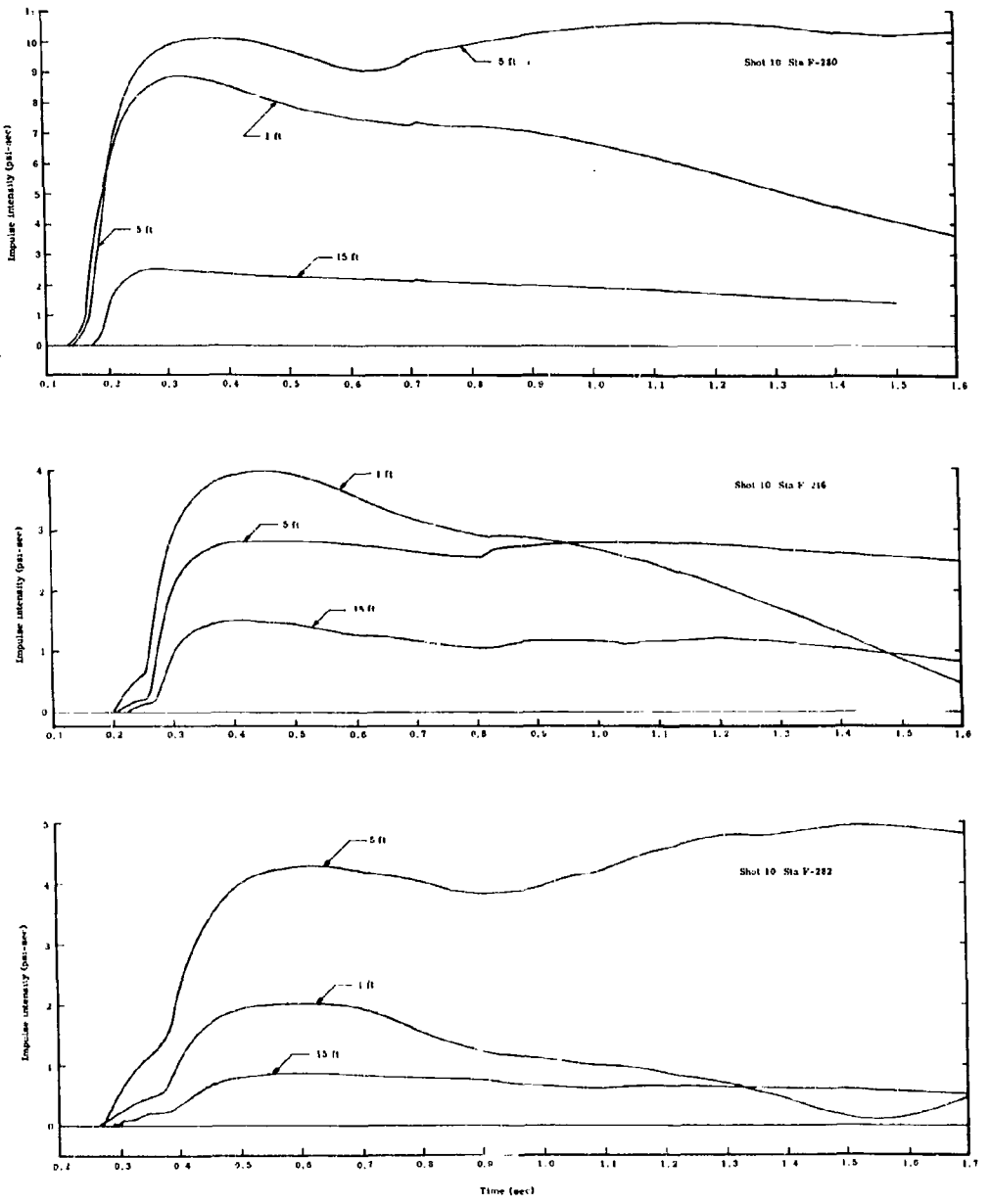

Fig. A.8 Impulse Intensity vs Time vs Depth

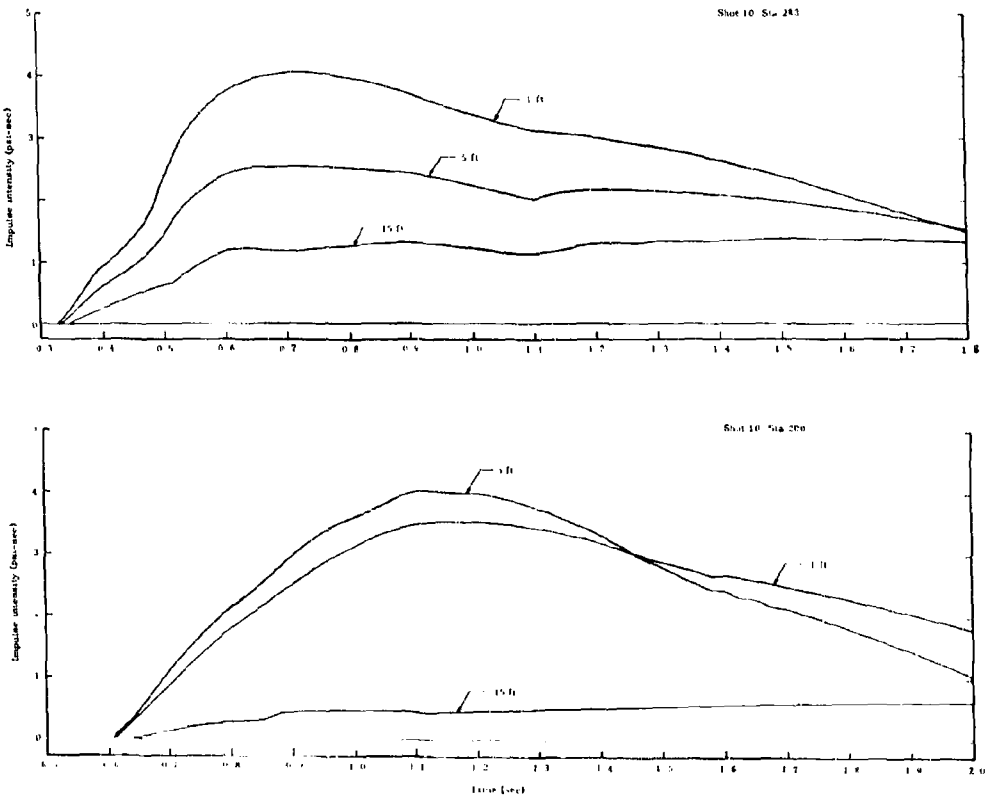

Fig. A.9 Impulse Intensity vs Time vs Depth

APPENDIX B

INSTALLATION OF GAGES FOR PROJECT 1.4b

Earth stress and earth strain gages were placed in trenches 5 ft deep which were perpendicular to the blast lines at Stations 3-285 and F-281. Location stakes were set prior to excavation to show the centerline of the trench and permit reasonably precise positioning of the gages. Each trench, as excavated by a backhoe, had a bottom width of about 2 ft and a width of about 7 ft at the surface. The length of each trench was sufficient to accommodate the full complement of gages (Figs. 2.1 and 2.2).

The bottom of each trench was tamped after cutting down or adding moist backfill as needed to permit installation of all gages with response axes at the prescribed depth of 5 ft within ± 0.1 ft.

The position of each gage in the trenches was determined from two rows of location stakes (Fig. B.1), set to grade at 3-ft intervals along the length of the trenches, one row 7 ft toward ground zero and the other 7 ft away from ground zero with respect to the centerline. These stakes, undisturbed by excavation, permitted exact positioning of the stress gages by means of a 5 ft plumb line dropped from the midpoint of a tape stretched between corresponding stakes in each line. Strain gages were placed approximately midway between adjacent stress gages.

Instruments were placed in the trench in sequence from the end nearest the blast line. Each gage was oriented with respect to ground zero by means of a sighting tube (Fig. B.2) and relative to the vertical axis by means of a spirit level and protractor (Fig. B.3).

Backfill material, consisting of soil free of rock and gravel, was mixed with water and allowed to season for about a day to approximately optimum compaction consistency. This material was screened and hand tamped around each instrument (Fig. B.4). Backfill was placed in thin lifts, about 2 in. for hand tamping and 6 to 12 in. for pneumatic tamping (Fig. B.5), and compacted to uniform densities somewhat greater than the natural density of the surrounding soil. A few density determinations of the undisturbed soil and of the compacted backfill were made for control purposes. Backfill was placed to an elevation of about 2 ft above each gage before the next one was installed.

Fig. B.1 Instrument Trench, Location Stakes and Gages in Prescribed Positions

Fig. B.2 Orientation of Earth Strain Gage

Fig. B.3 Orientation of Earth Strain Gage

Fig. B.4 Placement of Backfill Around Gage

Earth strain gages require more meticulous placement than stress gages. The very short ranges (0.010 in. for a 5 in. gage length) through which the gage must operate after completion of all backfill and the short range of linear response (0.040 in.) of the transducers indicate the precision with which control must be exercised during placement. Clamping devices intended to restrain the gages in proper mechanical alignment are impractical.

Fig. B.5 Tamping Backfill Over a Gage

Requisite control of strain gage alignment was accomplished by monitoring the output of each unit during its placement through a portable single-channel carrier-amplifier unit (Consolidated Type 113B). The amplifier output was under observation by the man compacting the backfill around the gage throughout the operation. Alternation of tamping operations between areas which caused extension of the gage and those which produced compression permitted thorough compaction and attained remarkably good ultimate mechanical alignment. This monitoring procedure permitted extension or compression of a gage during compaction beyond its linear range without loss of control.

Pneumatic tamping replaced hand tamping after sufficient fill had been placed to ensure protection of the gages from mechanical damage. Soil immediately adjacent to the gages was compacted to densities closely approximating that of the surrounding fill and exceeding that of the undisturbed soil.

Considerably greater difficulty was experienced in control of vertical strain gages than of those which responded to other components. The source of this difficulty appears to be a thin layer of soil directly beneath the upper plate of the vertically placed gage. This soil must be compacted by very indirect methods. The procedure found most effective for vertical gages was to compact the soil between the end plates sufficiently to extend the gage through several set ranges prior to final compaction of the overlying soil. This latter operation usually followed placement of a little less than 1 foot of fill above and around the gage. Compaction operations above the gages after they had been covered by more than 1 foot of compacted fill did not generally result in permanent mechanical zero changes of more than a few tenths of set range.

The two vertical earth strain gages at Sta 3-285 were not very well zeroed. The final set of ES-1 was off true mechanical zero by an appreciable fraction of a set range, and that of ES-7 was even more

seriously out of alignment. However, neither departure exceeded the linear range of the gage. The corresponding gages at Sta F-281 were zeroed so that the final set was within a very small fraction of a set range from true mechanical zero.

Compaction of the final 3 ft of fill above the gages did not affect the mechanical setting of the strain gages. All gages responded to the tamper loading but returned to their initial as-placed zeros.

APPENDIX C

PARAMETER TIME RECORDS

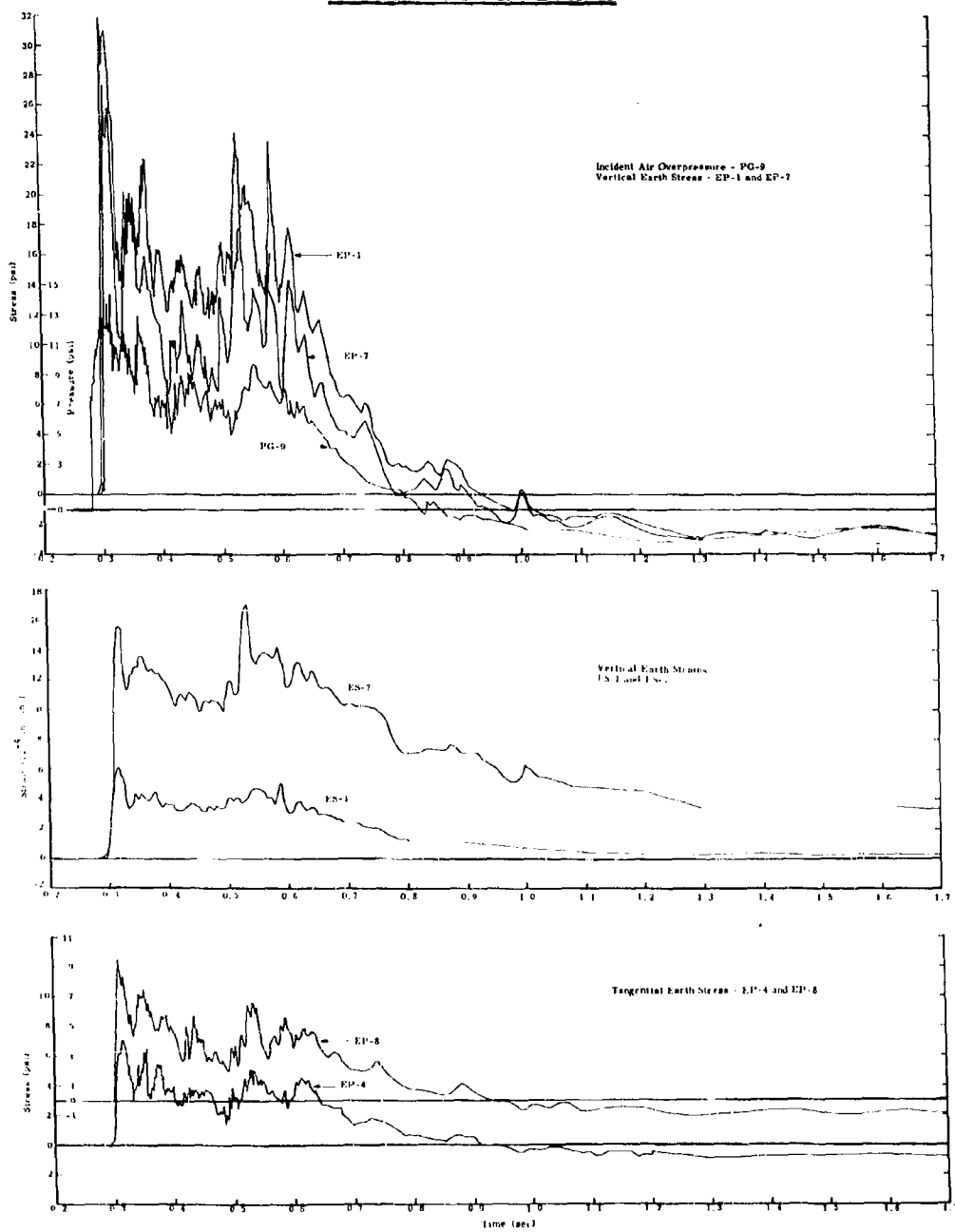

Fig. C.1 Earth Stress, Strain, and Air Overpressure vs Time - Shot 1

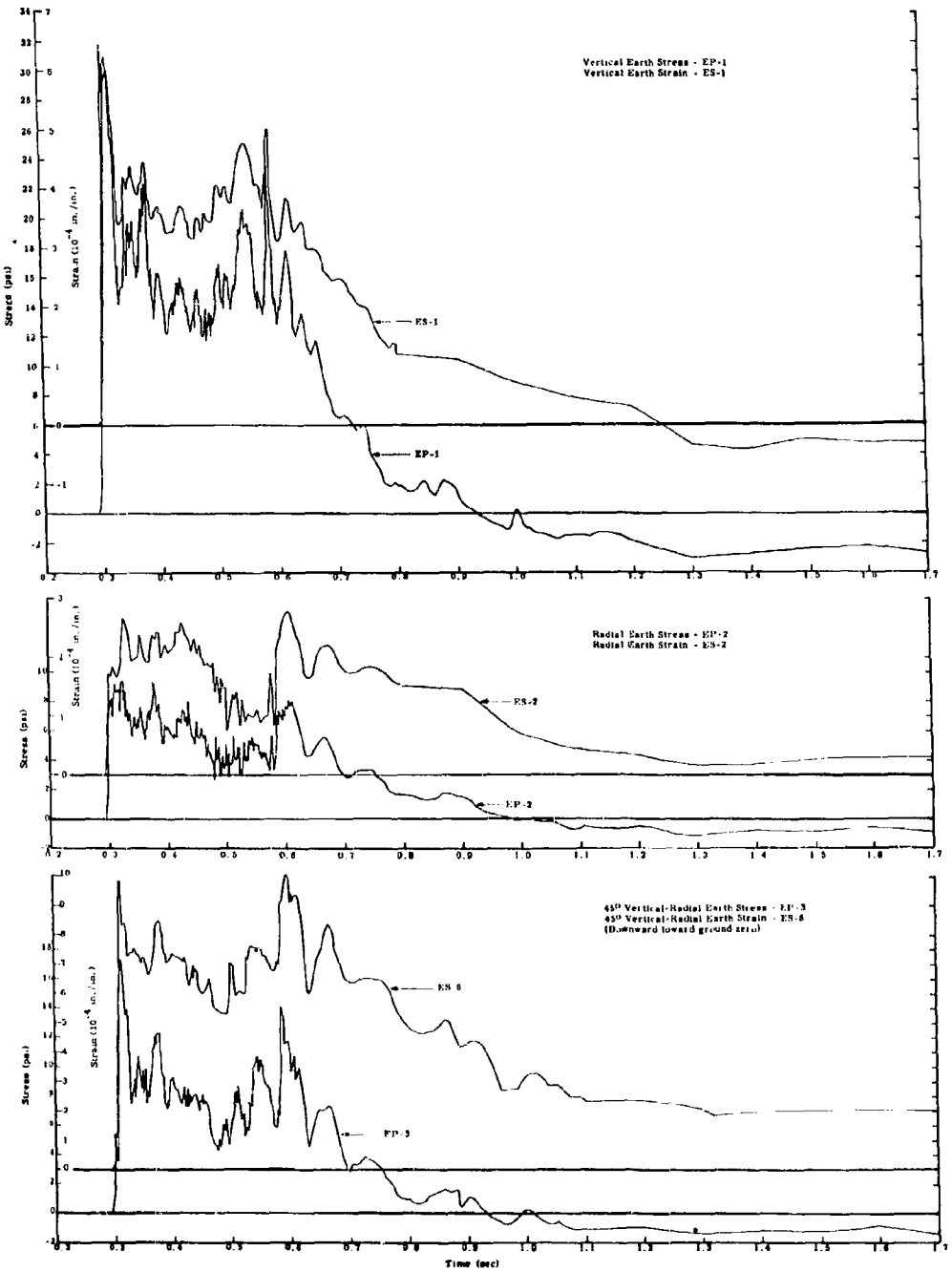

Fig. C.2 Earth Stress and Strain vs Time - Shot 1

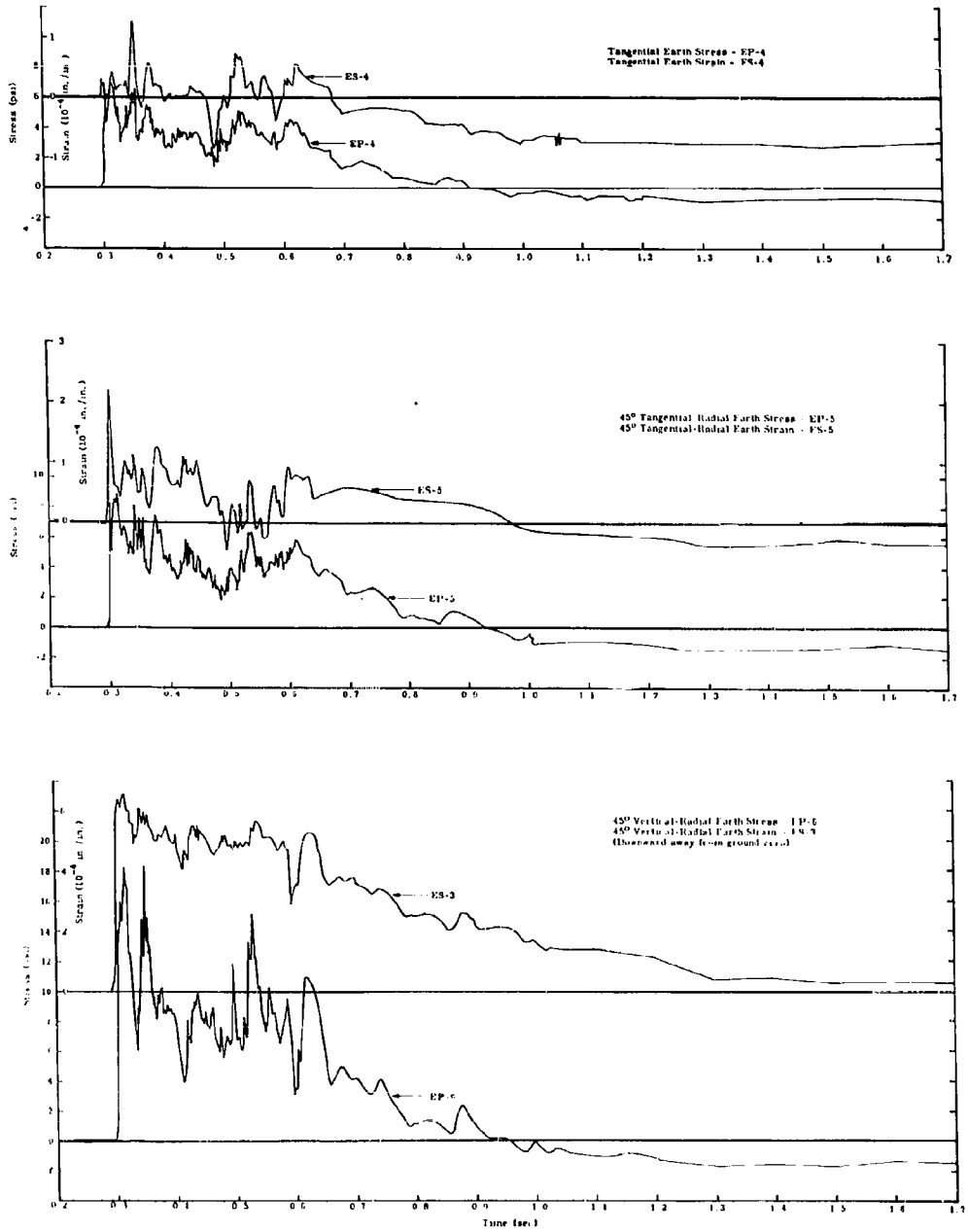

Fig. C.3 Earth Stress and Strain vs Time - Shot 1

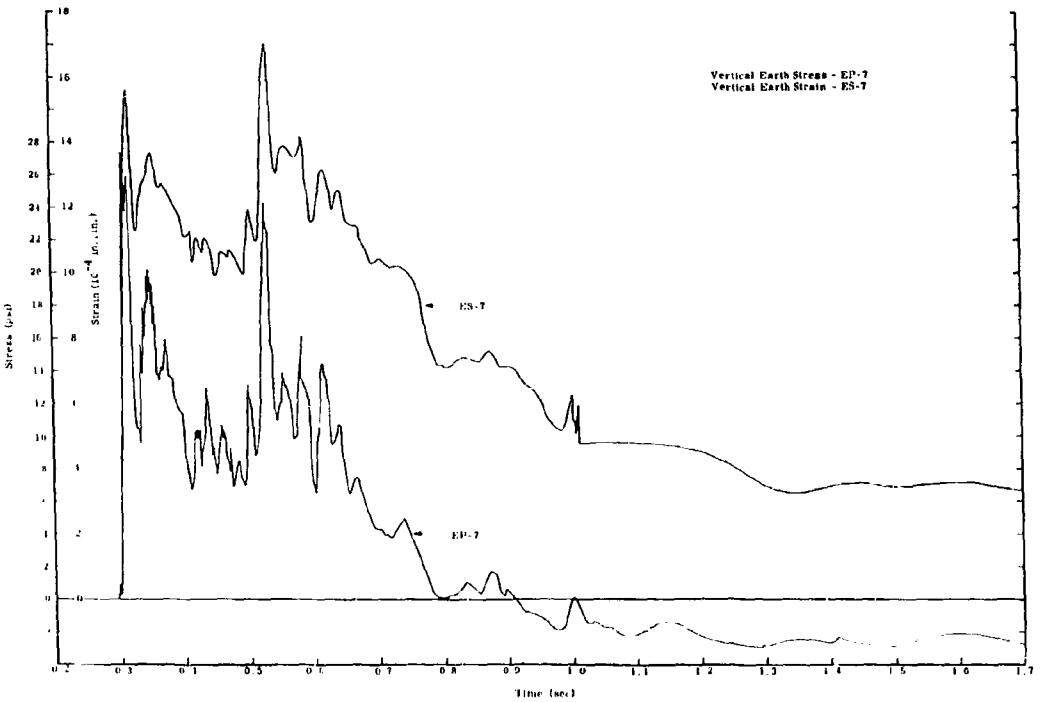

Fig. C.4 Earth Stress and Strain vs Time - Shot 1

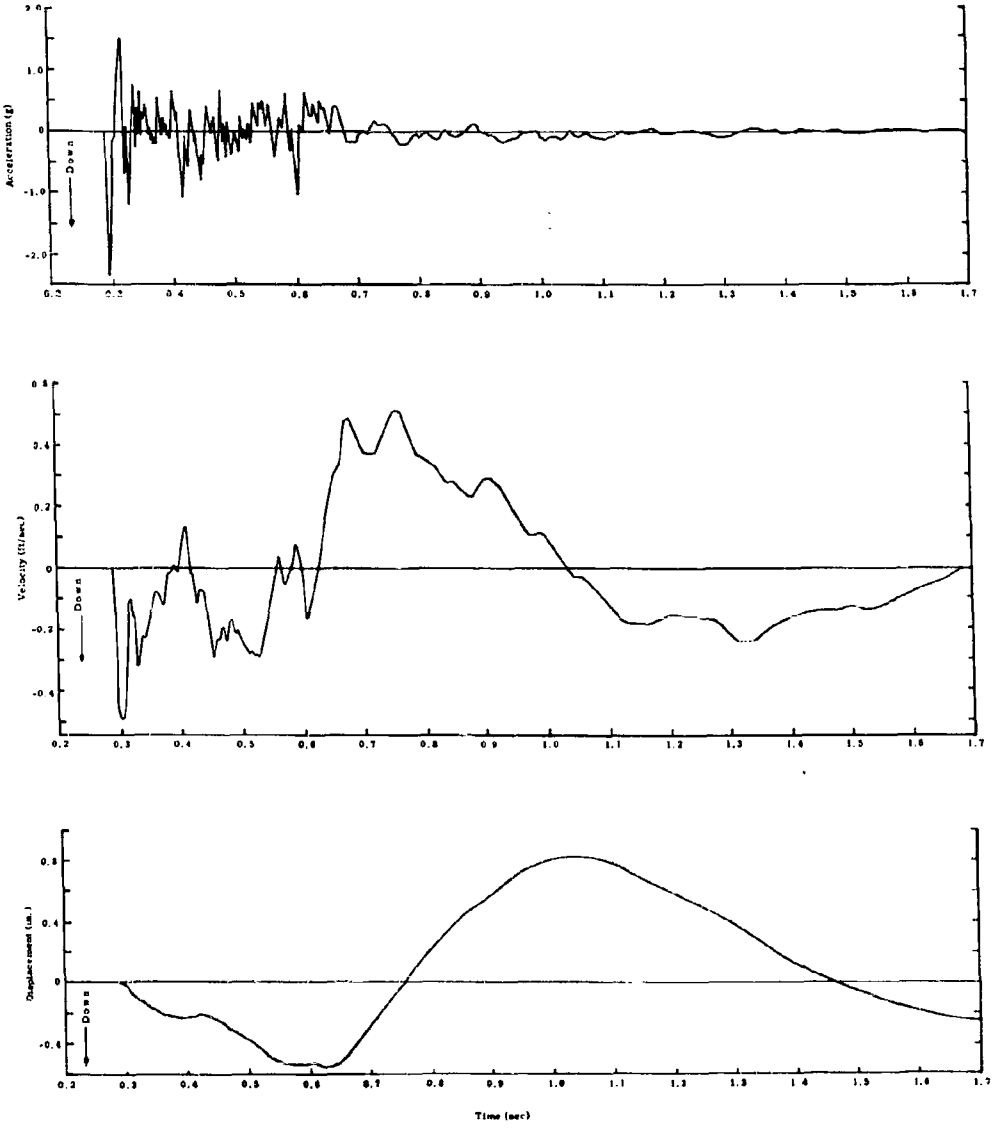

Fig. C.5 Vertical Ground Acceleration, Velocity, and Displacement vs Time - Shot 1

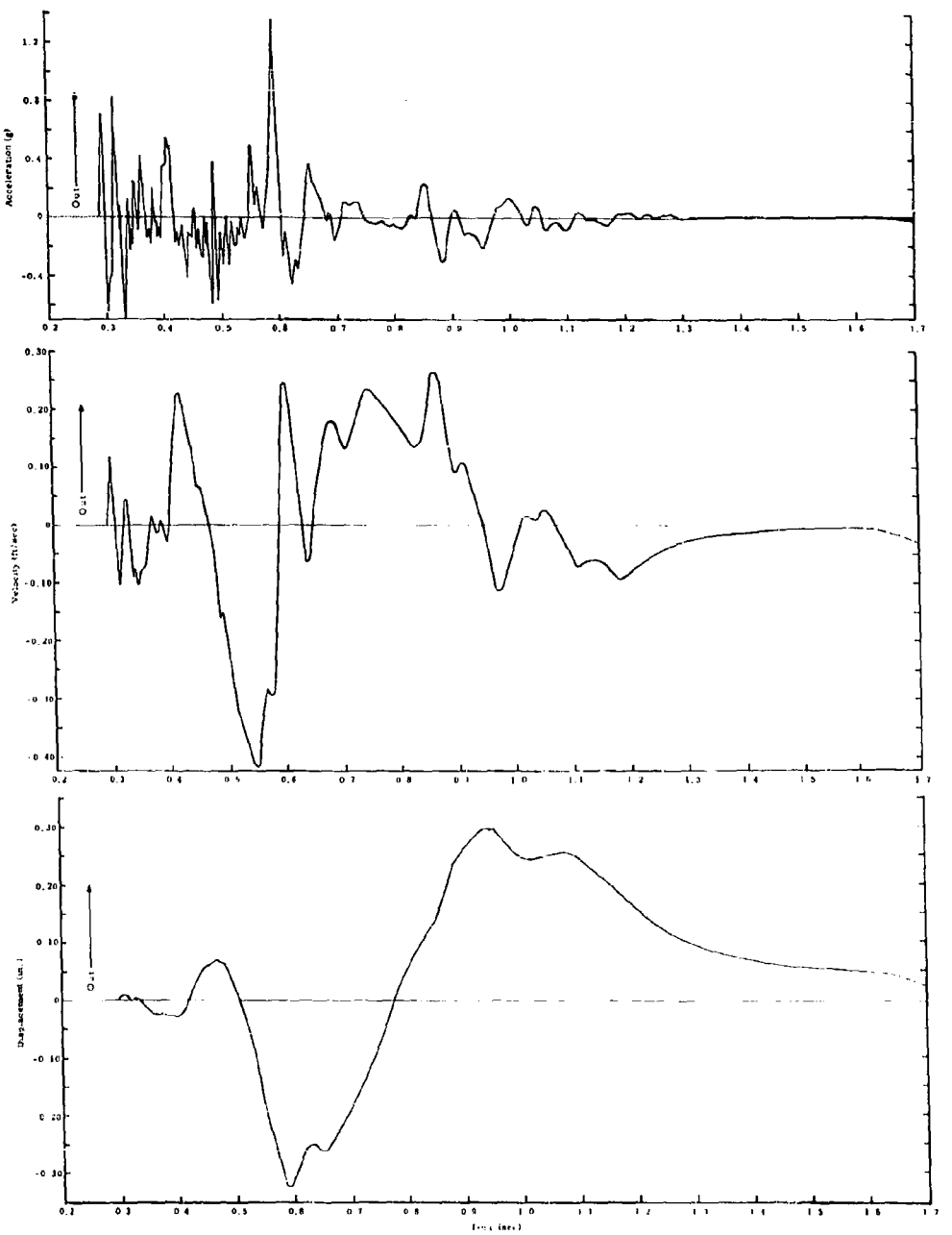

Fig. C.6 Radial Ground Acceleration, Velocity, and Displacement vs Time - Shot 1

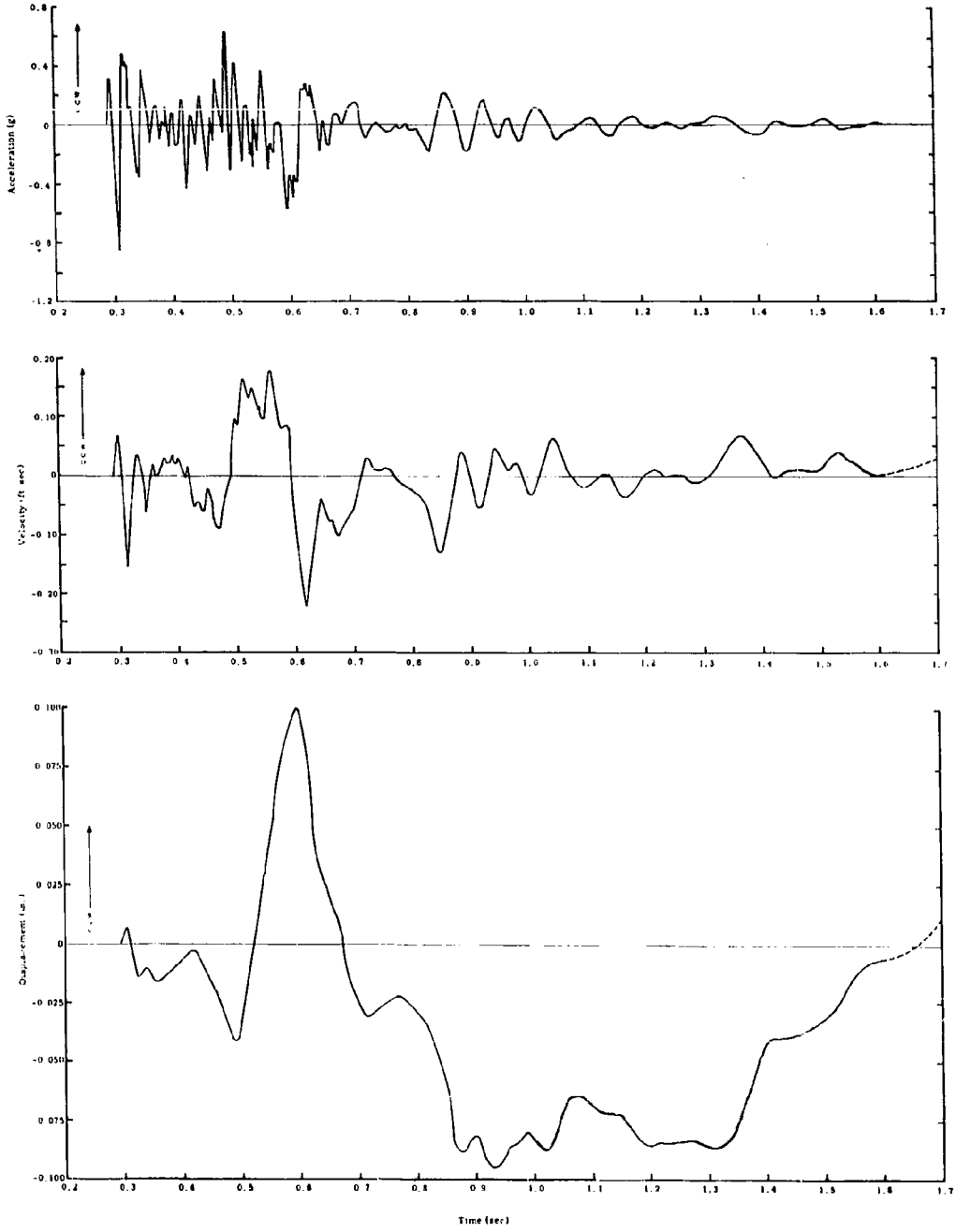

Fig. C.7 Tangential Ground Acceleration, Velocity, and Displacement vs Time - Shot 1

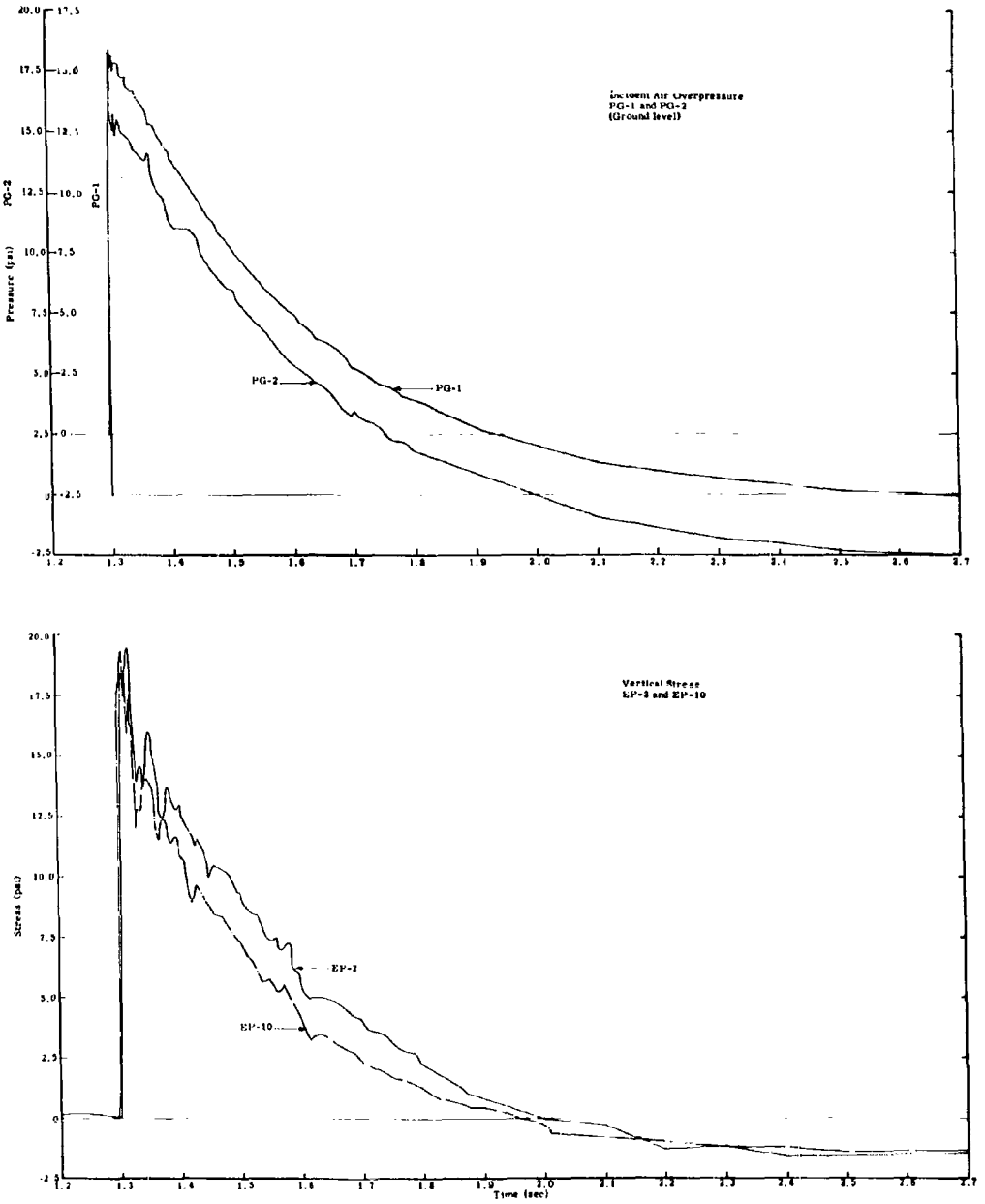

Fig. C.8 Air Overpressure and Earth Stress vs Time - Shot 9

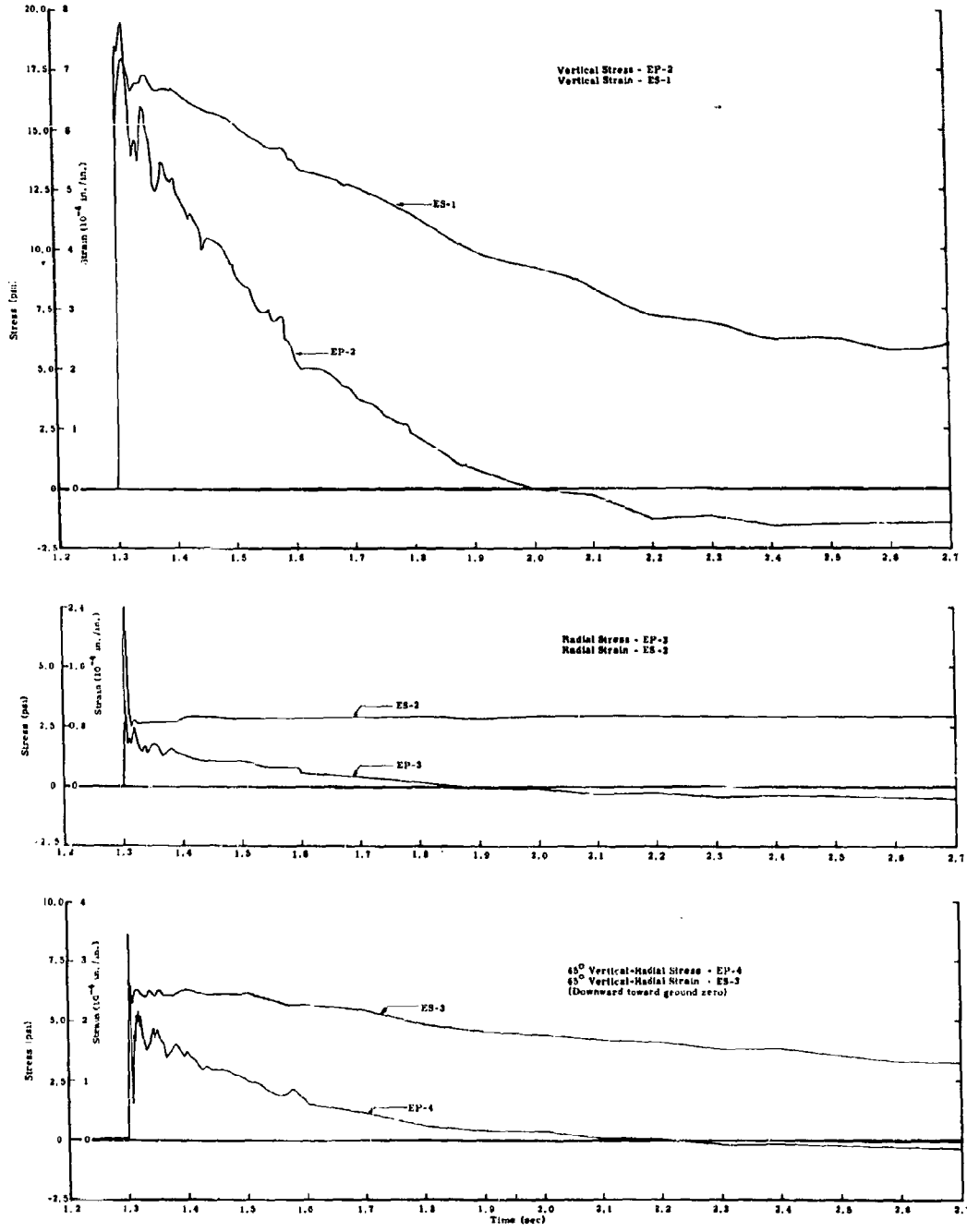

Fig. C.9 Earth Stress and Strain vs Time - Shot 9

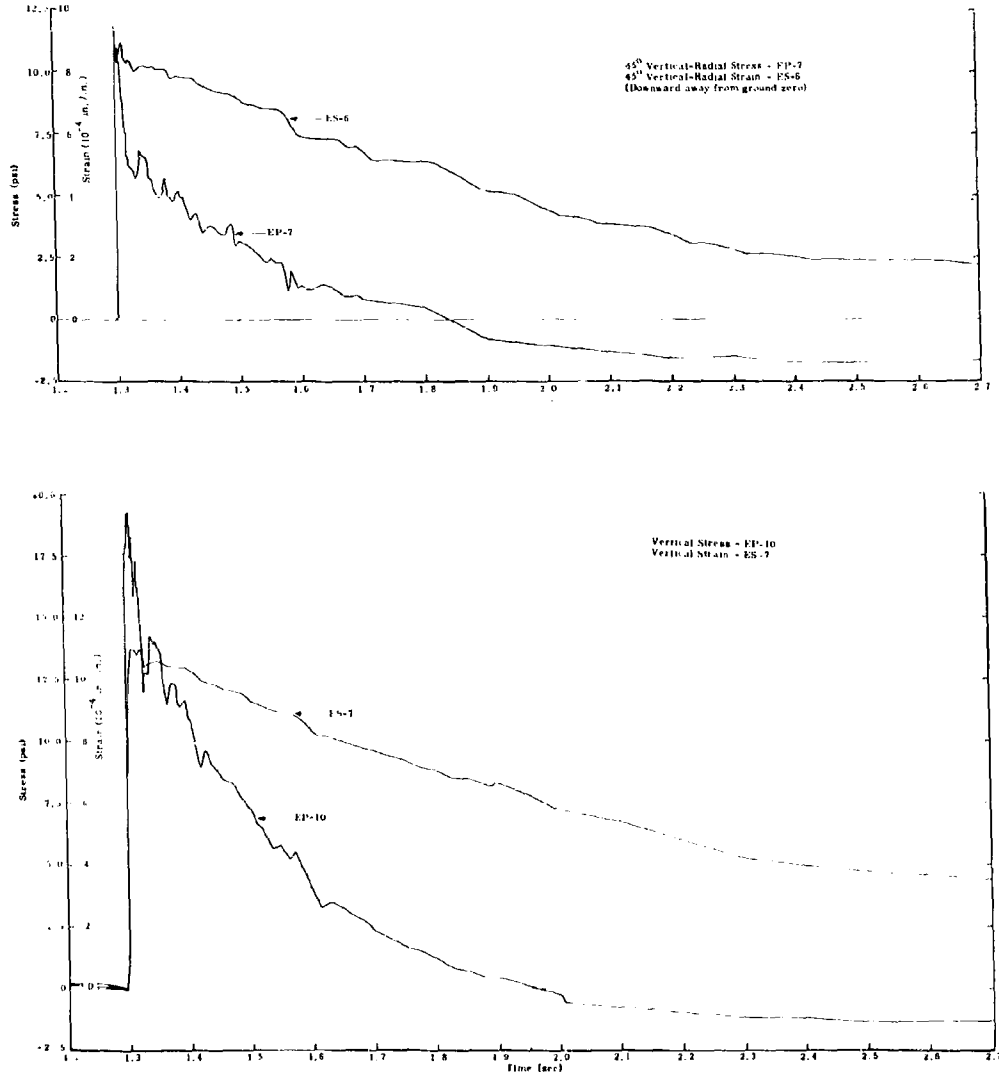

Fig. C.10 Earth Stress and Strain vs Time - Shot 9

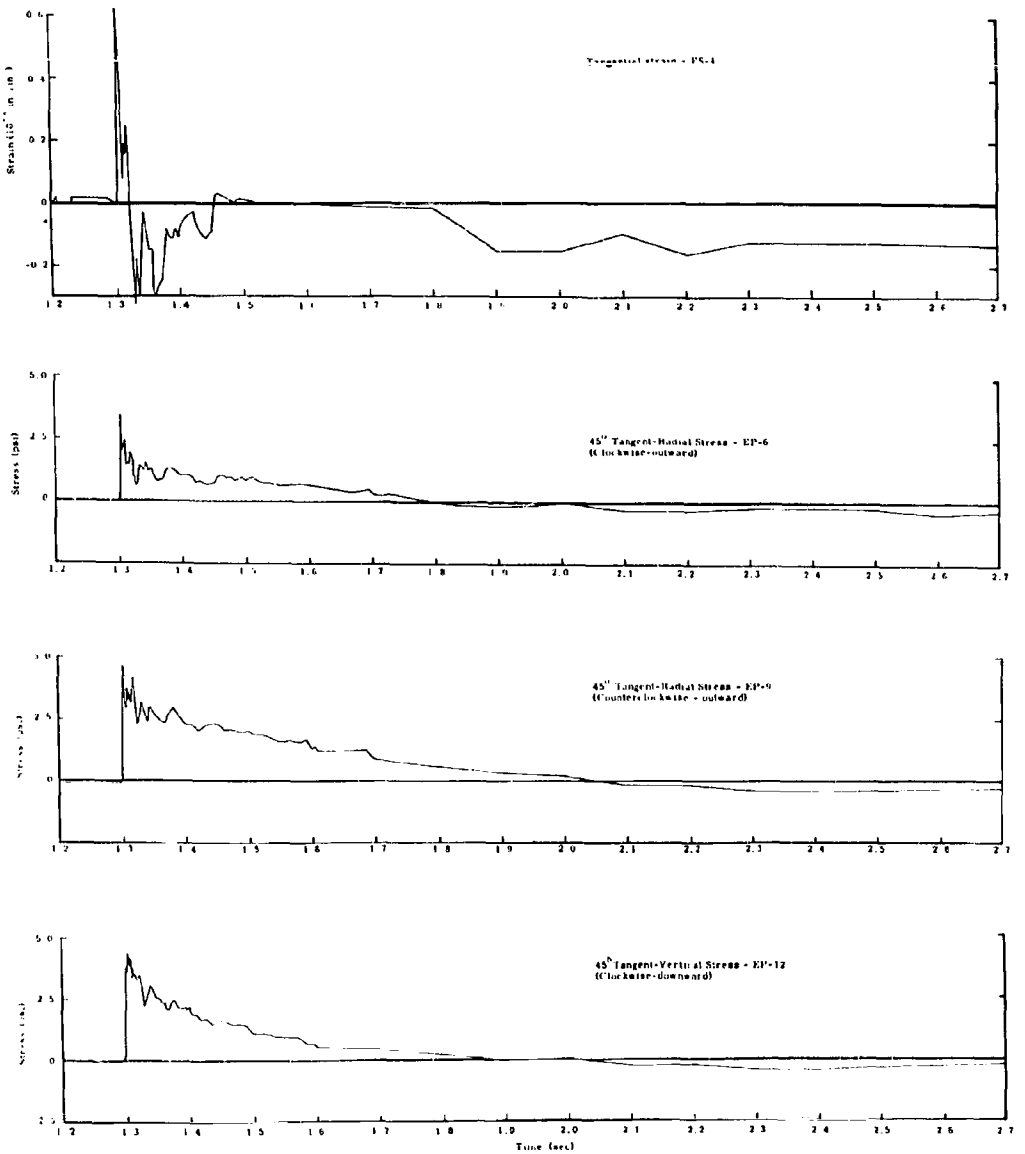

Fig. C.11 Earth Stress and Strain vs Time - Shot 9

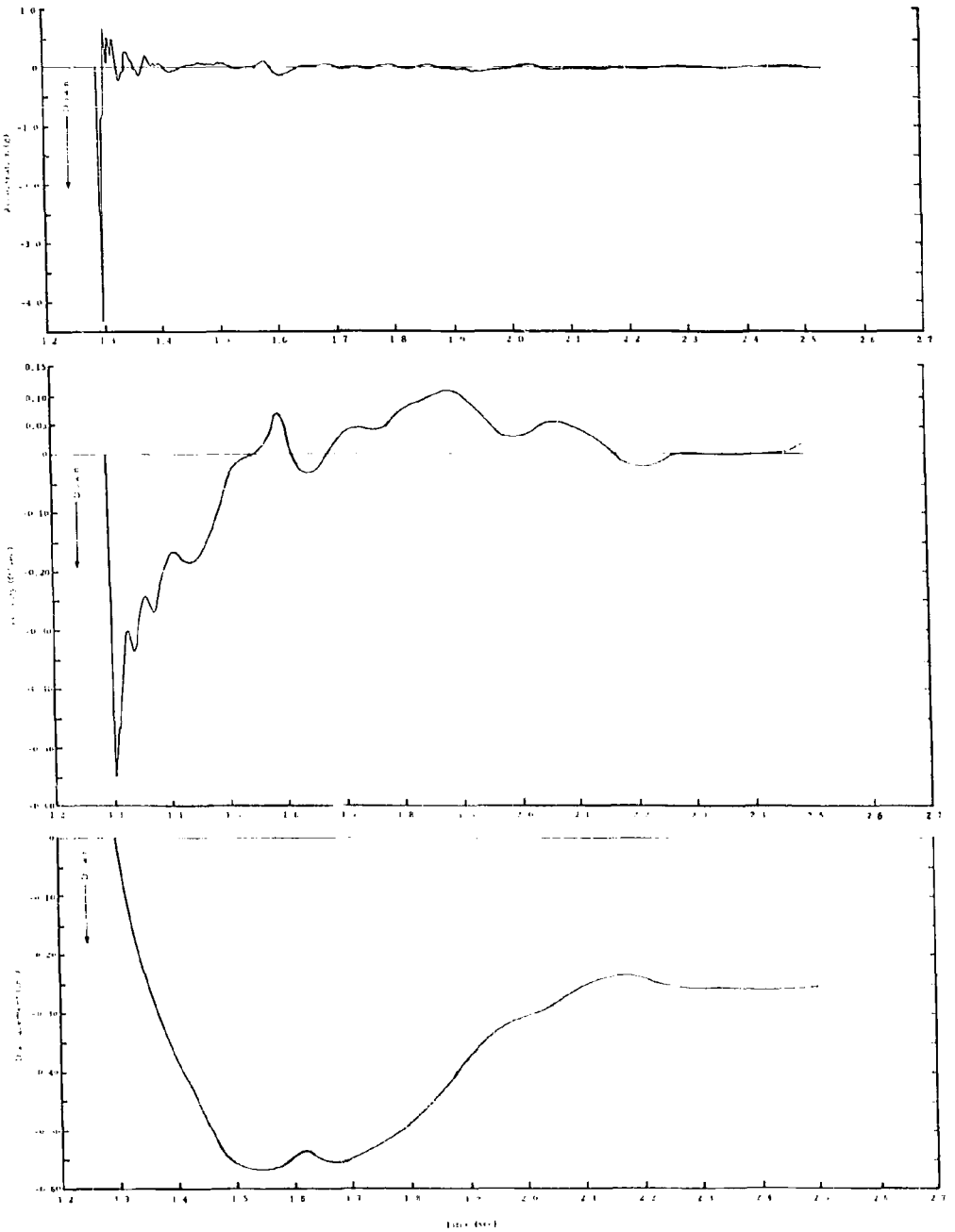

Fig. C.12 Vertical Ground Acceleration, Velocity, and Displacement vs Time - Shot 9

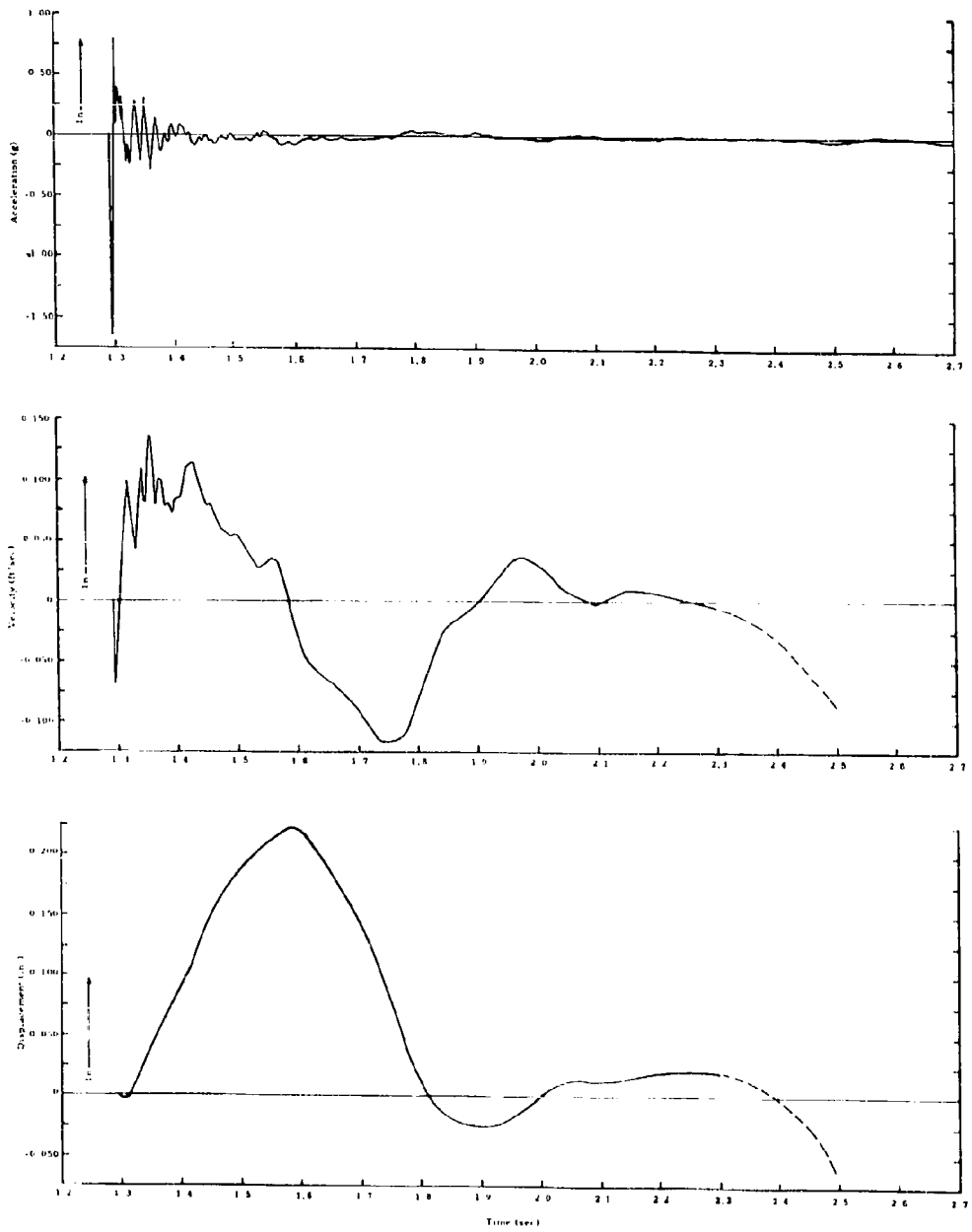

Fig. C.13 Radial Ground Acceleration, Velocity, and Displacement vs Time - Shot 9

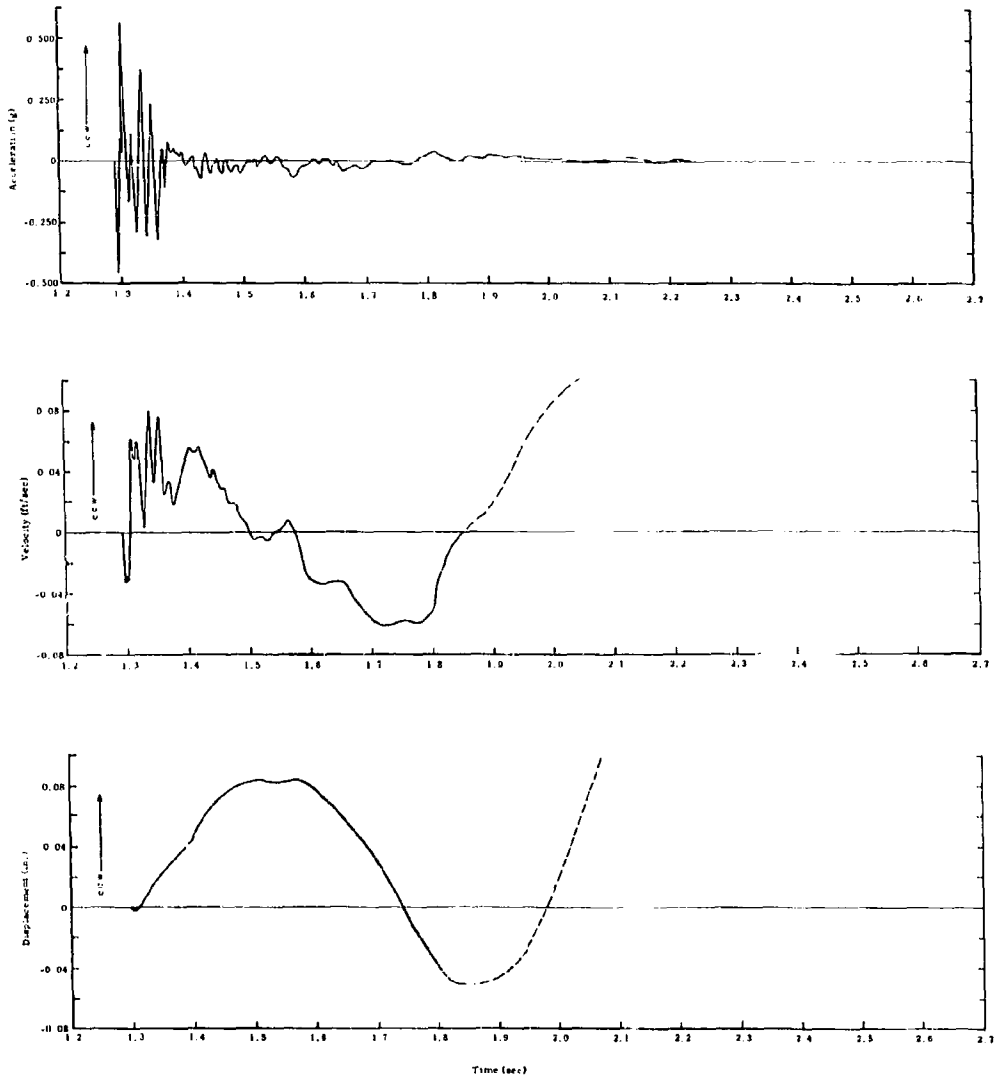

Fig. C.14 Tangential Ground Acceleration, Velocity, and Displacement vs Time - Shot 9

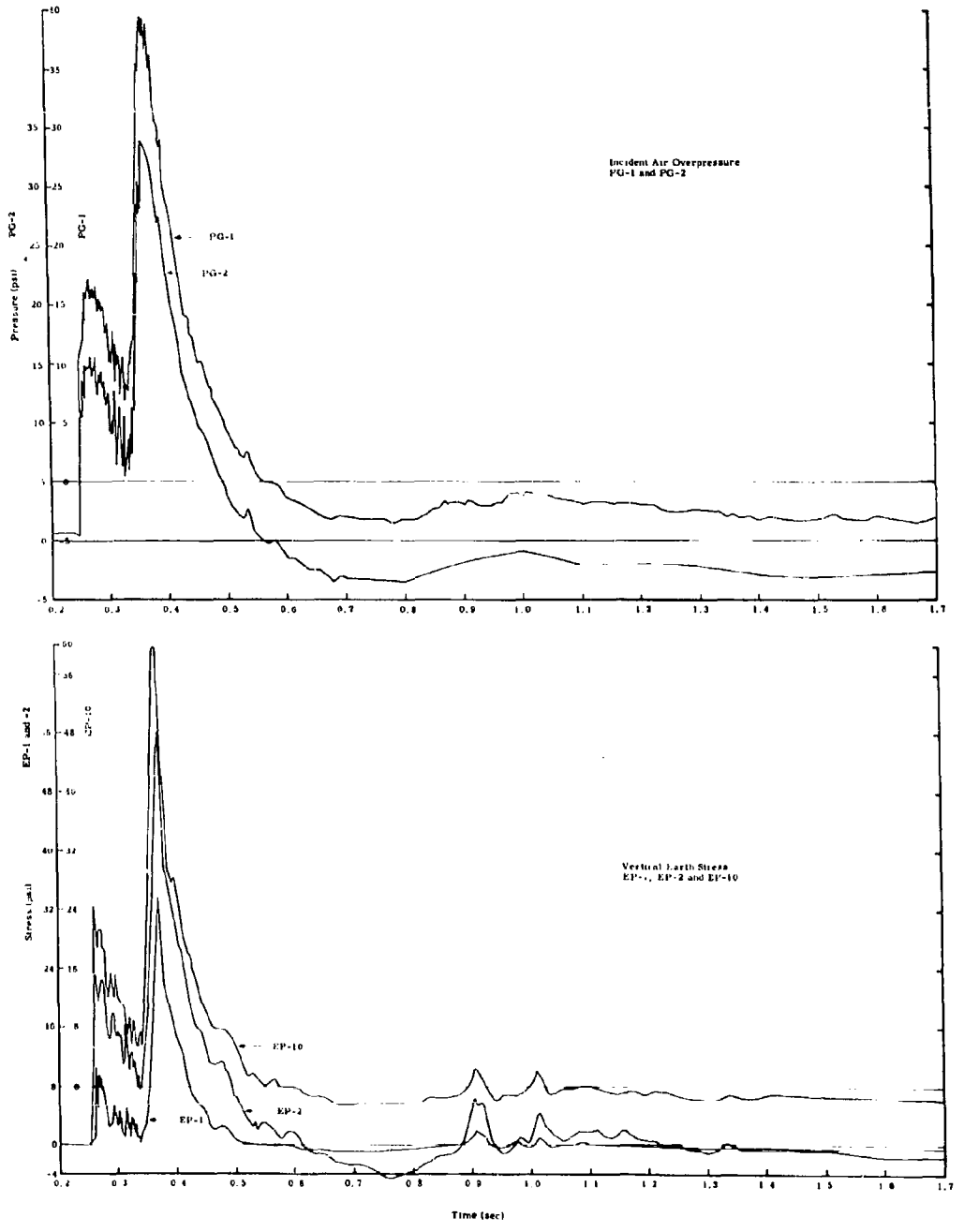

Fig. C.15 Air Overpressure and Earth Stress vs Time - Shot 10

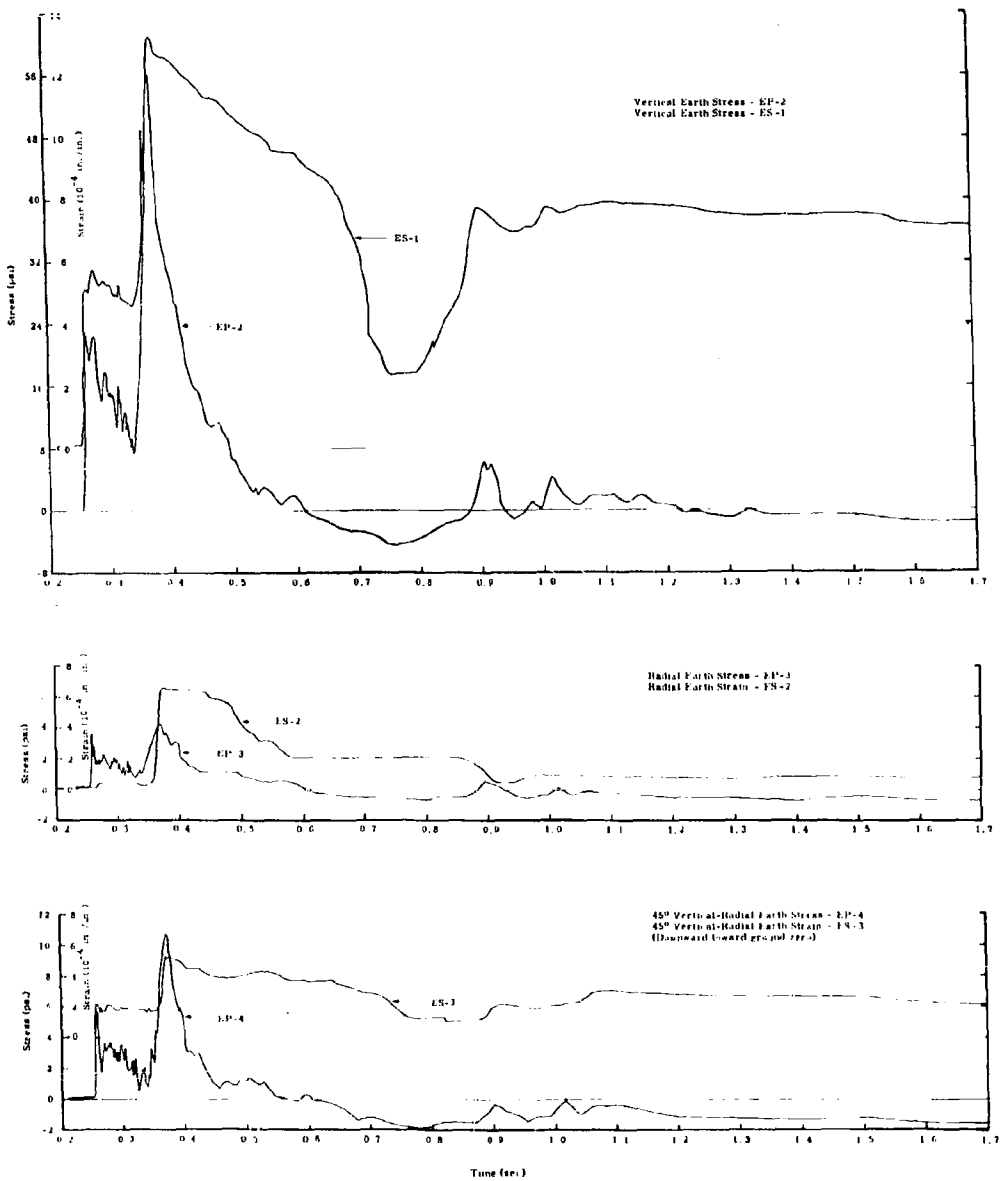

Fig. C.16 Earth Stress and Strain vs Time - Shot 10

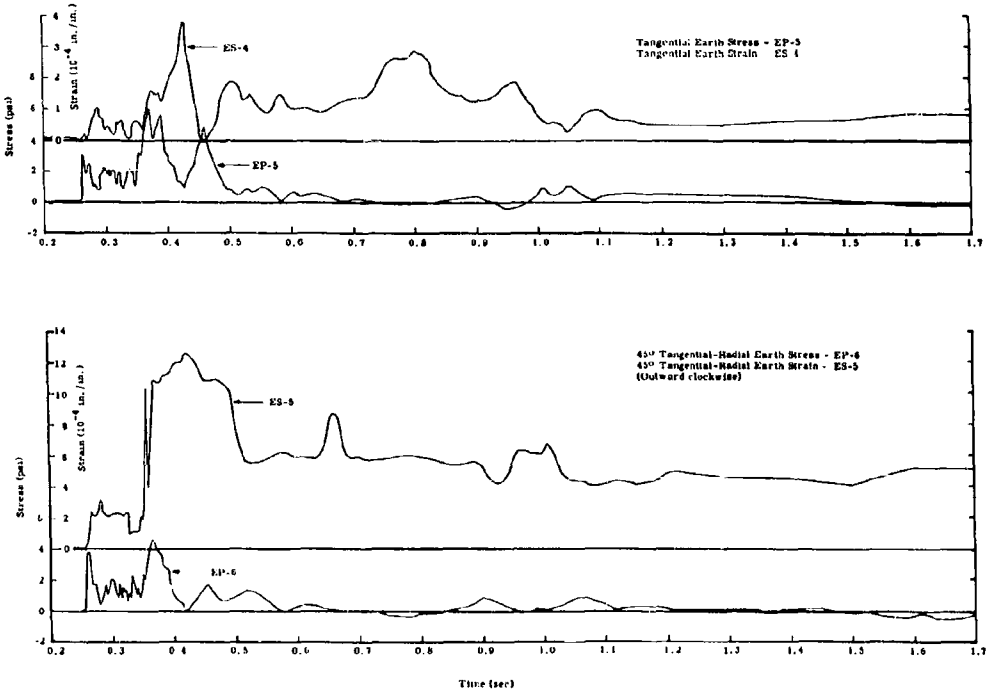

Fig. C.17 Earth Stress and Strain vs Time - Shot 10

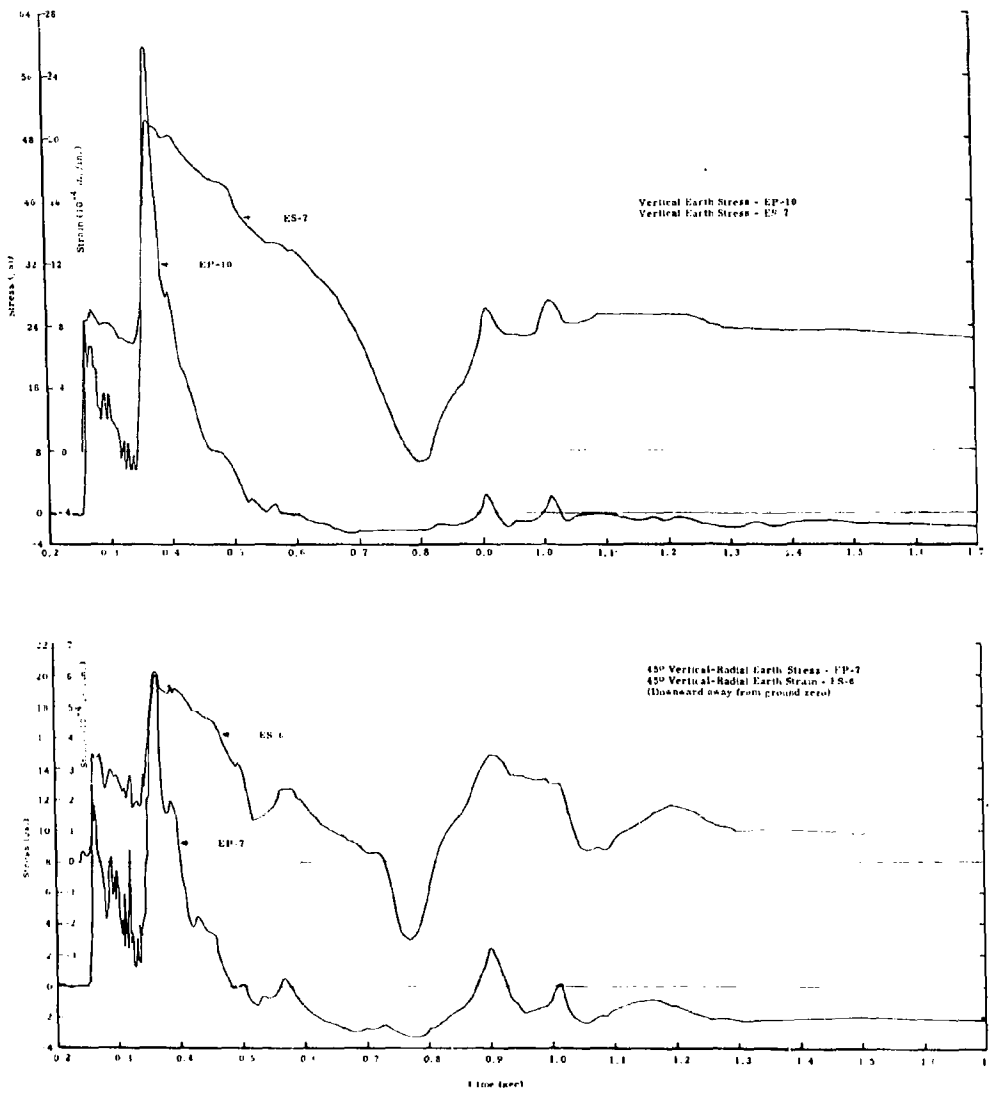

Fig. C.18 Earth Stress and Strain vs Time - Shot 10

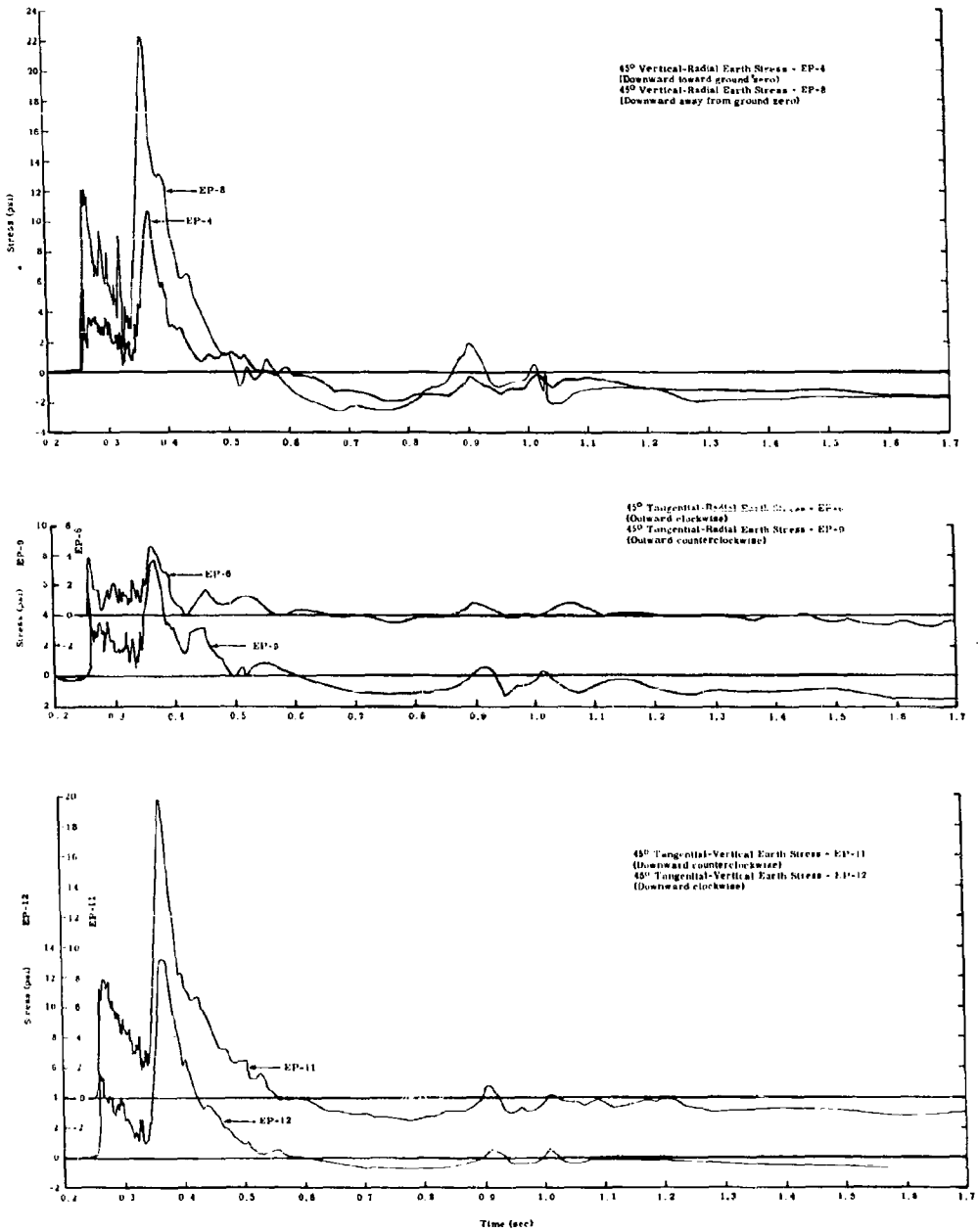

Fig. C.19 Earth Stress vs Time - Shot 10

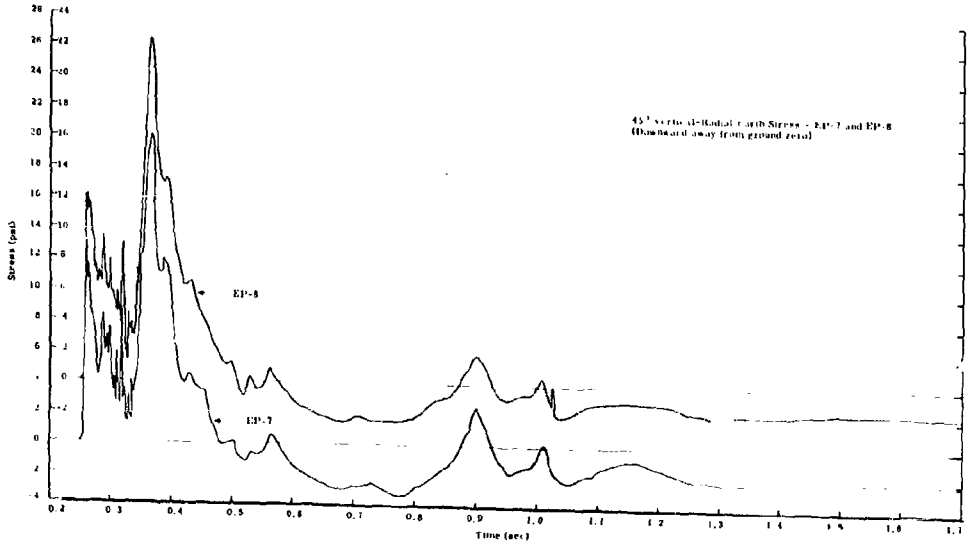

Fig. C.20 Earth Stress vs Time - Shot 10

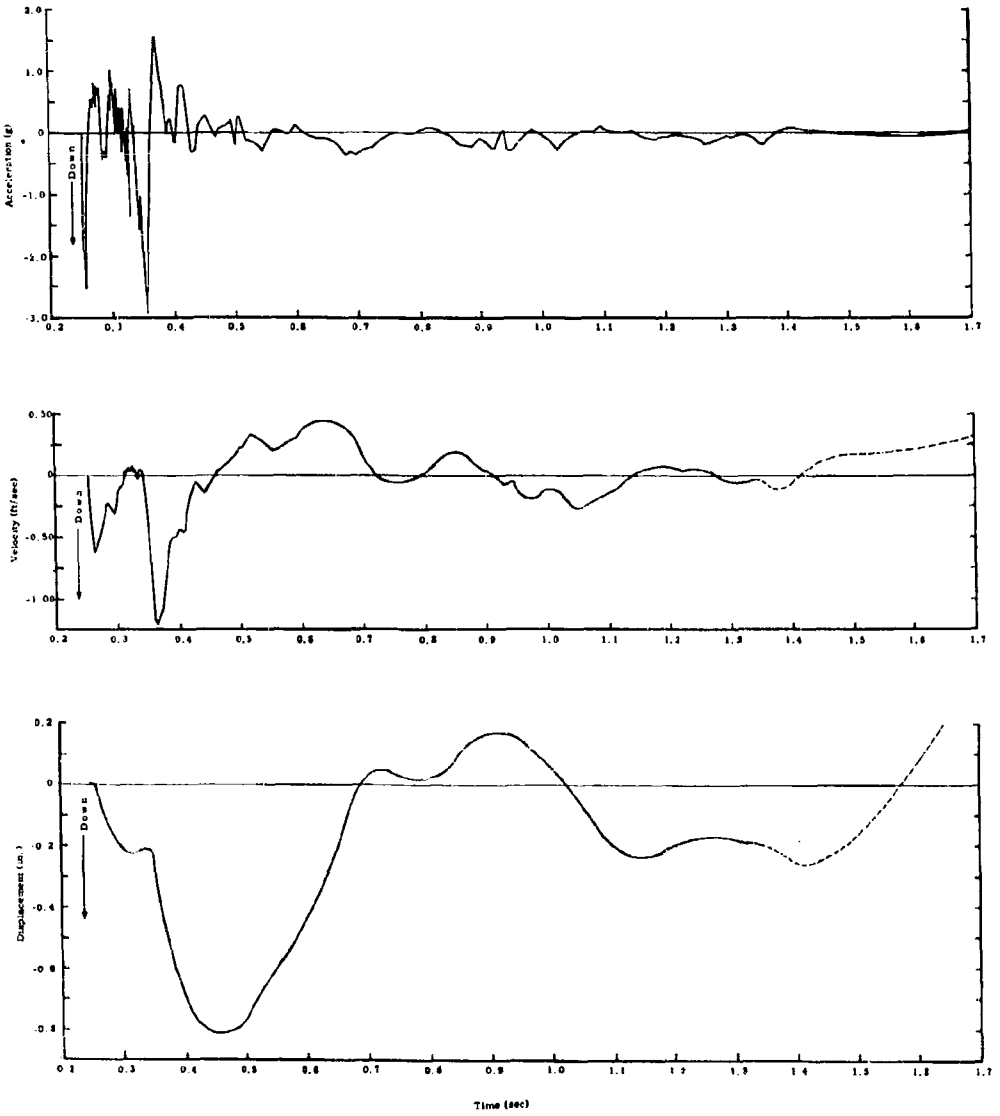

Fig. C.21 Vertical Ground Acceleration, Velocity, and Displacement vs Time - Shot 10

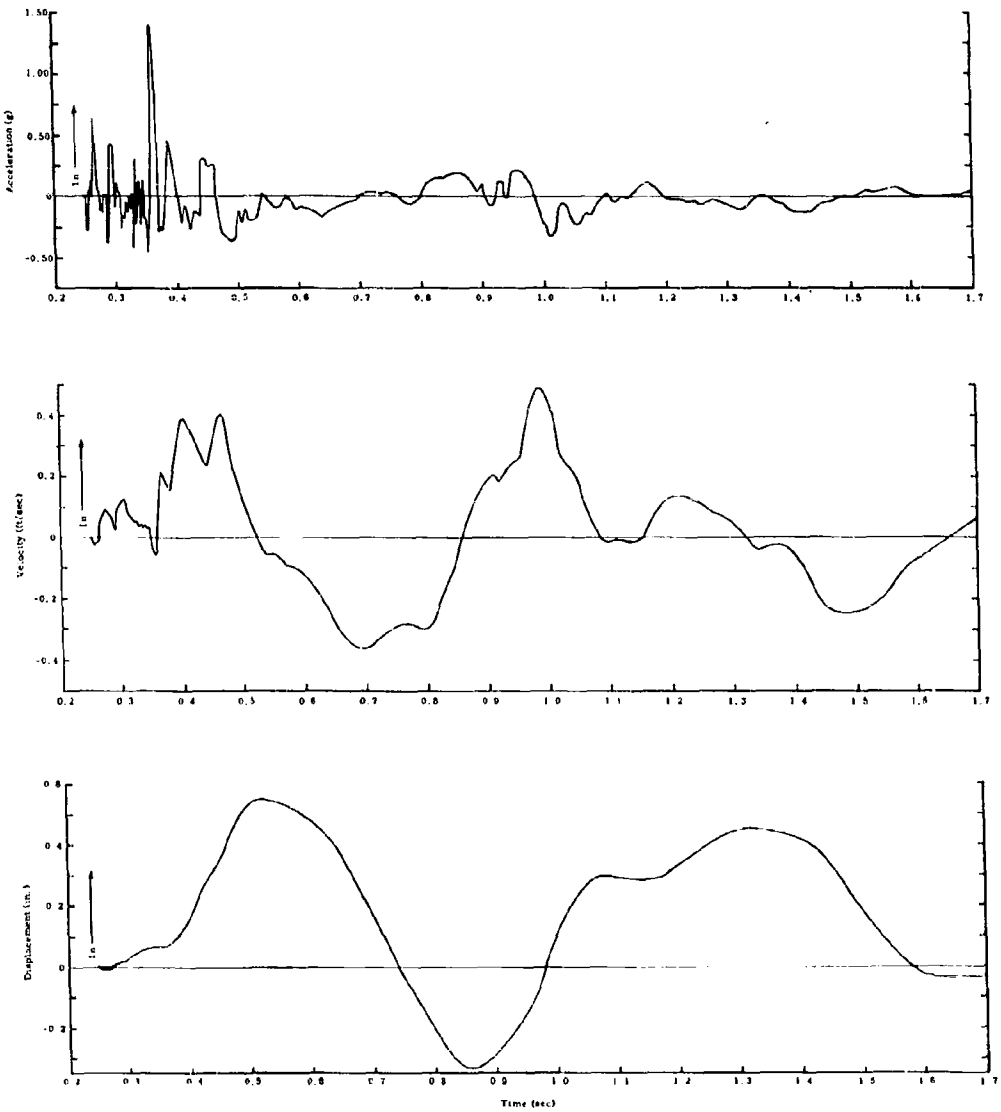

Fig. C.22 Radial Ground Acceleration, Velocity, and Displacement vs Time - Shot 10

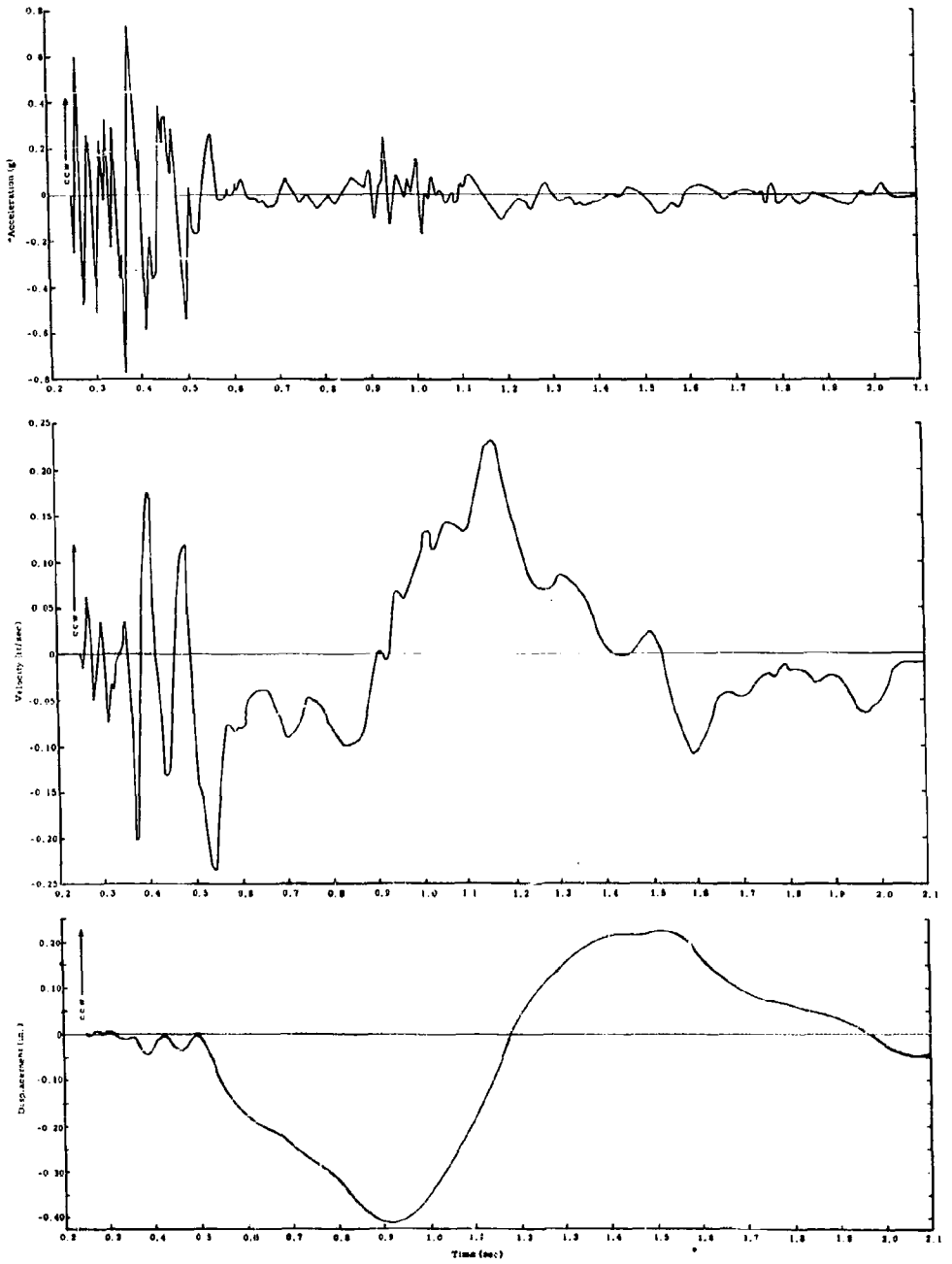

Fig. C.23 Tangential Ground Acceleration, Velocity, and Displacement vs Time - Shot 10

APPENDIX D

STRESS TENSOR - PRINCIPAL STRESS DERIVATION

Stress is the normal or tangential component of pressure acting on a surface within a solid or quasi-solid. Stresses, like pressures, represent intensity of force per unit area. The stress tensor is the mathematical expression which represents completely the condition of stress acting through a point.

The stress tensor is defined by all stresses acting on three mutually orthogonal planes. In the general case this definition requires knowledge of nine stress components, one normal to each plane and two, usually mutually perpendicular, tangent to each plane. However, equilibrium of stresses is necessary for analysis of the system, and this condition requires equality of three pairs of tangential stresses. Consequently the general stress tensor is defined by six stress components. There is, in addition to this definition of the tensor, a special case which results from the fact that for any point in a solid in which stresses are in equilibrium there exists one orientation of three mutually orthogonal planes such that all tangential stresses on them vanish. These are the principal planes. This special case completely defines the stress tensor in terms of only the three normal stresses on the principal planes, i.e., the principal stresses.

The purpose of this appendix is to show how data from practical field measurements of earth stress components may be treated mathematically to define the stress tensor in terms of the three principal stresses. Figure D.1 defines the terminology and geometry of the stresses involved. As noted in Part II, the direction of a plane is defined by the normal to it; thus direction of a plane and its normal stress are defined by the same symbol. Three mutually orthogonal planes through the point, O, of the diagram, are: the V-plane which is horizontal and below the ground surface at the depth of the instruments as depicted in the upper part of the diagram; the R-plane which is vertical and normal to the radius from ground zero at O; and the T-plane which is also vertical and normal to the tangential axis through O. These planes are chosen for discussion since the normal stresses on them, σ_V, σ_R, and σ_T, at O correspond to three of the measured stresses discussed in Section 2.5.3. The upper portion of the diagram shows a fourth plane, which for purposes of analysis

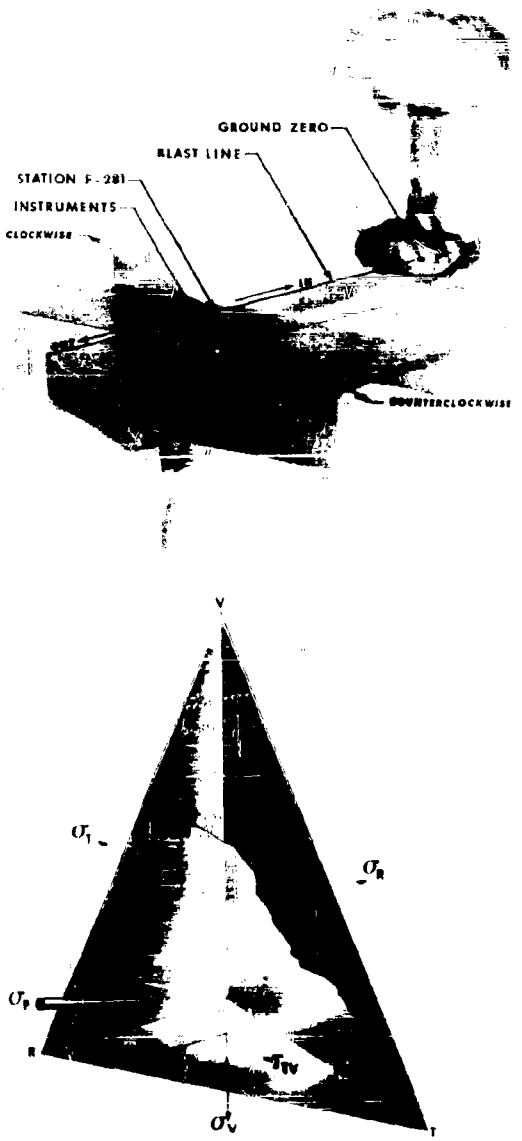

Fig. D.1 Schematic Diagram of Coordinate System and Stress Components

represents a principal plane, although its orientation, as shown, is wholly arbitrary and was chosen only to ensure contrast with the V-, R-, and T-planes.

The tetrahedron in the lower part of Fig. D.1 represents an infinitesimal portion of the four planes at O. The three stresses on each of the orthogonal planes at O are represented by arrows, and the normal stress on the arbitrary plane is represented by a perspective arrow. The stress arrows in the V-, R-, and T-planes were drawn as tension for clarity in the drawing but should all point inward to represent compression as does the σ_P-arrow. Compressive stresses are taken positive in accordance with soil mechanics convention and contrary to general stress analysis usage. Normal stress is identified by σ with a subscript representing the plane on which they act; shear stress is designated by τ with two subscripts, indicating the direction of the shear in terms of (1) the axis to which it is parallel and (2) the plane in which it acts. Thus σ_V is the normal stress on the V-plane and τ_{RV} is the shear parallel to the R-axis in the V-plane. σ_P is the normal stress on the arbitrary or P-plane, which, because of its definition as a principal plane, has no shear stresses associated with it.

The stress tensor is defined by the nine components σ_V, σ_R, σ_T, τ_{RV}, τ_{TV}, τ_{VR}, τ_{TR}, τ_{VT}, and τ_{RT}. However, since stress equilibrium must be assumed for analysis, it is necessary that $\tau_{VR} = \tau_{RV}$, $\tau_{VT} = \tau_{TV}$, and $\tau_{RT} = \tau_{TR}$; whence the stress tensor is defined by six components, σ_V, σ_R, σ_T, τ_{VR}, τ_{VT}, and τ_{RT}.

Equilibrium of stresses at O requires that all forces on the infinitesimal tetrahedron be in equilibrium. These forces are the product of the stresses by the areas over which they act. If A represents the triangular area of the P-plane included as a face of the tetrahedron, then Ak, Am, and An are the triangular areas of the faces in the V-, R-, and T-planes and k, m, and n are directional cosines of the P-plane with respect to the V-, R-, and T-axes, i.e., $k = \cos(P,V)$, $m = \cos(P,R)$, and $n = \cos(P,T)$. The force $A\sigma_P$ on the P-plane may be resolved into components parallel to the axes, and each of these component forces must be equal in magnitude and opposite in direction to the corresponding forces derived from the stresses on the V-, R-, and T-faces of the tetrahedron. Thus for equilibrium three equations of the type

$$\sigma_P\, Ak - \sigma_V\, Ak - \tau_{VR}\, Am - \tau_{VT}\, An = 0$$

must be satisfied. The equilibrium equations from which the area terms have been cancelled are

$$(\sigma_P - \sigma_V)\, k - \tau_{VR} m - \tau_{VT} n = 0 \qquad \text{(D.1)}$$

$$-\tau_{VR}\, k + (\sigma_P - \sigma_R)\, m - \tau_{RT} n = 0 \qquad \text{(D.2)}$$

$$-\tau_{VT}\, k - \tau_{RT}\, m + (\sigma_P - \sigma_T)\, n = 0. \qquad \text{(D.3)}$$

This group of simultaneous equations may be solved to yield the directional cosines if the values of σ_P are known. These solutions can differ from zero only if their determinant vanishes. That is, only if

$$\Delta = \begin{vmatrix} (\sigma_P - \sigma_V) & -\tau_{VR} & -\tau_{VT} \\ -\tau_{VR} & (\sigma_P - \sigma_R) & -\tau_{TR} \\ -\tau_{VT} & -\tau_{RT} & (\sigma_P - \sigma_T) \end{vmatrix} = 0. \quad (D.4)$$

This determinant may be restated as the cubic equation in σ_P,

$$\sigma_P^3 + p\sigma_P^2 + q\sigma_P + r = 0, \quad (D.5)$$

where

$$p = -(\sigma_V + \sigma_R + \sigma_T)$$

$$q = +(\sigma_V\sigma_R + \sigma_R\sigma_T + \sigma_V\sigma_T - \tau_{VR}^2 - \tau_{RT}^2 - \tau_{VT}^2)$$

$$r = -(\sigma_V\sigma_R\sigma_T + 2\tau_{VR}\tau_{RT}\tau_{VT} - \sigma_V\tau_{RT}^2 - \sigma_R\tau_{VT}^2 - \sigma_T\tau_{VR}^2).$$

The three roots of this equation, σ_1, σ_2, and σ_3, are normal stresses on three mutually orthogonal planes in which shear stresses vanish and are consequently the principal stresses at O.

Solution of the cubic equation requires elimination of the square term and conversion of the resultant to a quadratic equation in cubes. Thus if $\sigma_P = x + c$, Eq D.5 becomes

$$x^3 + (3c + p)\,x^2 + (3c^2 + 2pc + q)\,x + (c^3 + pc^2 + qc + r) = 0,$$

and if $3c + p = 0$, the x^2 -term vanishes and $c = -p/3$. Eq D.5 is now

$$x^3 + ax + b = 0. \quad (D.6)$$

Then

$$a = q - \frac{p^2}{3} \quad (D.7)$$

$$b = \frac{r + (2p^3 - 9pq)}{27}. \quad (D.8)$$

Equation D.6 may be converted to a quadratic form by placing $x = y + z$, whence

$$y^3 + z^3 + (3yz + a)(y + z) + b = 0 \qquad (D.9)$$

from which the $(y + z)$-term may be eliminated by making $(3yz + a)$ vanish. That is, if $3yz + a = 0$, $z = -a/3y$, Eq D.9 becomes

$$y^3 - \left(\frac{-a^3}{27y^3}\right) + b = 0$$

or

$$y^6 + by^3 - \frac{a^3}{27} = 0 \qquad (D.10)$$

The last equation is a quadratic in y^3 which has the more familiar form $s^2 + bs - a^3/27 = 0$ if $y3$ is replaced by s.

The solution of this quadratic equation is

$$s = y^3 = \frac{-b}{2} + \sqrt{\frac{b^2}{4} + \frac{a^3}{27}} \qquad (D.11)$$

and similarly,

$$z^3 = \frac{-b}{2} - \sqrt{\frac{b^2}{4} + \frac{a^3}{27}} \; . \qquad (D.12)$$

The solution of Eq D.6 is the sum of the three cube roots of Eqs D.11 and D.12 since $x = y + z$. However, there will be three possible sets of roots, depending on whether the quantity beneath the radical in Eqs D.11 and D.12 is greater than, equal to, or less than zero. For if $b^2/4 + a^3/27 > 0$, only one root will be real and the other two conjugate complex; if $b^2/4 + a^3/27 = 0$, all roots will be real, but two will be equal; and if $b^2/4 + a^3/27 < 0$, all roots will be real and unequal. The last of these conditions is the only one that is of real concern to the derivation of principal stresses. Unfortunately this case is also the one which is algebraically irreducible; algebraic manipulation of the equation leads only to identical equations because of the conjugate complex character of Eqs D.11 and D.12 when $b^2/4 + a^3/27$ is less than zero. It is feasible, however, to derive trigonometric solutions for Eqs D.11 and D.12 which yield usable information for evaluation of x and subsequently of σ_p.

The quantities y^3 and $z3$ are conjugate complex functions if $b^2/4 + a^3/27 < 0$, i.e., if $a^3/27$ is negative and numerically greater than $b^2/4$ when the latter is positive. Equations D.11 and D.12 may be rewritten in the trigonometric form

$$y^3 = \frac{-b}{2} + i\sqrt{-\left(\frac{b^2}{4} + \frac{a^3}{27}\right)} = w(\cos\theta + i \sin\theta) \qquad (D.13)$$

$$z^3 = \frac{-b}{2} - i\sqrt{-\left(\frac{b^2}{4} + \frac{a^3}{27}\right)} = w\,(\cos\theta - i\sin\theta) \qquad \text{(D.14)}$$

where, if

$$u = w\cos\theta = \frac{-b}{2}$$

and

$$v = w\sin\theta = \sqrt{-\left(\frac{b^2}{4} + \frac{a^3}{27}\right)}, \qquad \text{(D.15)}$$

$$w = \sqrt{u^2 + w^2} = \left(-\frac{a^3}{27}\right)^{1/2}$$

and

$$\cos\theta = \frac{-b}{2}\left(-\frac{27}{a^3}\right)^{1/2}. \qquad \text{(D.16)}$$

Equations D.13 and D.14 may now be evaluated by taking the cube roots of the trigonometric expressions

$$y_1 = w^{1/3}\,(\cos\theta + i\sin\theta)^{1/3} \times (1)^{1/3}$$

$$z_1 = w^{1/3}\,(\cos\theta - i\sin\theta)^{1/3} \times (1)^{1/3},$$

where $(1)^{1/3}$ has the values 1, $(\cos 2\pi/3 + i\sin 2\pi/3)$, and $(\cos 4\pi/3 + i\sin 4\pi/3)$. The result is three values each for y and z:

$$y_1 = w^{1/3}\left(\cos\frac{\theta}{3} + i\sin\frac{\theta}{3}\right)$$

$$y_2 = w^{1/3}\left(\cos\frac{\theta + 2\pi}{3} + i\sin\frac{\theta + 2\pi}{3}\right)$$

$$y_3 = w^{1/3}\left(\cos\frac{\theta + 4\pi}{3} + i\sin\frac{\theta + 4\pi}{3}\right)$$

$$z_1 = w^{1/3}\left(\cos\frac{\theta}{3} - i\sin\frac{\theta}{3}\right)$$

$$z_2 = w^{1/3}\left(\cos\frac{\theta + 2\pi}{3} - i\sin\frac{\theta + 2\pi}{3}\right)$$

$$z_3 = w^{1/3}\left(\cos\frac{\theta + 4\pi}{3} - i\sin\frac{\theta + 4\pi}{3}\right).$$

Consequently the solutions of Eq D.6 are the sums of these expressions:

$$x_1 = 2\,w^{1/3}\cos\frac{\theta}{3},$$

$$x_2 = 2\,w^{1/3}\cos\frac{\theta+2\pi}{3} = -2\,w^{1/3}\cos\left(60^\circ - \frac{\theta}{3}\right),$$

$$x_3 = 2\,w^{1/3}\cos\frac{\theta+4\pi}{3} = -2\,w^{1/3}\cos\left(60^\circ + \frac{\theta}{3}\right).$$

However, since $w = (-a^3/27)^{1/2}$ and $\sigma_p = x + c = x - p/3$, the solutions for Eq D.5 are

$$\sigma_1 = 2\left(\frac{-a}{3}\right)^{1/2}\cos\left(\frac{\theta}{3}\right) - \frac{p}{3} \qquad (D.17)$$

$$\sigma_2 = -2\left(\frac{-a}{3}\right)^{1/2}\cos\left(60^\circ - \frac{\theta}{3}\right) - \frac{p}{3} \qquad (D.18)$$

and

$$\sigma_3 = -2\left(\frac{-a}{3}\right)^{1/2}\cos\left(60^\circ + \frac{\theta}{3}\right) - \frac{p}{3}. \qquad (D.19)$$

Equations D.17, D.18, and D.19 are the three principal stresses at the origin O of Fig. D.1. They may be evaluated completely from measured values of the normal stress, σ_V, σ_R, and σ_T, and measured or derived values of the shear stresses τ_{VR}, τ_{RT}, and τ_{VT} at that point through the definition of the quantities p, q, and r for Eq D.5, of a and b in Eqs D.7 and D.8, and the expression for cos θ in Eq D.16. The subscripts used to identify the three stresses of Eqs D.17, D.18, and D.19 are those customarily used to distinguish the major, intermediate, and minor principal stresses, a distinction based upon magnitude. The relative magnitudes will depend upon both the magnitudes and the signs of the observed normal and shear stresses and will not necessarily result in values such that $\sigma_1 > \sigma_2 > \sigma_3$ in the notation given above. Consequently it may be convenient in practice to interchange the subscripts of the principal stresses given by Eqs D.17, D.18, and D.19 to conform with customary usage.

A further problem in application of the analytical methods to data from earth stress measurements is that introduced by the lack of suitable instruments for direct observation of transient earth shear stresses (Section 2.5.3). This problem has been solved by utilizing the normal stresses measured on two orthogonal planes to derive the shear stresses on the plane which bisects the angle between them. Thus normal stresses $\sigma_{VR\ DT}$ and $\sigma_{VR\ DA}$, measured on planes directed at 45° downward toward ground zero and downward away from ground zero between the vertical and radial planes, were used to derive the shear stresses, τ_{VR} and τ_{RV}, on the radial and vertical planes by means of the equation

$$\tau_{VR} = \tau_{RV} = \frac{\left(\sigma_{VR\ DT} - \sigma_{VR\ DA}\right)}{2} . \qquad (D.20)$$

The final step in defining the stress tensor by the principal stresses is determination of the direction of these stresses with respect to the coordinate axes. These directions are expressed as three directional cosines for each stress, representing the angles between the stress and each axis. A directional cosine is the ratio of a directional number to the unit vector representing the principal stress, and directional number is the projection of the unit principal stress vector on a coordinate axis.

The factors k, m, and n of the simultaneous Eqs D.1, D.2, and D.3 were defined as the directional cosines of the P-plane. Solutions of these equations will be directional numbers which by normalization are converted to directional cosines. Thus if $\bar{k}$, $\bar{m}$, and $\bar{n}$ are solutions of the simultaneous equations, the directional cosines are given by

$$k = \frac{\bar{k}}{\left(\bar{k}^2 + \bar{m}^2 + \bar{n}^2\right)^{1/2}} \qquad (D.21)$$

$$m = \frac{\bar{m}}{\left(\bar{k}^2 + \bar{m}^2 + \bar{n}^2\right)^{1/2}} \qquad (D.22)$$

and

$$n = \frac{\bar{n}}{\left(\bar{k}^2 + \bar{m}^2 + \bar{n}^2\right)^{1/2}} . \qquad (D.23)$$

The determinant Δ (Eq D.4) of the simultaneous equations must vanish if their solutions are different from zero. The minors of the three terms of any row of the determinant can be shown to be solutions of the simultaneous equations if they satisfy the equations. Thus if the minors of the terms of the first row $(\sigma_P - \sigma_V)$, $-\tau_{VR}$, and $-\tau_{VT}$ are $\bar{k}$, $\bar{m}$, and $\bar{n}$, then from Eq D.1 substitution of $\bar{k}$, $\bar{m}$, and $\bar{n}$ for k, m, and n gives $(\sigma_P - \sigma_V)\bar{k} - \tau_{VR}\bar{m} - \tau_{VT}\bar{m}$ which must vanish since it is exactly the determinant Δ. Similar substitutions in Eqs D.2 and D.3 give

$$-\tau_{VR}\bar{k} + \left(\sigma_P - \sigma_R\right)\bar{m} - \tau_{RT}\bar{n}$$

and

$$-\tau_{VT}\bar{k} - \tau_{RT}\bar{m} + \left(\sigma_P - \sigma_R\right)\bar{n} ,$$

both of which are determinants in which two rows contain identical terms and must consequently vanish. Thus the minors of the first row

satisfy the simultaneous equations and are solutions. The directional numbers for the P-plane are therefore $\bar{k}$, $\bar{m}$, and $\bar{n}$, the minors of the first-row terms of the determinant, and corresponding directional cosines are given by Eqs D.21, D.22, and D.23.

The P-plane has been defined as one of the principal planes and σ_P as the corresponding principal stress. Therefore, the directional cosines of the principal stress defining the angles between it and the coordinate axes V, R, and T are

$$k = \cos\left(\sigma_P, V\right) = \cos \alpha_P$$

$$m = \cos\left(\sigma_P, R\right) = \cos \beta_P$$

and

$$n = \cos\left(\sigma_P, T\right) = \cos \gamma_P,$$

where the subscript P has the values 1, 2, and 3 as the major, intermediate, and minor principal stresses are used in determining the directional numbers.

DISTRIBUTION

Military Distribution Categories 5-22

ARMY ACTIVITIES

1 Asst. Chief of Staff, G-3, D/A, Washington 25, D.C. ATTN: Dep. CofS, G-3 (RR&SW)
2 Deputy Chief of Staff for Logistics, D/A, Washington 25, D.C. ATTN: Director of Research & Development
3 Chief of Ordnance, D/A, Washington 25, D.C. ATTN: ORDTX-AR
4- 6 Chief Signal Officer, D/A, P&O Division, Washington 25, D.C. ATTN: SIGOP
7 The Surgeon General, D/A, Washington 25, D.C. ATTN: Chief, R&D Division
8- 9 Chief Chemical Officer, D/A, Washington 25, D.C.
10 The Quartermaster General, CBR, Liaison Officer, Research and Development Div., D/A, Washington 25, D.C.
11- 15 Chief of Engineers, D/A, Washington 25, D.C. ATTN: ENGNB
16 Chief of Transportation, Military Planning and Intelligence Div., Washington 25, D.C.
17- 19 Commanding General, Continental Army Command, Ft. Monroe, Va.
20 President, Board #1, Headquarters, Continental Army Command, Ft. Bragg, N.C.
21 President, Board #2, Headquarters, Continental Army Command, Ft. Knox, Ky.
22 President, Board #4, Headquarters, Continental Army Command, Ft. Bliss, Tex.
23 Commanding General, U.S. Army Caribbean, Ft. Amador, C.Z. ATTN: Cml. Off.
24- 25 Commander-in-Chief, Far East Command, APO 500, c/o PM, San Francisco, Calif. ATTN: ACofS, J-3
26- 27 Commanding General, U.S. Army Europe, APO 403, c/o PM, New York, N.Y. ATTN: OPOT Div., Combat Dev. Br.
28- 29 Commandant, Command and General Staff College, Ft. Leavenworth, Kan. ATTN: ALLLS(AS)
30 Commandant, The Artillery School, Ft. Sill, Okla.
31 Secretary, The AA&GM Branch, The Artillery School, Ft. Bliss, Tex. ATTN: Lt. Col. Albert D. Epley, Dept. of Tactics and Combined Arms
32 Commanding General, Medical Field Service School, Brooke Army Medical Center, Ft. Sam Houston, Tex.
33 Director, Special Weapons Development Office, Ft. Bliss, Tex. ATTN: Lt. Arthur Jaskierny
34 Commandant, Army Medical Service Graduate School, Walter Reed Army Medical Center, Washington 25, D.C.
35 Superintendent, U.S. Military Academy, West Point, N.Y. ATTN: Prof. of Ordnance
36 Commandant, Chemical Corps School, Chemical Corps Training Command, Ft. McClellan, Ala.
37 Commanding General, Research and Engineering Command, Army Chemical Center, Md. ATTN: Deputy for RW and Non-Toxic Material
38- 39 Commanding General, Aberdeen Proving Grounds, Md. (inner envelope) ATTN: RD Control Officer (for Director, Ballistics Research Laboratory)
40- 42 Commanding General, The Engineer Center, Ft. Belvoir, Va. ATTN: Asst. Commandant, Engineer School
43 Commanding Officer, Engineer Research and Development Laboratory, Ft. Belvoir, Va. ATTN: Chief, Technical Intelligence Branch
44 Commanding Officer, Picatinny Arsenal, Dover, N.J. ATTN: ORDBB-TK
45 Commanding Officer, Army Medical Research Laboratory, Ft. Knox, Ky.
46- 47 Commanding Officer, Chemical Corps Chemical and Radiological Laboratory, Army Chemical Center, Md. ATTN: Tech. Library
48 Commanding Officer, Transportation R&D Station, Ft. Eustis, Va.
49 Director, Technical Documents Center, Evans Signal Laboratory, Belmar, N.J.
50 Director, Waterways Experiment Station, PO Box 631, Vicksburg, Miss. ATTN: Library
51 Director, Armed Forces Institute of Pathology, 7th and Independence Avenue, S.W., Washington 25, D.C.
52 Director, Operations Research Office, Johns Hopkins University, 7100 Connecticut Ave., Chevy Chase, Md. ATTN: Library
53- 59 Technical Information Service, Oak Ridge, Tenn. (Surplus)

NAVY ACTIVITIES

60- 61 Chief of Naval Operations, D/N, Washington 25, D.C. ATTN: OP-36
62 Chief of Naval Operations, D/N, Washington 25, D.C. ATTN: OP-03EG
63 Director of Naval Intelligence, D/N, Washington 25, D.C. ATTN: OP-922V
64 Chief, Bureau of Medicine and Surgery, D/N, Washington 25, D.C. ATTN: Special Weapons Defense Div.
65 Chief, Bureau of Ordnance, D/N, Washington 25, D.C.
66 Chief, Bureau of Ships, D/N, Washington 25, D.C. ATTN: Code 348
67 Chief, Bureau of Yards and Docks, D/N, Washington 25, D.C. ATTN: D-440
68 Chief, Bureau of Supplies and Accounts, D/N, Washington 25, D.C.
69- 70 Chief, Bureau of Aeronautics, D/N, Washington 25, D.C.
71 Chief of Naval Research, Department of the Navy Washington 25, D.C. ATTN: LT(jg) F. McKee, USN
72 Commander-in-Chief, U.S. Pacific Fleet, Fleet Post Office, San Francisco, Calif.
73 Commander-in-Chief, U.S. Atlantic Fleet, U.S. Naval Base, Norfolk 11, Va.
74- 77 Commandant, U.S. Marine Corps, Washington 25, D.C. ATTN: Code A03H
78 President, U.S. Naval War College, Newport, R.I.
79 Superintendent, U.S. Naval Postgraduate School, Monterey, Calif.
80 Commanding Officer, U.S. Naval Schools Command, U.S. Naval Station, Treasure Island, San Francisco, Calif.
81 Commanding Officer, U.S. Fleet Training Center, Naval Base, Norfolk 11, Va. ATTN: Special Weapons School
82- 83 Commanding Officer, U.S. Fleet Training Center, Naval Station, San Diego 36, Calif. ATTN: (SPWP School)
84 Commanding Officer, U.S. Naval Damage Control Training Center, Naval Base, Philadelphia 12, Pa. ATTN: ABC Defense Course
85 Commanding Officer, U.S. Naval Unit, Chemical Corps School, Army Chemical Training Center, Ft. McClellan, Ala.
86 Commander, U.S. Naval Ordnance Laboratory, Silver Spring 19, Md. ATTN: EE
87 Commander, U.S. Naval Ordnance Laboratory, Silver Spring 19, Md. ATTN: R
88 Commander, U.S. Naval Ordnance Test Station, Inyokern, China Lake, Calif.
89 Officer-in-Charge, U.S. Naval Civil Engineering Res. and Evaluation Lab., U.S. Naval Construction Battalion Center, Port Hueneme, Calif. ATTN: Code 753
90 Commanding Officer, U.S. Naval Medical Research Inst., National Naval Medical Center, Bethesda 14, Md.
91 Director, U.S. Naval Research Laboratory, Washington 25, D.C. ATTN: Code 2029
92 Commanding Officer and Director, U.S. Navy Electronics Laboratory, San Diego 52, Calif. ATTN: Code 4223

[redacted]

(104 - 106)

93- 94 Commanding Officer, U.S. Naval Radiological Defense Laboratory, San Francisco 24, Calif. ATTN: Technical Information Division
95 Director, Naval Air Experimental Station, Air Material Center, U.S. Naval Base, Philadelphia, Penn.
96- 97 Commanding Officer and Director, David W. Taylor Model Basin, Washington 7, D.C. ATTN: Library
98 Commander, U.S. Naval Air Development Center, Johnsville, Pa.
99 Director, Office of Naval Research Branch Office, 1000 Geary St., San Francisco, Calif.
100 Commanding Officer and Director, U.S. Naval Engineering Experiment Station, Annapolis, Md. ATTN: Code 155
101-107 Technical Information Service, Oak Ridge, Tenn. (Surplus)

AIR FORCE ACTIVITIES

108 Asst. for Atomic Energy, Headquarters, USAF, Washington 25, D.C. ATTN: DCS/O
109 Director of Operations, Headquarters, USAF, Washington 25, D.C. ATTN: Operations Analysis
110 Director of Plans, Headquarters, USAF, Washington 25, D.C. ATTN: War Plans Div.
111 Director of Research and Development, Headquarters, USAF, Washington 25, D.C. ATTN: Combat Components Div.
112-113 Director of Intelligence, Headquarters, USAF, Washington 25, D.C. ATTN: AFOIN-1B2
114 The Surgeon General, Headquarters, USAF, Washington 25, D.C. ATTN: Bio. Def. Br., Pre. Med. Div.
115 Deputy Chief of Staff, Intelligence, Headquarters, U.S. Air Forces Europe, APO 633, c/o PM, New York, N.Y. ATTN: Directorate of Air Targets
116 Commander, 497th Reconnaissance Technical Squadron (Augmented), APO 633, c/o PM, New York, N.Y.
117 Commander, Far East Air Forces, APO 925, c/o PM, San Francisco, Calif.
118 Commander, Strategic Air Command, Offutt Air Force Base, Omaha, Nebraska. ATTN: Special Weapons Branch, Inspection Div., Inspector General
119 Commander, Tactical Air Command, Langley AFB, Va. ATTN: Documents Security Branch
120 Commander, Air Defense Command, Ent AFB, Colo.
121-122 Commander, Wright Air Development Center, Wright-Patterson AFB, Dayton, O. ATTN: WCRRN, Blast Effects Research
123 Commander, Air Training Command, Scott AFB, Belleville, Ill. ATTN: DCS/O GTF
124 Commander, Air Research and Development Command, PO Box 1395, Baltimore, Md. ATTN: RDDN
125 Commander, Air Proving Ground Command, Eglin AFB, Fla. ATTN: AG/TRB
126-127 Director, Air University Library, Maxwell AFB, Ala.
128-135 Commander, Flying Training Air Force, Waco, Tex. ATTN: Director of Observer Training
136 Commander, Crew Training Air Force, Randolph Field, Tex. ATTN: 2CTS, DCS/O
137 Commander, Headquarters, Technical Training Air Force, Gulfport, Miss. ATTN: TA&D
138-139 Commandant, Air Force School of Aviation Medicine, Randolph AFB, Tex.

140-145
146-147
148-150
151
152
153
154-155
156-162
163
164
165
166
167
168-173
174-175
176-184
185
186-192
ATC
193-195
196-198
199-203
204-206
207
208-220